

# UC Berkeley

## UC Berkeley Electronic Theses and Dissertations

### Title

Controlled Self Assembly of Conjugated Polymer Containing Block Copolymers

### Permalink

<https://escholarship.org/uc/item/9hm6c4b5>

### Author

McCulloch, Bryan

### Publication Date

2012

Peer reviewed|Thesis/dissertation

Controlled Self Assembly of Conjugated Polymer Containing Block Copolymers

By

Bryan McCulloch

A dissertation submitted in partial satisfaction of the

requirements for the degree of

Doctor of Philosophy

in

Chemical Engineering

in the

Graduate Division

of the

University of California, Berkeley

Committee in charge:

Professor Rachel A. Segalman, Chair

Professor Nitash P. Balsara

Professor Ronald Gronsky

Fall 2012

Controlled Self Assembly of Conjugated Polymer Containing Block Copolymers

© 2012

By Bryan McCulloch

## Abstract

### Controlled Self Assembly of Conjugated Polymer Containing Block Copolymers

by

Bryan McCulloch

Doctor of Philosophy in Chemical Engineering

University of California, Berkeley

Professor Rachel A. Segalman, Chair

The discovery and development of conjugated polymers has led to a large and vibrant research field due to their unique semiconducting properties and possibility of offering a completely new paradigm due to their abundant, lightweight, flexible and solution processable properties. In particular, the optoelectronic properties of these materials make them very well suited to applications such as organic light emitting diodes or organic photovoltaics and their relatively high charge mobility also make them useful in organic circuits. There are several reasons why the performance of these materials is presently limited compared to inorganic alternatives. Recently, significant work has been done trying to improve the performance of these materials by synthetically tuning the electronic properties such as the band gap and energy levels. There have been many other studies trying to improve intermolecular transport by enhancing crystallinity through annealing. In all of these studies the performance organic electronics still tends to be limited because the morphology of these materials is very complex and difficult to optimize. Many different length scales must be simultaneously optimized because the structure of a single polymer chain, their interactions with other polymer chains, the orientation of these chains and their degree of mixing with other components in the device all are extremely important to the performance of these materials.

In this work, block copolymers containing conjugated polymers are used to optimize the morphology of these materials through self assembly processes. Block copolymers can be used to produce a wide variety of thermodynamically stable morphologies with long range order and tunable domain sizes. The self assembly of conjugated polymers using block copolymers is complicated because the delocalization of electrons along the backbone, which produces their interesting semiconducting properties, also makes these polymers rod-like, liquid crystalline and drastically increases their intermolecular interactions. This thesis focuses on some of the basic issues that must be understood when trying to create and optimize techniques that can be used to produce self assembled structures containing conjugated polymers using block copolymers.



The chain shape of conjugated polymers is related to their intramolecular interactions and is a fundamental property of the polymer chemistry. This contributes to their specific properties that make every conjugated polymer behave slightly differently, making it difficult to build design rules that can be used for all conjugated polymers or even classes of polymers. By understanding the chain shape of these conjugated polymers, we can begin to understand how to tune their intermolecular interactions and block copolymer phase diagram. In this work we have examined the chain shape of polythiophenes, one of the most commonly used classes of conjugated polymers. We have also explored the use of polythiophenes in block copolymers to control the morphology in polymer photovoltaics. In order to optimize the properties of these materials it is also important develop techniques to align the block copolymer structure and the conjugated polymer backbone. This work examines the use of magnetic field alignment as a method to achieve these two goals. It has been shown that high degrees of alignment have been achieved with easily accessible field strengths. Additionally, work has been done examining methods to optimize the alignment procedure for magnetic field alignment of block copolymers by examining the effect of the field strength on the block copolymer phase behavior and through detailed work focusing on the dynamics of the alignment process. By building methods to optimize the morphology of block copolymer containing conjugated polymers we hope see these techniques applied to increase the performance of polymer optoelectronics.

## Table of Contents

Table of Contents.....	i
List of Figures.....	iii
List of Tables.....	v
Chapter 1. Introduction.....	1
1.1 Chain Shape of Conjugated Polymers.....	4
1.1.1 Understanding Conformations of Conjugated Polymers.....	4
1.1.2 Impact of Chain Shape on Conjugated Polymer Properties.....	8
1.2. Self Assembly of Conjugated Polymers.....	8
1.2.1 Conjugated Polymer in Block Copolymers.....	9
1.2.2 Functional Conjugated Block Copolymers.....	9
1.2.3 Alignment of Conjugated Block Copolymers.....	10
1.3. Motivation and Thesis Outline.....	12
1.4. References.....	13
Chapter 2. Polymer Chain Shape of Poly(3-alkyl thiophenes) in Solution Using Small Angle Neutron Scattering.....	19
2.1. Introduction.....	19
2.2. Experimental Section.....	23
2.2.1 Materials.....	23
2.2.2 Small Angle Neutron Scattering.....	25
2.2.3 SANS Intensity Modeling.....	25
2.3. Discussion.....	28
2.4. Conclusions.....	39
2.5. Appendix.....	40
2.6. Acknowledgments.....	43
2.7. References.....	43
Chapter 3. The Relationship Between Morphology and Performance of Donor Acceptor Rod-Coil Block Copolymers Solar Cells.....	48
3.1. Introduction.....	48
3.2. Experimental Methods.....	53
3.2.1 General methods.....	53
3.2.2 Materials.....	54

3.2.3 Devices Fabrication and Measurement.....	60
3.2.4 Transmission Electron Microscopy.....	61
3.2.5 Atomic Force Microscopy.....	61
3.3. Results and Discussion.....	61
3.3.1 Synthesis of Block Copolymers.....	61
3.3.2 Self-Assembly of the Bifunctional Block Copolymer.....	63
3.3.3 Device Behavior of Self-Assembled Film.....	67
3.3.4 The Effect of Chemical Structure.....	72
3.4. Conclusions.....	73
3.5. Acknowledgments.....	73
3.6. References.....	73
Chapter 4. Increased Order-Disorder Transition Temperature for a Rod-Coil Block Copolymer in the Presence of a Magnetic Field.....	81
4.1 Introduction.....	81
4.2. Experimental Section.....	83
4.3. Results and Discussion.....	86
4.4. Conclusions.....	90
4.5. Appendix.....	91
4.6. Acknowledgments.....	93
4.7. References.....	93
Chapter 5. Dynamics of Magnetic Alignment in Rod-Coil Block Copolymers.....	96
5.1. Introduction.....	96
5.2. Experimental Section.....	99
5.3. Results and Discussion.....	103
5.4. Conclusions.....	117
5.5. Appendix.....	118
5.6. Acknowledgments.....	125
5.7. References.....	125
Chapter 6. Conclusions and Future Outlook.....	129

## List of Figures

Figure 1.1. Polymer photovoltaic device geometries.....	3
Figure 1.2. Chain shape of common conjugated polymers.....	7
Figure 2.1. Polythiophene conformations and regioregularity.....	22
Figure 2.2. P3HT molecular weight distribution.....	24
Figure 2.3. Scattering intensity from P3HT.....	29
Figure 2.4. Comparison of models for P3AT SANS.....	31
Figure 2.5. Persistence length of P3ATs.....	32
Figure 2.6. Bond angles of P3ATs.....	35
Figure 2.7. Characteristic lengths of P3ATs as a function of temperature.....	37
Figure 2.8. Absorption maxima of polymers studied.....	40
Figure 2.9. Comparison of P3HT scattering at different concentrations.....	40
Figure 2.10. Statistical segment length of P3HT as a function of TCNQ doping concentration.....	41
Figure 2.11. Characteristic ratio of P3ATs.....	42
Figure 2.12. Conformation population from Boltzmann model.....	42
Figure 3.1. Photovoltaic Morphologies.....	50
Figure 3.2. Block Copolymer Photovoltaic Structure.....	52
Figure 3.3. Synthetic Scheme of Block Copolymer.....	55
Figure 3.4. Chemical structures for block copolymers.....	56
Figure 3.5. Block Copolymer GPC.....	58
Figure 3.4. Block Copolymer Nanostructure.....	64
Figure 3.5. Internal film Morphology.....	66
Figure 3.6. Photovoltaic device performance.....	68
Figure 3.7. Effect of ordering on efficiency.....	69
Figure 3.8. Effect of butyl acrylate on morphology.....	70
Figure 3.9. Effect of butyl acrylate on device performance.....	71
Figure 4.1. Chemical structure and morphology.....	84
Figure 4.2. Experimental setup for in situ SAXS.....	85
Figure 4.3. Increased order-disorder transition temperature.....	88
Figure 4.4. Distinguishing an order-disorder transition.....	89
Figure 4.5. Order-disorder transition in a 2T magnetic field.....	91

Figure 4.6. Order-disorder transition outside of a magnetic field.....	92
Figure 5.1. PPV-PI chemical structure and morphology.....	100
Figure 5.2. In situ SAXS used for studying magnetic alignment.....	102
Figure 5.3. Magnetic alignment of PPV-PI block copolymers.....	104
Figure 5.4. Maximum observed alignment as a function of field strength.....	105
Figure 5.5. Dynamics at low field strength.....	107
Figure 5.6. PPV-PI morphology during alignment at low field strength.....	108
Figure 5.7. Scattering during alignment at high field strengths upon cooling.....	109
Figure 5.8. Alignment as a function of time at high fields upon cooling.....	110
Figure 5.9. PPV-PI morphology during alignment at high field strength.....	111
Figure 5.10. Scattering during alignment at high field strengths upon heating.....	113
Figure 5.11. Alignment as a function of time at high fields upon heating.....	114
Figure 5.12. Alignment as a function of temperature and field strength.....	116
Figure 5.13. Alignment after rotation at high fields.....	118
Figure 5.14. Angular intensity of alignment after rotation.....	119
Figure 5.15. Scattering upon cooling at 2T.....	120
Figure 5.16. Alignment upon cooling at 2T.....	121
Figure 5.17. Alignment of PPV at low field strengths.....	122
Figure 5.18. Alignment of ex situ quenched samples at 6T.....	123
Figure 5.19. Effect of crosslinking on block copolymer morphology.....	124

## List of Tables

Table 2.1. Characteristics of Polymer Samples.....	24
Table 2.2. Model Comparison of chain shape parameters.....	31
Table 2.3. Comparison of chain shape parameters for different polymers and solvent conditions.....	32
Table 3.1. Block Copolymer Compositions.....	59

## Chapter 1. Introduction

Delocalization of electrons along the backbone of conjugated polymers leads to interesting optoelectronic properties useful to numerous applications. In particular, conjugated polymers have been the source of intense investigation in field effect transistors (FETs), organic light emitting diodes (OLEDs) and organic photovoltaics (OPVs).<sup>1</sup> Conjugated polymers can be precisely tuned through chemical modification to optimize their properties and are unique when compared to traditional inorganic systems because polymers are flexible, lightweight, created from abundant resources, can be solution processed and are much less expensive. While currently applications for conjugated polymers may best fit mobile consumer or disposable applications, rapid advances in the field have given hope that these materials will be used widespread, increasing efficiency, reducing costs or enabling new applications in the fields of display technology, indoor lighting and power generation. In order to improve the performance of these materials further optimization of the polymer morphology is crucial.

Due to the delocalization of electrons along  $\pi$ -orbitals, the backbone of conjugate polymers is planar making them behave more rod-like than traditional polymers which often thought of as flexible coils. Their rod-like nature and strong  $\pi$ - $\pi$  interactions lead to liquid crystallinity and crystallinity which drastically alter their behavior, often decreasing solubility and increasing kinetically trapped metastable structures. Though there are many synthetic challenges in discovering new and useful conjugated polymers, one of the major challenges in the field has been to find ways to optimize the morphology of these materials.<sup>2,3</sup>

FETs are one of the simplest organic electronic devices, requiring a high charge mobility, however improving the crystallinity and optimizing chain orientation in these devices is still a major field of research. OLEDs and OPVs are even more complex because they require a blend of p-type and n-type organic semiconductors in the active layer. For example, during the operation of an OPV many different processes must be simultaneously optimized in order to create an efficient device. First, light must be absorbed necessitating a material with a high absorbance and a band gap well suited to the solar spectrum. Since conjugated polymers have a low dielectric constant, free charges are not formed. Instead, a bound electron-hole pair (exciton) is formed which must diffuse to a junction between the p-type conjugated polymer and n-type, usually a fullerene derivative before the exciton decays (around 10 nm). This requirement necessitates a large number of interfaces throughout the active material in order to separate charges efficiently. Finally, electrons and holes must be transported through the bulk of the material to their respective electrodes. To achieve this, the most common device architecture involves a kinetically trapped phase separated blend of an electron donating polymer and electron accepting small molecule which is referred to as a bulk heterojunction. Ideally this morphology can achieve a large number of interfaces and continuous pathways throughout the material. Unfortunately in practice it is very difficult to achieve this and whenever any component or process is altered, the morphology must be optimized. Typically, even after optimization the bulk heterojunction is still limited because it is nearly impossible to achieve small domain

sizes and continuous pathways throughout the material because phase separation is an uncontrolled process and tradeoffs are always made. As a device is annealed, the domain size increases, decreasing charge separation as connectivity throughout the active layer increases leading to better charge transport. The performance of OLEDs also depends critically on the morphology of the active layer to optimize charge transport, photoluminescence and efficiency. To achieve the optimum geometry, many groups have examined ways to create ordered bulk heterojunctions using a variety of top-down processes such as stamping or templating techniques<sup>4-6</sup> and bottom up strategies taking advantage of self assembly processes.

In this work, we study methods of controlling a bottom up approach using the self assembly of conjugated polymer containing block copolymers as a technique to optimize the morphology of these interesting materials. Block copolymers have been used in numerous applications to create thermodynamically stable nanoscale structures. They are made up of two chemically distinct polymer chains which are covalently bonded together. Depending on the strength of segregation and volume fraction of each polymer chain, these materials can phase separate into a wide variety of structures and the domain size of these structures can be easily tuned by varying the degree of polymerization. While there are decades of research using block copolymers based on traditional vinyl and olefin based polymer, relatively little research has been done applying these concepts to the self assembly of block copolymers containing conjugated polymers.<sup>7</sup>

The increased rigidity of the backbone in conjugated polymers and their strong intermolecular interactions leading to liquid crystallinity and crystallinity, drastically alter their behavior in block copolymers and also introduce new difficulties such as an increase in kinetically trapped structures. The chain shape of many conjugated polymers is not well known and has not been extensively studied due to their strong intermolecular interactions and their relatively recent discovery. While it is clear that conjugation along the backbone should stiffen these polymers it is unclear to what degree it affects the overall persistence length in these materials. Balancing the complex driving forces for microphase separation and crystallinity is also crucial in developing new block copolymers containing conjugated polymers. The self assembly of these block copolymers is even more complex after incorporation of n-type small molecules. Finally, in order to optimize the performance of these materials it will be important to develop novel methods of aligning the block copolymer structure and the conjugated polymer within the self assembled structure. We have studied a relatively new technique using magnetic fields to align conjugated polymer containing block copolymers.



## Three Common Polymeric Photovoltaic Device Geometries

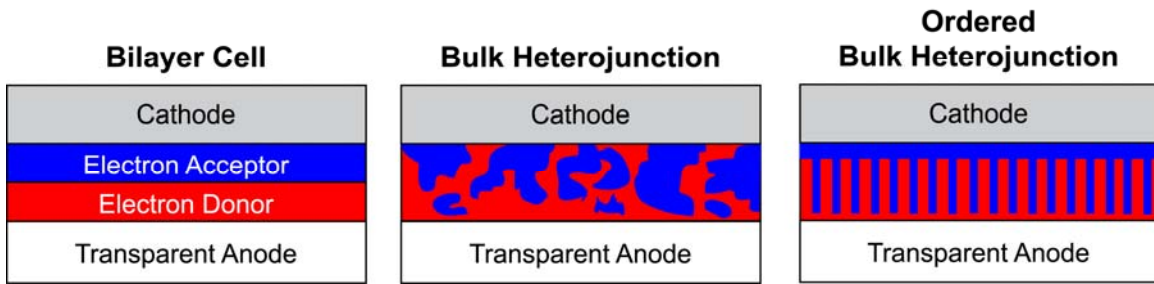


**Figure 1.1. Polymer photovoltaic device geometries**

Bilayer photovoltaic geometries are most common with small molecule organic photovoltaics and has the best charge transport to the electrodes but is limited because charge separation only can occur close to the donor-acceptor junction limiting efficiencies. Typically polymer photovoltaics are made using bulk heterojunctions where a conjugated polymer is blended with a n-type small molecule. This geometry ideally can lead to large number of interfaces and continuous pathways throughout the active material maximizing charge separation and charge transport; however, in practice it is extremely difficult to optimize the bulk heterojunction morphology. Ideally, an ordered bulk heterojunction could be patterned or self assembled where the domain size and orientation of phase separation can be precisely controlled.

## Chapter 1.1. Chain Shape of Conjugated Polymers

Polymer chain shape is one of the most basic properties of a polymer and is dominated by the intramolecular interactions between monomers.<sup>8</sup> The flexibility of a polymer controls many of the fundamental properties such as mechanical properties and impacts phenomena such as crystallization and self-assembly behavior. Intermolecular interactions such as sterics, hydrogen bonding and electron delocalization influence chain stiffness. Typically, classical polymers have very flexible backbones because of many possible configurations that have similar energetics.<sup>9</sup> As the energetics of these configurations are altered by the presence of intermolecular interactions, preferred orientations along the backbone tend to dominate and leads to a stiffer backbone, causing a transition from a random coil to a rod-like polymer.

Steric interactions can be very important to polymer chain stiffness causing polymers of similar backbones to have drastically different persistence lengths by slightly altering the polymer sidechain. By introducing bulky sidechains, rotation along the polymer backbone becomes hindered causing rod-like behavior and imparts liquid crystallinity showing that changes in the intramolecular interactions can lead to drastic changes in the intermolecular interactions and polymer properties.<sup>10</sup> Polypeptides have strong hydrogen bonding intermolecular interactions that can lead to secondary structures such as alpha-helices with very long persistence lengths.<sup>11</sup> Polyelectrolytes or other charged polymers can have strong coulombic interactions also resulting in increased polymer chain stiffness.<sup>12</sup> Understanding polymer chain shape is a complex problem because many of these interactions are long range between many monomers along the polymer chain leading to challenges theoretically predicting persistence lengths.

Conjugated polymers have increased stiffness due to the delocalization of electrons along the backbone, which also leads to their interesting electronic properties. Electron delocalization locks in a planar conformation between monomers and has been shown to lead to rod-like behavior and liquid crystallinity in some of these materials.<sup>13, 14</sup> The chain shape of these materials also has important ramifications on charge transport along the chain axis and intermolecular packing that can impact charge transport, excited state energetics and crystallization.<sup>15, 16</sup> While delocalization of electrons may lead to planarity, the distance over which electron delocalization occurs is limited and therefore these materials have finite conjugation lengths. The persistence lengths of these materials are also strongly affected by steric intramolecular interactions,<sup>10</sup> chemical defects along the chain and the number of possible conformations that may exist. While conjugated polymers tend to be much stiffer than traditional polymers, these factors lead to a wide range of persistence lengths and is one of the contributing reasons that conjugated polymers have a large variation in their polymer properties.

### 1.1.1 Understanding Conformations of Conjugated Polymers

Polymers typically lose bond correlations quickly and appear to behave like flexible coils. Between monomer segments along the backbone there are typically

several possible states that are accessible at room temperature. Semi-flexible and rod-like polymers have specific interactions that affect the energetics of these states and alter the population of possible conformations. In the extreme case, a perfectly rod-like polymer will only have one single possible bond angle with no backbone torsion, however, this is effectively impossible because of thermal energy. Conjugated polymers have increased stiffness because electron delocalization induces planarity along the backbone however there may be multiple states that are planar. One measure of the degree of delocalization is the conjugation length. The conjugation length is defined as the effective distance over which the electrons are delocalized and is typically estimated by measuring the optical band gap of a polymer while varying the degree of polymerization until the optical band gap asymptotes to its final value.<sup>17, 18</sup> In literature, it is common to associate the conjugation length as a measure of chain stiffness because a longer conjugation length requires a longer average planar distance along the polymer backbone. While measuring the optical properties of polymer is relatively simple, knowing the conjugation length is insufficient to determine the persistence length of a conjugated polymer.

Even in a perfectly planar conjugated polymer with no backbone torsion, if two different bond angles are possible, the persistence length is limited as the polymer will undergo a 2-D random walk. While conjugation may encourage a planar conformation, there are actually a range of torsion angles that still possess some orbital overlap and preserve some degree of conjugation.<sup>19</sup> This means that many conjugated polymers can also have relatively large average torsion angles, giving another mechanism for decreasing the persistence length. Sterics also play an important roll in the chain shape of conjugated polymers, just as they do in all polymers. The sidechains attached to the conjugated backbone to improve solubility and processing can have a large impact on the chain shape by altering the intramolecular interactions. For example, in poly(phenylene vinylene) (PPV) and polyflourene (PF), increasing the size of the sidechains can make the cis conformation very unfavorable and therefore leads to one predominant conformation along the polymer chain.<sup>20-22</sup> In PPV it has been shown that the persistence length can increase from 5 nm to over 20 nm by adding increasingly bulky sidechains. Conversely, adding longer sidechains to poly(paraphenylene) (PPP) can lead to increased backbone torsion or in poly(3-alkyl thiophene) (P3AT) affecting both the distribution of conformations along the backbone and the degree of backbone torsion, leading to a decrease in the persistence length.

There are also geometric factors that can influence the chain shape of these polymers. PPP and PF appear quite similar chemically and one may think PF should have a longer persistence length than PPP because essentially they are the same polymers however PF has a bridged linker that decreases backbone torsion, however, PPP has a persistence length, which is an order of magnitude longer. This arises because PPP has a 0° bond angle between monomers so all directional correlation between monomers is transmitted along the backbone even if there is significant torsion between monomers. PF has significantly less backbone torsion and a longer conjugation length, however, since there is a slight bend in the monomer structure, PF has a significantly shorter persistence length. This is one example that shows that while the conjugation length may

be related to the persistence length, it is not sufficient to determine the chain shape of a polymer.

There are several methods used to measure the chain shape of polymers that can be applied to conjugated polymers, however, the strong intermolecular interactions and unique optical properties can make these techniques quite difficult in practice. The most common way to measure chain shape involves scattering techniques using visible light, x-rays or neutrons.<sup>23-26</sup> All of these techniques can be used to examine the correlations within a sample and are used to examine the size of a single polymer chain. Static light scattering and x-ray scattering by using Zimm plots and Guiner plots respectively can access the radius of gyration of a polymer chain. If a series of polymers with known degrees of polymerization are used, fundamental parameters governing chain shape such as the statistical segment length or persistence length can be extracted. Unfortunately in both of these techniques, there is very little information gained on the structure of the polymer chain at the atomic level. In light scattering the wavelength is too large to have the resolution to extract correlations between monomers. In x-ray scattering, it is theoretically possible to resolve correlations between monomer units however the contrast between the solvent and polymer chain is usually too low. Neutron scattering has been a powerful tool used in polymer physics to study the chain shape of polymers because contrast can be drastically increased by using deuterated solvents and resolution can be achieved to gather data about correlations along the backbone of a polymer chain, providing substantially more information about the polymer chain shape. Since contrast can be achieved through selective deuteration, the chain shape in a polymer melt can be studied. Other techniques that can be used to access information about polymer chain size, and therefore chain shape include dilute solution viscometry and dynamic light scattering. The chain shape of conjugated polymers have been measured using all of the above techniques however there are significant challenges in working with these materials and obtaining reliable results.

Due to the strong intermolecular interactions arising from liquid crystallinity and strong  $\pi$ - $\pi$  stacking in conjugated polymers, it is often difficult to decouple single chain statistics from interactions throughout the material.<sup>10</sup> Often it is difficult to completely dissolve these polymers due to poor solubility and even when fully dispersed, aggregation between polymer chains is common. In all these techniques we rely on the fact that there are no correlations between measured chains because it is very difficult to deconvolute correlations within a single chain and correlations between chains. Depending on the wavelength used, light scattering techniques are also difficult with conjugated polymers because much of the light may be absorbed by the polymer chain leading to systematic errors. Finally, measurement of the persistence length of optically active conjugated polymers in the melt have remained elusive because of very strong low-angle scattering caused by correlations over very long distances.<sup>10</sup> It is unclear what the source of these correlations is, however, it has been hypothesized that it may be caused by packing frustrations from these rod-like materials or from very strong intermolecular aggregation that produces order in a seemingly disordered polymer melt. Since measurement of the persistence lengths of these materials in the melt has remained elusive, nearly all measurements of chain shape have been done in solution.

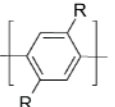
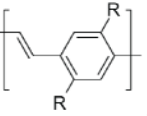
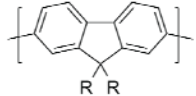
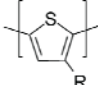
Polymer	Conformations	Conjugation Length	Persistence Length
Polyparaphenylene (PPP) 	1	~ 3.5 nm	~ 20 nm
Poly(phenylene vinylene) (PPV) 	2	6 - 11 nm	5 - 20 nm
Polyfluorene (PF) 	2	~ 9 nm	7 - 8 nm
Poly(3-alkyl thiophene) (P3AT) 	2	3 - 4 nm	2 - 30 nm

Figure 1.2. Chain shape of common conjugated polymers<sup>10, 17, 18, 20-22, 27-30</sup>

Conjugated polymers are in general stiffer than typical coil-like polymers however there is a wide range in their measured persistence lengths. The persistence length is related to the conjugation length of the material but is also related to the geometry of bond conformations along the backbone and the sterics associated with the sidechains.

Theoretically, the quality of solvent may alter the radius of gyration, it should not drastically affect the observed persistence length. In practice, depending on the specific interactions between the solvent and polymer chain, the persistence length can be slightly altered by solvent choice however these measurements give a good estimation of the polymer chain shape.

### **1.1.2 Impact of Chain Shape on Conjugated Polymer Properties**

The persistence length of conjugated polymers is a fundamental polymer property affecting its electronic, mechanical, and morphological properties. Most importantly, the stiffness imparted to conjugated polymers often leads to liquid crystallinity, increasing the order within the material and leading to methods of increasing the overall crystallinity of a material. For example, poly(2,5-bis(3-hexadecylthiophen-2-yl)thieno[3,2-b]thiophene) (PBTTT) contains a fused thiophene ring along the backbone that drastically increases the backbone stiffness compared to P3ATs. This leads to a smectic liquid crystalline phase and also changes the crystalline morphology. The smectic liquid crystalline phase allows the polymer chains to form well ordered sheet structures since the smectic phase is an ordered phase with high enough mobility to overcome kinetic trapping that usually limits crystal size in P3ATs. Liquid crystallinity and chain stiffness also alter the crystal structure to form well ordered sheets instead of crystalline fibers, drastically improving the charge mobility in PBTTT.<sup>31</sup>

Changes in the chain shape also have an important impact on the mechanical properties of the polymer. A very stiff polymer such as Kevlar or polyimide will be extremely tough and thermally robust because the polymer chains can not be easily deformed. In fact, PPP is often used to take advantage of these properties and is rarely used for any of its electronic properties.<sup>10</sup> While stiff polymers may be useful for certain applications, most commonly used polymers are very flexible, useful because they are easily processed and have useful elastic properties. Polymers with shorter persistence lengths tend to become more easily entangled, which is a critical phenomena to achieve tough and elastic materials.<sup>32</sup> Because flexible polymers can sample more conformations and take up a smaller hydrodynamic radius, the viscosity of polymer melts is also dependent on the polymer chain shape such that more flexible polymers flow more easily. In devices such as photovoltaics, one of the major failure mechanisms is associated with delamination between the active layer and the metal electrodes due to thermal cycling soft or more flexible polymer active layers could improve this.<sup>33</sup> It is also desired to use polymer electronics in applications where flexibility is very important and demands that the polymer not fail under large stresses. In order to meet these challenges it is important to design polymers that contain all of the desired electronic properties and also are able to meet the mechanical requirements of the final application by balancing the degree of stiffness in the final material.

## **1.2. Self Assembly of Conjugated Polymers**

The nanoscale morphology, crystallinity, orientation, domain size and degree of mixing are all critical parameters in optoelectronic devices using conjugated polymers.

Block copolymer self assembly techniques can be used to create a scalable, thermodynamically stable material that optimizes all of these parameters. Coil-like block copolymers, work has shown that the morphology of block copolymers can be optimized by simply altering the volume fraction of one block ( $\phi$ ) and the strength of segregation ( $\chi N$ ) where  $\chi$  is the Flory-Huggins interactions parameter and  $N$  is the degree of polymerization.<sup>34</sup> The Flory-Huggins interaction parameter is related to the unfavorable interactions between the two different polymer blocks and is dependent on temperature. The wide variety of different morphologies and domain sizes only depend on these two simple parameters, making it possible to predict the self assembly of a wide variety of block copolymers. The self assembly of block copolymers containing conjugated polymers is much more complicated due to the strong intermolecular interactions and packing constraints arising from their stiff backbone.<sup>7</sup>

### 1.2.1 Conjugated Polymer in Block Copolymers

One of the major challenges in the field of block copolymers is to incorporate functional polymers, which often do not have Gaussian chain shapes. Rod-coil block copolymers, where one block behaves rod-like, have been constructed using a wide variety of other polymers including biological, charged or mechanically robust polymers and is not just made of block copolymers containing conjugated polymers.<sup>7</sup> Rod-coil block copolymers behave fundamentally differently than the well understood coil-coil block copolymers. Both systems are parameterized by the Flory Huggins interactions ( $\chi N$ ) and the volume fraction of each block ( $\phi$ ). In addition, rod-coil systems require two additional parameters; the rod-rod interactions characterized by the Maier Saupe parameter ( $\mu N$ ) and a geometric scaling term to account for the difference in chain conformations between the rod-like and coil-like chains ( $v$ ). These four parameters have been used to formulate a phase diagram for a weakly segregated rod-coil system where theory and experiment both show drastic differences compared to the traditional block copolymer phase diagram.<sup>7, 35-39</sup> In the weakly segregated case, the rod-rod interactions and the reduced flexibility of the rod block stabilizes lamellar and liquid crystalline phases over a wide range of phase space. It also introduces a penalty for interfacial curvature preventing bicontinuous, cylindrical, or spherical phases. A hexagonal “hockey puck” phase replaces these phases at high coil fraction<sup>37</sup>. Recent experiments have shown that the ratio of the Flory Huggins and Maier Saupe interactions ( $\chi/\mu$ ) is also a relevant parameter and as this ratio increases, traditional coil-coil block copolymer structures with higher levels of curvature such as cylinders may be stabilized<sup>40</sup>. Many works have shown complex morphologies due to differences in interactions and solvent processing, which may lead to kinetically trapped structures.<sup>41-45</sup> A major challenge in the field of rod-coil block copolymers involves constructing systems that can reach stable morphologies since the rod-rod interactions can be quite strong and the rod-like block reduces the mobility of the system. Because of the rigid backbone and strong rod-rod interactions, rod-coil block copolymers behave distinctly differently than coil-coil systems with different governing parameters changing the chain conformation, amount of interfacial curvature and observed phase diagram.

### 1.2.2 Functional Conjugated Block Copolymers

There have been many areas of work where block copolymers have been used to enhance the performance of optoelectronic organic devices. One strategy of optimizing the morphology of an OPV has been to use a block copolymer to control the domain size and morphology of the bulk heterojunction.<sup>46</sup> Instead of a phase separated blend, a block copolymer is used containing one block uses a p-type conjugated polymer and the other contains an n-type small molecule. Several groups have constructed promising block copolymers for photovoltaics however it appears efficiencies tend to be limited by two major factors; their inability to self assemble into clearly defined morphology and instead form kinetically trapped structures due to the highly crystalline components or the low charge mobilities of many organic materials, which can be used to make systems that self assemble more easily. The Hadziioannou group was one of the first to construct a block copolymer photovoltaic by making a rod-coil block copolymer where the rod block consisted of poly(phenylene vinylene) (PPV) and the coil block had C<sub>60</sub> derivatives attached pendant to the chain.<sup>47</sup> This material failed to self assemble into structures with long range order because the C<sub>60</sub> crystallized too strongly, kinetically trapping the polymer morphology and limiting control over the resulting morphology. Another approach used by Thelakkat group has been to create coil-coil block copolymers where electron donating triphenylamine and electron accepting perylene were attached pendant to the chain.<sup>48</sup> This increases the chain mobility, which allows this system to self assemble into block copolymer morphologies. This work indicated that block copolymers could be used to form thermodynamically stable morphologies that improved device performance, however, the absolute efficiencies of these devices were limited by poor charge transport and significantly lower light absorbance of the inferior semiconducting small molecules compared to bulk heterojunction devices using C<sub>60</sub> and conjugated polymers, such as P3HT. In order to improve the performance of these devices, several groups have worked on rod-coil systems where conjugated polymer, P3HT, was used as the electron donor and perylene attached pendant to the coil block was used as the electron acceptor.<sup>49-51</sup> These block copolymers have also struggled to demonstrate self assembled structures because the P3HT domain crystallizes strongly. Work with P3HT block copolymers has been able to improve device performance by controlling the phase behavior of these materials however their performance still lags behind P3HT/PCBM heterojunction cells. It appears these block copolymers form crystalline P3HT fibrils, similar to the morphology of P3HT homopolymer,<sup>52</sup> lying parallel to the electrode that ultimately limits charge transport.<sup>51</sup> Work done on block copolymer photovoltaics appears promising however there are major challenges left in this field. In particular, strategies must be developed to control the self assembly of these block copolymers, utilize rod-like conjugated polymers. Once this is achieved, the impact of important parameters such as domain size, orientation and the degree of mixing on device efficiency can be systematically studied.

### **1.2.3 Alignment of Conjugated Block Copolymers**

While there are many exciting challenges in optimizing the morphology of block copolymers containing conjugated polymers, one of the major tasks will be controlling the orientation of the block copolymer domains and the conjugated polymer backbone.



To use functional block copolymers in optoelectronic devices such as photovoltaics, OLEDs or transistors it is crucial that the domains are aligned to improve charge transport.<sup>16, 53, 54</sup> For example, if block copolymer lamella are oriented perpendicular to the conduction axis, nearly no current will pass through the device. Aligning the conjugated polymer backbone can also improve absorbance or photoluminescence because optical transitions in the anisotropic backbone are very dependent on its orientation. This has been shown to improve the performance of photovoltaics by drastically increasing absorbance or incorporating interesting new properties such as polarized absorbance or photoluminescence.<sup>55-58</sup> An ideal alignment technique would align both the conjugated polymer and block copolymer structure.

There are many techniques that have been used to align block copolymers in the past included mechanical shear, surface functionalization, electric fields and magnetic fields. Each of these techniques have been able to achieve very high degrees of alignment however all of these have their own set of strengths and weaknesses. Mechanically shearing, pulling or rubbing polymer samples has been the most common way of producing aligned polymer samples.<sup>59, 60</sup> This usually works by stretching the polymer chains in the shear direction. This technique is widely used to align homopolymer samples to enhance strength of materials in a particular direction and can easily be obtained during the extrusion of thermoplastics. This makes it an excellent way to align bulk polymer samples, however, since it requires physically contacting a sample its application to thin polymer films may be limited. Rubbing thin films has been used in the past to align conjugated polymers however this technique can physically scratch the films making it difficult to reproducibly obtain high quality samples.<sup>16</sup>

One of the major applications for block copolymers has been in nanopatterning and nanolithography where a self assembled block copolymer thin film is used to transfer its structure to an underlying substrate.<sup>61</sup> In order to do this effectively, it is useful to align the block copolymer structure perpendicular to the surface. Typically, the surface energy of the polymer-substrate or air-polymer interfaces lead to preferential wetting of one of the block copolymer domains causing the block copolymer to instead orient parallel relative to the substrate, preventing any attempt to use the block copolymer for nanopatterning. By controlling the surface energy of the bottom surface and the film thickness, many groups have shown that block copolymers can be preferentially aligned perpendicular to the substrate.<sup>62</sup> Unfortunately in many optoelectronic applications it is not feasible to control the surface energies because the interfaces are critically important in charge transport and collection so any changes will decrease performance. This technique often only works for very thin films, which may be impractical for many applications and it may also be impossible to alter the surface energies to the degree needed to control alignment.

Another technique to align block copolymer nanostructures has been to use an electric field that orients the block copolymer structure perpendicular to the field, minimizing the capacitive energy of the system.<sup>63, 64</sup> Electric field alignment can achieve high degrees of alignment but requires extremely high fields. Usually to obtain these high fields, electrodes must be deposited directly on the block copolymer sample. It also

requires a fairly high difference in the dielectric constants between polymer blocks to produce a driving force for alignment. While it may be useful in particular systems such as polyelectrolytes, it is difficult to apply electric field alignment to conjugated polymer containing block copolymers because the high field strengths required will induce very large and damaging currents in these materials.

Finally, magnetic field alignment has been used successfully on a variety of liquid crystalline block copolymers, including systems with conjugated polymers.<sup>37, 65-67</sup> Magnetic field alignment has been widely used on liquid crystals and acts on the anisotropy in the magnetic susceptibility produced by the ordering of large grains made up of highly anisotropic rod-like molecules. Block copolymers have been aligned where small molecule liquid crystals are attached pendant to the backbone of one block. These small molecules can be aligned in the field, inducing alignment in the block copolymer structure. Alternatively, one of the block copolymer domains can be replaced with a rod-like liquid crystalline polymer such as a conjugated polymer. The liquid crystalline conjugated polymer can be aligned in the field and templates the block copolymer ordering. Both of these techniques have been shown to achieve highly aligned materials and work at readily accessible field strengths. The major advantages of using magnetic fields are that alignment can occur without contacting the polymer sample and any arbitrary orientation can be achieved by simply altering the field direction. This technique is well-suited to align the liquid crystalline conjugated polymers in optoelectronic block copolymers however there still exist a number of challenges because these systems often are kinetically trapped due to the strong intermolecular interactions. Additionally, magnetic alignment of block copolymer works best on bulk samples because the driving force for alignment is relatively small compared to the surface forces present in thin films.

### **1.3. Motivation and Thesis Outline**

Block copolymers offer a route to precisely control the morphology of conjugated polymers useful for optoelectronic devices. Because of the rod-like nature of many conjugated polymers, the self assembly of these block copolymers is much more complicated than model block copolymer systems. Conjugated polymers, due to their inherent backbone stiffness have strong intermolecular interactions and are often liquid crystalline, complicating their processing and drastically altering the block copolymer phase diagram. First, we must be able to understand what affects the chain shape of conjugated polymers, how the chain shape of these materials impacts their properties and how we can actively control the stiffness of these polymers to fit our desired application. Only then can we start to begin how to understand to self-assemble functional block copolymers. For applications such as polymer photovoltaics where a block copolymer is used containing both a p-type conjugated polymer and n-type small molecule, the block copolymer self assembly driving forces must be carefully balanced with other intermolecular interactions to produced the desired morphology. Alignment in these block copolymer systems is also important in optimizing their performance because many of the optoelectronic properties such as charge transport and light absorbance are highly anisotropic. In order to realize these objectives, we must have a deep understanding of

the complex interactions which control the block copolymer self assembly, intermolecular interactions from the conjugated polymer and the effects of chain shape.

This thesis will explore the fundamentals behind controlling the self assembly of block copolymers containing a conjugated polymer. Chapter 2 examine the chain shape of one of the most commonly studied classes of conjugated polymers, poly(3-alkyl thiophenes) (P3ATs) and shows how these polymers are actually better thought of as semi-flexible chains. Chapter 3 explores the self assembly behavior of a functional block copolymer containing both a p-type conjugated polymer and n-type small molecule. Chapter 4 demonstrates that the magnetic field used to align rod-coil block copolymers can also drastically affect the phase behavior, stabilizing the ordered phase. Finally, Chapter 5 looks closely at the mechanisms of magnetic alignment in rod-coil block copolymers and demonstrates several ways to improve alignment.

#### 1.4. References

1. Nelson, J., *The physics of solar cells*. Imperial College Press ; Distributed by World Scientific Pub. Co.: London River Edge, NJ, 2003; p xix, 363 p.
2. Greenham, N. C.; Moratti, S. C.; Bradley, D. D. C.; Friend, R. H.; Holmes, A. B., Efficient Light-Emitting-Diodes Based on Polymers with High Electron-Affinities. *Nature* **1993**, 365, (6447), 628-630.
3. Yu, G.; Gao, J.; Hummelen, J. C.; Wudl, F.; Heeger, A. J., Polymer Photovoltaic Cells - Enhanced Efficiencies Via a Network of Internal Donor-Acceptor Heterojunctions. *Science* **1995**, 270, (5243), 1789-1791.
4. Wiedemann, W.; Sims, L.; Abdellah, A.; Exner, A.; Meier, R.; Musselman, K. P.; MacManus-Driscoll, J. L.; Muller-Buschbaum, P.; Scarpa, G.; Lugli, P.; Schmidt-Mende, L., Nanostructured interfaces in polymer solar cells. *Applied Physics Letters* **2010**, 96, (26).
5. Scarpa, G.; Abdellah, A.; Exner, A.; Harrer, S.; Blanco, G. P.; Wiedemann, W.; Schmidt-Mende, L.; Lugli, P., Patterning Poly(3-Hexylthiophene) in the Sub-50-nm Region by Nanoimprint Lithography. *Ieee Transactions on Nanotechnology* **2011**, 10, (3), 482-488.
6. Park, L. Y.; Munro, A. M.; Ginger, D. S., Controlling Film Morphology in Conjugated Polymer: Fullerene Blends with Surface Patterning. *Journal of the American Chemical Society* **2008**, 130, (47), 15916-15926.
7. Olsen, B. D.; Segalman, R. A., Self-assembly of rod-coil block copolymers. *Materials Science & Engineering R-Reports* **2008**, 62, (2), 37-66.
8. Birshstein, T. M.; Ptitsyn, O. B., *Conformations of macromolecules*. Interscience Publishers: New York,, 1966; p xiv, 350 p.

9. Gennes, P. G. d., *Scaling concepts in polymer physics*. Cornell University Press: Ithaca, N.Y., 1979; p 324 p.
10. Vaia, R. A.; Krishnamoorti, R.; Benner, C.; Trimer, M., Chain conformation of rod-like polymers in the melt: Small-angle neutron scattering of poly(benzoyl paraphenylene). *Journal of Polymer Science Part B-Polymer Physics* **1998**, 36, (13), 2449-2459.
11. Lu, Y. J.; Weers, B.; Stellwagen, N. C., DNA persistence length revisited. *Biopolymers* **2001**, 61, (4), 261-275.
12. Brulet, A.; Boue, F.; Cotton, J. P., About the experimental determination of the persistence length of wormlike chains of polystyrene. *Journal De Physique Ii* **1996**, 6, (6), 885-891.
13. Chow, A. W.; Bitler, S. P.; Penwell, P. E.; Osborne, D. J.; Wolfe, J. F., Synthesis and Solution Properties of Extended Chain Poly(2,6-Benzothiazole) and Poly(2,5-Benzoxazole). *Macromolecules* **1989**, 22, (9), 3514-3520.
14. Yu, L. P.; Bao, Z. N., Conjugated Polymers Exhibiting Liquid Crystallinity. *Advanced Materials* **1994**, 6, (2), 156-159.
15. Snyder, C. R.; Henry, J. S.; DeLongchamp, D. M., Effect of Regioregularity on the Semicrystalline Structure of Poly(3-hexylthiophene). *Macromolecules* **2011**, 44, (18), 7088-7091.
16. Hartmann, L.; Tremel, K.; Uttiya, S.; Crossland, E.; Ludwigs, S.; Kayunkid, N.; Vergnat, C.; Brinkmann, M., 2D Versus 3D Crystalline Order in Thin Films of Regioregular Poly(3-hexylthiophene) Oriented by Mechanical Rubbing and Epitaxy. *Advanced Functional Materials* **2011**, 21, (21), 4047-4057.
17. Thienpont, H.; Rikken, G. L. J. A.; Meijer, E. W.; Tenhoeve, W.; Wynberg, H., Saturation of the Hyperpolarizability of Oligothiophenes. *Physical Review Letters* **1990**, 65, (17), 2141-2144.
18. Meier, H.; Stalmach, U.; Kolshorn, H., Effective conjugation length and UV/vis spectra of oligomers. *Acta Polymerica* **1997**, 48, (9), 379-384.
19. Darling, S. B.; Sternberg, M., Importance of Side Chains and Backbone Length in Defect Modeling of Poly(3-alkylthiophenes). *Journal of Physical Chemistry B* **2009**, 113, (18), 6215-6218.
20. Fytas, G.; Nothofer, H. G.; Scherf, U.; Vlassopoulos, D.; Meier, G., Structure and dynamics of nondilute polyfluorene solutions. *Macromolecules* **2002**, 35, (2), 481-488.
21. Gettinger, C. L.; Heeger, A. J.; Drake, J. M.; Pine, D. J., The Effect of Intrinsic Rigidity on the Optical-Properties of Ppv Derivatives. *Molecular Crystals and Liquid*

*Crystals Science and Technology Section a-Molecular Crystals and Liquid Crystals* **1994**, 256, 507-512.

22. Gettinger, C. L.; Heeger, A. J.; Drake, J. M.; Pine, D. J., A Photoluminescence Study of Poly(Phenylene Vinylene) Derivatives - the Effect of Intrinsic Persistence Length. *Journal of Chemical Physics* **1994**, 101, (2), 1673-1678.

23. Debye, P., Molecular-Weight Determination by Light Scattering. *Journal of Physical and Colloid Chemistry* **1947**, 51, (1), 18-32.

24. Flory, P. J., The Configuration of Real Polymer Chains. *Journal of Chemical Physics* **1949**, 17, (3), 303-310.

25. Benoit, H.; Doty, P., Light Scattering from Non-Gaussian Chains. *Journal of Physical Chemistry* **1954**, 57, (9), 958-963.

26. Sharp, P.; Bloomfield, V., Light Scattering from Wormlike Chains with Excluded Volume Effects. *Biopolymers* **1968**, 6, (8), 1201-&.

27. Aime, J. P.; Bargain, F.; Schott, M.; Eckhardt, H.; Elsenbaumer, R. L.; Miller, G. G.; McDonnell, M. E.; Zero, K., Structural Study of Conducting Polymers in Solution. *Synthetic Metals* **1989**, 28, (1-2), C407-C417.

28. Aime, J. P.; Bargain, F.; Schott, M.; Eckhardt, H.; Miller, G. G.; Elsenbaumer, R. L., Structural Study of Doped and Undoped Polythiophene in Solution by Small-Angle Neutron-Scattering. *Physical Review Letters* **1989**, 62, (1), 55-58.

29. Klaerner, G.; Miller, R. D., Polyfluorene derivatives: Effective conjugation lengths from well-defined oligomers. *Macromolecules* **1998**, 31, (6), 2007-2009.

30. Socci, E. P.; Farmer, B. L.; Adams, W. W., Molecular-Dynamics Simulations of a Poly(P-Phenylene) Oligomer. *Journal of Polymer Science Part B-Polymer Physics* **1993**, 31, (13), 1975-1982.

31. McCulloch, I.; Heeney, M.; Bailey, C.; Genevicius, K.; I, M.; Shkunov, M.; Sparrowe, D.; Tierney, S.; Wagner, R.; Zhang, W. M.; Chabinyc, M. L.; Kline, R. J.; McGehee, M. D.; Toney, M. F., Liquid-crystalline semiconducting polymers with high charge-carrier mobility. *Nature Materials* **2006**, 5, (4), 328-333.

32. Fetters, L. J.; Lohse, D. J.; Milner, S. T.; Graessley, W. W., Packing length influence in linear polymer melts on the entanglement, critical, and reptation molecular weights. *Macromolecules* **1999**, 32, (20), 6847-6851.

33. Jorgensen, M.; Norrman, K.; Gevorgyan, S. A.; Tromholt, T.; Andreasen, B.; Krebs, F. C., Stability of Polymer Solar Cells. *Advanced Materials* **2012**, 24, (5), 580-612.

34. Bates, F. S.; Fredrickson, G. H., Block copolymers - Designer soft materials. *Physics Today* **1999**, 52, (2), 32-38.

35. Olsen, B. D.; Segalman, R. A., Structure and thermodynamics of weakly segregated rod-coil block copolymers. *Macromolecules* **2005**, 38, (24), 10127-10137.
36. Olsen, B. D.; Segalman, R. A., Phase transitions in asymmetric rod-coil block copolymers. *Macromolecules* **2006**, 39, (20), 7078-7083.
37. Tao, Y. F.; Zohar, H.; Olsen, B. D.; Segalman, R. A., Hierarchical nanostructure control in rod-coil block copolymers with magnetic fields. *Nano Letters* **2007**, 7, (9), 2742-2746.
38. Olsen, B. D.; Shah, M.; Ganesan, V.; Segalman, R. A., Universalization of the phase diagram for a model rod-coil diblock copolymer. *Macromolecules* **2008**, 41, (18), 6809-6817.
39. Pryamitsyn, V.; Ganesan, V., Self-assembly of rod-coil block copolymers. *Journal of Chemical Physics* **2004**, 120, (12), 5824-5838.
40. Ho, C. C.; Lee, Y. H.; Dai, C. A.; Segalman, R. A.; Su, W. F., Synthesis and Self-Assembly of Poly(diethylhexyloxy-p-phenylenevinylene)-b-poly(methyl methacrylate) Rod-Coil Block Copolymers. *Macromolecules* **2009**, 42, (12), 4208-4219.
41. Chen, J. T.; Thomas, E. L.; Ober, C. K.; Hwang, S. S., Zigzag Morphology of a Poly(Styrene-B-Hexyl Isocyanate) Rod Coil Block-Copolymer. *Macromolecules* **1995**, 28, (5), 1688-1697.
42. Chen, J. T.; Thomas, E. L.; Ober, C. K.; Mao, G. P., Self-assembled smectic phases in rod-coil block copolymers. *Science* **1996**, 273, (5273), 343-346.
43. Lee, M.; Cho, B. K.; Zin, W. C., Supramolecular structures from rod-coil block copolymers. *Chemical Reviews* **2001**, 101, (12), 3869-3892.
44. Li, C. Y.; Tenneti, K. K.; Zhang, D.; Zhang, H. L.; Wan, X. H.; Chen, E. Q.; Zhou, Q. F.; Carlos, A. O.; Igos, S.; Hsiao, B. S., Hierarchical assembly of a series of rod-coil block copolymers: Supramolecular LC phase in nanoenvironment. *Macromolecules* **2004**, 37, (8), 2854-2860.
45. Radzilowski, L. H.; Carragher, B. O.; Stupp, S. I., Three-dimensional self-assembly of rodcoil copolymer nanostructures. *Macromolecules* **1997**, 30, (7), 2110-2119.
46. Segalman, R. A.; McCulloch, B.; Kirmayer, S.; Urban, J. J., Block Copolymers for Organic Optoelectronics. *Macromolecules* **2009**, 42, (23), 9205-9216.
47. van der Veen, M. H.; de Boer, B.; Stalmach, U.; van de wetering, K. I.; Hadziioannou, G., Donor-acceptor diblock copolymers based on PPV and C-60: Synthesis, thermal properties, and morphology. *Macromolecules* **2004**, 37, (10), 3673-3684.

48. Lindner, S. M.; Huttner, S.; Chiche, A.; Thelakkat, M.; Krausch, G., Charge separation at self-assembled nanostructured bulk interface in block copolymers. *Angewandte Chemie-International Edition* **2006**, 45, (20), 3364-3368.
49. Sommer, M.; Lang, A. S.; Thelakkat, M., Crystalline-crystalline donor-acceptor block copolymers. *Angewandte Chemie-International Edition* **2008**, 47, (41), 7901-7904.
50. Zhang, Q.; Cirpan, A.; Russell, T. P.; Emrick, T., Donor–Acceptor Poly(thiophene-block-perylene diimide) Copolymers: Synthesis and Solar Cell Fabrication. *Macromolecules* **2009**, 42, (4), 1079–1082.
51. Tao, Y. F.; McCulloch, B.; Kim, S.; Segalman, R. A., The relationship between morphology and performance of donor-acceptor rod-coil block copolymer solar cells. *Soft Matter* **2009**, 5, (21), 4219-4230.
52. Iovu, M.; Jeffries-El, M.; Sheina, E. E.; Krankowski, A.; Sauve, G.; McCullough, R. D., Synthesis and characterization of poly(3-hexylthiophene)-b-polystyrene di-block copolymers. *Abstracts of Papers of the American Chemical Society* **2004**, 228, U336-U336.
53. Liu, J. G.; Sun, Y.; Gao, X. A.; Xing, R. B.; Zheng, L. D.; Wu, S. P.; Geng, Y. H.; Han, Y. C., Oriented Poly(3-hexylthiophene) Nanofibril with the pi-pi Stacking Growth Direction by Solvent Directional Evaporation. *Langmuir* **2011**, 27, (7), 4212-4219.
54. O'Connor, B.; Kline, R. J.; Conrad, B. R.; Richter, L. J.; Gundlach, D.; Toney, M. F.; DeLongchamp, D. M., Anisotropic Structure and Charge Transport in Highly Strain-Aligned Regioregular Poly(3-hexylthiophene). *Advanced Functional Materials* **2011**, 21, (19), 3697-3705.
55. Zhu, R.; Kumar, A.; Yang, Y., Polarizing Organic Photovoltaics. *Advanced Materials* **2011**, 23, (36), 4193-+.
56. Whitehead, K. S.; Grell, M.; Bradley, D. D. C.; Jandke, M.; Strohriegel, P., Highly polarized blue electroluminescence from homogeneously aligned films of poly(9,9-dioctylfluorene). *Applied Physics Letters* **2000**, 76, (20), 2946-2948.
57. Weder, C.; Sarwa, C.; Bastiaansen, C.; Smith, P., Highly polarized luminescence from oriented conjugated polymer/polyethylene blend films. *Advanced Materials* **1997**, 9, (13), 1035-&.
58. Smilowitz, L.; Heeger, A. J., Photoinduced Absorption from Triplet Excitations in Poly(2-Methoxy, 5-(2'-Ethyl-Hexyloxy)-P-Phenylene Vinylene) Oriented by Gel-Processing in Polyethylene. *Synthetic Metals* **1992**, 48, (2), 193-202.
59. Frederickson, G. H., Steady Shear Alignment of Block-Copolymers near the Isotropic Lamellar Transition. *Journal of Rheology* **1994**, 38, (4), 1045-1067.

60. Hamley, I. W., The effect of shear on ordered block copolymer solutions. *Current Opinion in Colloid & Interface Science* **2000**, 5, (5-6), 342-350.
61. Segalman, R. A., Patterning with block copolymer thin films. *Materials Science & Engineering R-Reports* **2005**, 48, (6), 191-226.
62. Suh, H. S.; Kang, H. M.; Liu, C. C.; Nealey, P. F.; Char, K., Orientation of Block Copolymer Resists on Interlayer Dielectrics with Tunable Surface Energy. *Macromolecules* **2010**, 43, (1), 461-466.
63. Amundson, K.; Helfand, E.; Quan, X. N.; Hudson, S. D.; Smith, S. D., Alignment of Lamellar Block-Copolymer Microstructure in an Electric-Field .2. Mechanisms of Alignment. *Macromolecules* **1994**, 27, (22), 6559-6570.
64. Boker, A.; Elbs, H.; Hansel, H.; Knoll, A.; Ludwigs, S.; Zettl, H.; Zvelindovsky, A. V.; Sevink, G. J. A.; Urban, V.; Abetz, V.; Muller, A. H. E.; Krausch, G., Electric field induced alignment of concentrated block copolymer solutions. *Macromolecules* **2003**, 36, (21), 8078-8087.
65. Osuji, C.; Ferreira, P. J.; Mao, G. P.; Ober, C. K.; Vander Sande, J. B.; Thomas, E. L., Alignment of self-assembled hierarchical microstructure in liquid crystalline diblock copolymers using high magnetic fields. *Macromolecules* **2004**, 37, (26), 9903-9908.
66. Gopinadhan, M.; Majewski, P. W.; Osuji, C. O., Facile Alignment of Amorphous Poly(ethylene oxide) Microdomains in a Liquid Crystalline Block Copolymer Using Magnetic Fields: Toward Ordered Electrolyte Membranes. *Macromolecules* **2010**, 43, (7), 3286-3293.
67. Majewski, P. W.; Gopinadhan, M.; Jang, W. S.; Lutkenhaus, J. L.; Osuji, C. O., Anisotropic Ionic Conductivity in Block Copolymer Membranes by Magnetic Field Alignment. *Journal of the American Chemical Society* **2010**, 132, (49), 17516-17522.



## Chapter 2. Polymer Chain Shape of Poly(3-alkyl thiophenes) in Solution Using Small Angle Neutron Scattering

The chain shape of polymers affects many aspects of their behavior and is governed by their intramolecular interactions. Delocalization of electrons along the backbone of conjugated polymers has been shown to lead to increased chain rigidity by encouraging a planar conformation. Poly(3-hexyl thiophene) and other poly(3-alkyl thiophenes) (P3ATs) are interesting for organic electronics applications and it is clear that a hierarchy of structural features in these polymers control charge transport. While other conjugated polymers are very rigid, the molecular structure of P3AT allows for two different planar conformations and a significant degree of torsion at room temperature. It is unclear, however, how their chain shape depends on variables such as sidechain chemistry or regioregularity, both of which are key aspects in the molecular design of organic electronics. Small angle neutron scattering from dilute polymer solutions indicates that the chains adopt a random coil geometry with a semiflexible backbone. The measured persistence length is shorter than the estimated conjugation length due to the two planar conformations that preserve conjugation but not backbone correlations. The persistence length of regioregular P3HT has been measured to be 3 nm. Changes in the regioregularity, sidechain chemistry or synthetic defects can decrease the persistence length by 60 - 70%.

### 2.1. Introduction

Delocalization of electrons along the backbone of conjugated polymers leads to their interesting electronic properties as well as the potential for substantially increased backbone stiffness. Electron delocalization favors a planar conformation between neighboring monomers and has been shown to lead to rod-like behavior and liquid crystallinity in many of these materials.<sup>1,2</sup> The flexibility of conjugated polymers controls many of their fundamental properties such as their mechanical and optoelectronic properties and also impacts phenomena such as crystallization and self-assembly behavior (micelles, block copolymers, etc.).<sup>3</sup> Classical polymers have very flexible backbones because many possible configurations are populated, however, intermolecular interactions such as sterics, hydrogen bonding and columbic interactions can also affect chain stiffness. The chain shape of conjugated polymers has important ramifications on charge transport along the chain axis and structural defects such as hairpin turns have been shown to represent breaks in conjugation.<sup>4</sup> In bulk materials, intermolecular packing can further impact intermolecular charge transport, excited state energetics and crystallization.<sup>5,6</sup> Delocalization of electrons along the backbone, in combination with steric interactions, lead to a unique mechanism affecting the chain shape in conjugated polymers and are relevant in understanding the complex morphological behavior (phase separation, crystallization, and molecular orientation) observed in optoelectronic devices such as organic photovoltaics, light emitting diodes and transistors.

Even though conjugated polymers tend to be relatively rigid, there exists a wide range of observed persistence lengths for conjugated polymers due primarily to

differences in: sterics caused primarily by sidechain interactions, conjugation lengths due to different degrees of electronic delocalization, and geometric factors such as the bond angles between monomers. The chain shape of conjugated polymers has primarily been studied using dilute solution light scattering. For example, poly(2-methoxy-5-(2'-ethylhexyloxy)-p-phenylene vinylene) (MEH-PPV) has a conjugated backbone and exhibits a relatively high degree of stiffness with a measured persistence length around 6 nm.<sup>7,8</sup> After the addition of large bulky sidegroups, the persistence length of PPV derivatives can be increased to over 40 nm by sterically favoring the planar trans conformation.<sup>7,8</sup> Optical single molecule spectroscopy of conjugated polymers, pioneered by Barbara and coworkers, has also been used extensively to understand the conjugation length and arrangement of chromophores in conjugated polymers by dispersing a dilute concentration of polymers in a polymer matrix such as PMMA.<sup>4</sup> While this technique does not directly measure the chain shape of a polymer, it gives information about the orientation of chromophores within a molecule and can be used to model the polymer chain shape. Work done on MEH-PPV has shown that these chains appear to be semi-flexible however do not follow a random walk and instead aggregate upon themselves due to the strong intramolecular  $\pi$ -stacking interactions.<sup>9</sup> In the case of MEH-PPV, it has been suggested that the flexibility of these materials has been shown to be related to structural defects such as hairpin turns and chemical defects which cause a break in conjugation.<sup>10</sup> Similar to MEH-PPV, polyfluorene (PF) has a long persistence length of around 7 nm measured in dilute solution by light scattering.<sup>11</sup> The persistence length of PF is also limited by a combination of finite backbone torsion and non-zero bond angles between monomers leading to a polymer which is relatively stiff but would still undergoes a random walk at high molecular weights. Poly(para-phenylene) (PPP) is unique because this conjugated polymer has a single bond angle of  $0^\circ$  between monomers which leads to a long persistence length of around 28 nm limited by static bending of the polymer backbone even though there is significant backbone torsion and it has a shorter conjugation length.<sup>12-14</sup> While conjugated polymers tend to have longer persistence lengths than most polymers, they still are not as stiff as many rod-like polymers such as some biopolymers or polymers with bulky sidechains. For example, DNA has been shown to have a persistence length of around 50-70 nm.<sup>15</sup> Conjugated polymers typically do not achieve comparable persistence lengths to extremely stiff polymers such as DNA because there are typically two possible conformations (ex: cis/trans) that preserve planarity and a significant amount of backbone torsion often exists since electron delocalization can actually tolerate some torsion along the backbone without being significantly affected.

Poly(3-alkyl thiophenes) (P3ATs) represent one of the most studied classes of conjugated polymers due to their high hole mobility and a relatively low bandgap, however, it is still unclear how rigid these polymers are and how the persistence length of these polymers is affected by factors such as sidechain chemistry or regioregularity. P3ATs have two possible monomer conformations shown in Figure 2.1. Both the anti and syn conformations preserve conjugation along the backbone by retaining the planar geometry however the anti conformation is the lower energy state and is the only conformation that would produce a rigid polymer backbone.<sup>16</sup> Without any torsion between monomers, the backbone geometry would resemble a two dimensional random

walk from a distribution of anti and syn planar conformations. Flexibility of the P3AT backbone, which leads to a three dimensional polymer structure, comes from a distribution of syn and anti conformations as well as a finite amount of torsion between monomers.

The degree of flexibility in P3ATs has been discussed in many studies, however, there exist a wide range of estimates for the persistence length and it is unclear what influences the chain shape of these materials. Furthermore, this wide range of persistence lengths makes it unclear whether P3ATs should be thought of as being a rod-like polymer. The first studies into the chain shape of P3ATs were carried out by Aime et al. on poly(3-butyl thiophene) (P3BT) in nitrobenzene using small angle neutron scattering.<sup>17, 18</sup> They found that the persistence length of P3BT was around 5.5 nm however there was scattering at low angles due to chain aggregation which may have obscured the single polymer chain form factor. They also measured an increase in the persistence length to over 85 nm when doping with  $\text{NOSbF}_6$  attributed to increased electron delocalization. Heffner et al. used static light scattering and dilute solution viscometry to look at poly(3-hexyl thiophene) (P3HT) and poly(3-octyl thiophene) (P3OT) in THF and found that the persistence length of these materials was around 2.1 – 2.4 nm. These initial studies used  $\text{FeCl}_3$  catalyzed polymerizations which results in polymers with high polydispersity and relatively low regioregularity and may contain coupling defects along the backbone and catalytic impurities which may dope the polymer chain.<sup>19, 20</sup> After the development of new synthetic techniques, the chain shape of regioregular P3HT was first studied by Yamamoto et al. using static light scattering where it was suggested that the persistence length may be as high as 30 nm.<sup>21</sup> Single chain spectroscopy of dilute P3HT mixtures in a PMMA film showed that the chromophores in regiorandom P3HT are more disordered than regioregular P3HT suggesting that the chain shape may be more flexible for regiorandom P3HT.<sup>22</sup> There have also been theoretical predictions of the persistence length of P3ATs using a molecular dynamics simulations which predicted persistence lengths as high as 86 nm but showed a large decrease of around 25% for regiorandom polymers.<sup>23</sup> Conversely, recent work by on regioregular poly(3-(2'-ethyl)-hexylthiophene) (P3EHT) block copolymers in the disordered melt using small angle x-ray scattering combined with mean field random phase approximation theory estimated the persistence length to be around 6 nm.<sup>24</sup> There are several explanations for such a wide range of observed values including differing synthesis techniques, solvents, sidechain chemistry, regioregularity and measuring techniques. For example, strong light absorption over a wide range of wavelengths can make static light scattering difficult in polythiophenes. It is also important to note that P3ATs have strong intermolecular interactions which can cause polymer chain aggregation, even at low concentrations, which can make it difficult to extract single chain statistics. Studying the chain shape using small angle neutron scattering for polythiophenes in the melt, as well as other rod-like or conjugated polymer systems, has been difficult because these polymers suffer from a large amount of low-q scattering caused by long range correlations which overwhelms single chain scattering.<sup>25</sup>

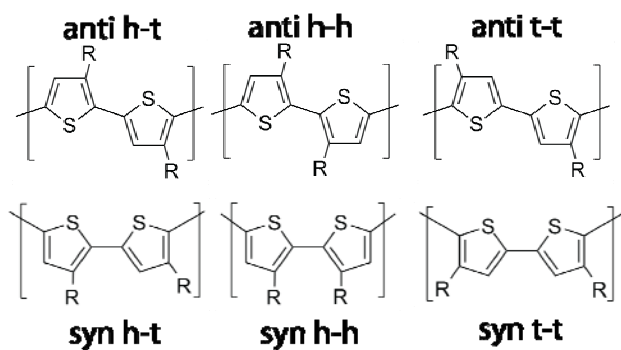


**Figure 2.1. Polythiophene conformations and regioregularity**

Polythiophene monomers can adopt two primary conformations. The anti conformation is energetically preferred to the syn conformation. Regioregularity, which is controlled synthetically, is associated with the position of the sidechain on thiophene rings of adjacent monomers and influences the possible backbone conformations. The head-to-tail coupling (h-t) produces less steric hindrance than the head-to-head (h-h) and tail-to-tail (t-t) couplings.

Previous studies have shown that there is a wide range of measured and predicted persistence lengths for P3ATs. This may be caused by effects from regioregularity, synthetic defects, sidechains as well as experimental difficulties measuring the persistence length. Polymer synthesized through  $\text{FeCl}_3$  catalyzed routes or polymer with low regioregularity may have drastically different persistence lengths because of backbone defects or increased backbone torsion compared to the high regioregularity polymers synthesized today using the GRIM and Rieke methods. The sidechain may also affect the polymer chain shape of P3ATs. For PPV derivatives a bulky sidechain leads to a stiffer polymer because it favors the trans conformation however in P3ATs as the sidechain increases in size, the backbone torsion may also increase leading to a less rigid backbone. In this work, we set out to systematically investigate the effect of regioregularity, sidechain chemistry, synthetic route, solvent choice, and temperature on the chain shape of P3ATs. Neutron scattering experiments show P3ATs follow random coil statistics, and while the backbone conjugation does impart some degree of stiffness, the measured persistence lengths are in the range where these materials should be thought of as semiflexible and not rod-like.

## 2.2. Experimental Section

### 2.2.1 Materials

Chemicals were purchased from Sigma-Aldrich and used without further purification unless otherwise noted. Poly(3-hexyl thiophene) (P3HT), poly(3-(2'-ethyl)-hexylthiophene) (P3EHT) and poly(3-dodecylthiophene) (P3DDT) were synthesized by standard procedures from literature via grignard metathesis polymerized (GRIM).<sup>26, 27</sup> P3HT and P3EHT were also synthesized by standard procedures from literature via a  $\text{FeCl}_3$  catalyzed polymerization.<sup>28</sup> All monomers were prepared according to standard procedures. Polymers were precipitated in methanol, purified by Soxhlet extraction, dried and stored under vacuum away from light. Regiorandom P3HT and Rieke P3DDT were purchased from Sigma-Aldrich.

A Malvern triple detector gel permeation chromatography system was used to measure the absolute molecular weight and absolute molecular weight distribution of these polymers. A representative absolute molecular weight distribution is shown in Figure 2.2. This technique utilizes an inline refractive index detector, viscometer and low angle light scattering detector (Malvern TDA 302 detector array) to access the absolute molecular weight distribution of a polymer. A monodisperse polystyrene standard is used to calibrate the detector responses of the system. THF was used as the mobile phase at a flow rate of  $1 \text{ mL min}^{-1}$ . A combination of Waters Styragel HR2, HR4 and two HR3 columns and polystyrene standards from Polymer Source were used.

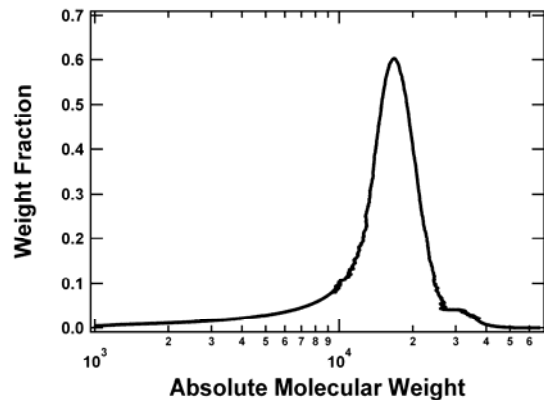


**Figure 2.2. P3HT molecular weight distribution**

Absolute molecular weight distribution of P3HT-1 obtained by triple detector GPC.

**Table 2.1. Characteristics of Polymer Samples**

<i>Polymer</i>	<i>Synthetic Route</i>	$M_N^a$ (kg/mol)	$PDI^a$	<i>Regioregularity (%)</i>
P3HT-1	GRIM	15.1	1.17	>97%
P3HT-2	GRIM	7.4	1.08	>97%
P3HT-3	Regiorandom	40.7	1.92	58%
P3HT-4	FeCl <sub>3</sub> Oxidation	63.9	2.42	79%
P3EHT-1	GRIM	10.0	1.13	>97%
P3EHT-2	GRIM	10.2	1.24	>97%
P3EHT-3	GRIM	18.4	1.44	>97%
P3EHT-4	GRIM	4.8	1.07	>97%
P3EHT-5	GRIM	20.1	1.33	>97%
P3EHT-6	GRIM	12.1	1.35	>96%
P3EHT-7	FeCl <sub>3</sub> Oxidation	38.0	1.90	80%
P3DDT-1	GRIM	22.9	1.32	>96%
P3DDT-2	GRIM	32.0	1.34	>96%
P3DDT-3	Rieke	33.4	1.57	>96%

<sup>a</sup>Based on the absolute molecular weight distribution measured by triple detector GPC

$^1\text{H}$  NMR spectra were measured on a Bruker AVQ-400 spectrometer using deuterated chloroform solutions. Molecular weights were confirmed by end group analysis from the  $^1\text{H}$  NMR spectra. NMR was also used to confirm the chemical composition of the final product and to calculate the polymer regioregularity. Due to signal-to-noise limitations and peak broadness it is difficult to ascertain differences between samples with very high degree of regioregularity. The density of these polymers was measured using a density gradient column (glycerin/isopropanol) to estimate the monomer volume. The monomer volume of P3HT was estimated to be  $0.300\text{ nm}^3$ , P3EHT was estimated to be  $0.388\text{ nm}^3$  and P3DDT was estimated to be  $0.466\text{ nm}^3$ . A reference volume of  $0.1\text{ nm}^3$  was assumed for statistical segment length calculations common with convention. UV-Vis absorbance measurements were made with Varian Cary 50 instrument between 350 and 900 nm on dilute polymer solutions in dichlorobenzene.

### 2.2.2 Small Angle Neutron Scattering

Small angle neutron scattering (SANS) studies were conducted at the extended Q-range small-angle neutron scattering diffractometer (EQ-SANS BL-6) line at the Spallation Neutron Source (SNS) located at Oak Ridge National Laboratory (ORNL). The measured intensity was corrected for detector sensitivity and the scattering contribution from the empty cells, and placed on an absolute scale using a direct beam measurement. Samples were dissolved at a concentration of  $2 - 5\text{ mg mL}^{-1}$  in deuterated solvent and stirred overnight. A range of concentrations were measured to confirm the absence of significant interchain interactions which would cause low  $q$  scattering. Titanium sample cells with quartz windows and a 1mm path length were used.

### 2.2.3 SANS Intensity Modeling

The scattering contrast in SANS originates from different scattering cross-sections of the deuterated solvent and the non-deuterated polymer chains. By operating in the dilute polymer limit where polymer chains are not interacting, SANS can be used to extract information related to correlations along a single polymer chain. Most polymer chains can be estimated to undergo a random walk and follow Gaussian chain statistics. For a random coil, the Debye function can be used to model the scattering of a single chain:

$$g(u) = \frac{2}{u^2} (u - 1 + e^{-u}) \quad (1)$$

where  $u$  is given by:

$$u = q^2 R_g^2 = q^2 \left( \frac{b^2 N}{6} \right) \quad (2)$$

and  $R_g$  is the radius of gyration of the polymer chain.<sup>29</sup> For a polymer undergoing a random walk,  $R_g$  can be replaced with an expression including  $b$ , the statistical segment length, and  $N$  which is the number of monomers in the chain. Both the statistical segment length ( $b$ ) and the degree of polymerization ( $N$ ) are calculated using the reference volume of  $0.1\text{ nm}^3$ . This equation is derived to correspond to monodisperse

polymer chains and for the remainder of this paper will be referred to as the standard Debye model.

The scattering intensity of a polymer can be fit using the following equation:

$$I(q) = Kg(q) + I_{inc} \quad (3)$$

where K is a scaling factor, g(q) is the form factor of a single chain and  $I_{inc}$  is the incoherent scattering intensity which is assumed independent of q. In theory, the scaling factor can be predicted from the scattering intensity, concentration and polymer molecular weight. However, in this analysis K has been treated as a fitting parameter to account for any errors in the absolute intensity calibration and because the amorphous density of P3ATs is not well known. There are only three fitting parameters in the resulting model: the incoherent background scattering intensity ( $I_{inc}$ ), the scaling factor (K), and the statistical segment length of the polymer (b) if the polymer molecule weight is known.

The standard Debye model has been used successfully despite the finite polydispersity of most polymers. If the molecular weight distribution follows an ideal distribution, the standard Debye model can be analytically corrected<sup>30</sup> however often molecular weight distributions are non-ideal and can not be represented by a simple function. To correct the standard Debye model for the effects of polydispersity, it is possible to numerically integrate the single chain scattering over the entire molecular weight distribution using the following function:

$$I(q) = K \int_{N=0}^{N=\infty} w_i g(u_{N_i}) N_i dN_i + I_{inc} \quad (4)$$

where  $w_i$  is the weight fraction at a particular molecular and  $N_i$  is the degree of polymerization and  $g(u_{N_i})$  is the standard Debye model evaluated at  $N_i$ .<sup>31</sup> The absolute molecular weight distribution is characterized using triple detector GPC as shown in Figure 2.2. Similar to the standard Debye model, K and  $I_{inc}$  have been treated as fitting parameters. The model in Equation 4 will be referred to as the polydispersity corrected Debye model.

While the Debye model for Gaussian coils should fit well for high polymers, deviations occur when the polymer contour length is less than or roughly equal to the persistence length. This occurs for low molecular weight polymers or relatively rigid polymers. The Debye model is also unable to fit data at high q values when the length scale probed begins to behave rod-like. The worm-like chain model is able to account for these effects and for this work the approximate form for single chain scattering formulated by Sharp and Bloomfield is used:

$$g(u) = \frac{2}{u^2} (u - 1 + e^{-u}) + \frac{2}{5q^2 L^2} [4u - 11ue^{-u} + 7(1 - e^{-u})] \quad (5)$$

where L is the contour length of the chain ( $L = nl_0$ , where n is the number of thiophene monomers per chain and  $l_0$  is the contour length of each thiophene monomer).<sup>32</sup> It is important to note that n is the actual number of thiophene rings per chain and is not normalized by a reference volume. For P3ATs,  $l_0$  corresponds to the length of one monomer and is taken to be 0.39 nm, confirmed by theory and crystallography.<sup>18,33</sup> For



the wormlike chain model there is also a more complex form for  $R_g$  leading to the following expression:

$$u = q^2 R_g^2 = q^2 \left[ \frac{Ll_p}{3} - l_p + \frac{2l_p^3}{L} \left( 1 - \frac{l_p}{L} + \frac{l_p}{L} e^{-L/l_p} \right) \right] \quad (6)$$

where  $l_p$  is the persistence length.<sup>34</sup> This expression can be corrected for finite polydispersity similar to the polydispersity corrected Debye model shown above by integrating over the molecular weight distribution in a similar manner with the following equation.

$$I(q) = K \int_{n=0}^{n=\infty} w_i g(u_{n_i}) n_i dn_i + I_{inc} \quad (7)$$

While the form of this equation is more complicated, it still contains only three fitting parameter which is the same number as in the standard Debye model. Random error in the measured scattering intensity and molecular weight distribution has also been propagated through this analysis.

While both the statistical segment length and persistence length quantify the polymer chain shape, they give different values and fundamentally describe slightly different but related quantities. The statistical segment length is derived to describe the distance between uncorrelated random walks within a Gaussian coil. The persistence length describes the decay in directional correlations between monomers along the polymer backbone. The statistical segment length is normalized to the monomer volume of the polymer and a chosen reference volume. This makes it useful when comparing between polymers of different chemistry, however, the absolute statistical segment length depends on the chosen reference volume. The monomer volume also depends on the density of the amorphous polymer which has been estimated and is a source of error. In comparison, the persistence length depends on the monomer length which is well known and ties the value for the persistence length directly to the length over which the backbone is rigid, an unambiguous physical parameter. The rest of the discussion will therefore focus primarily on the use of the wormlike chain model and the derived persistence length from this model. It is important to note that it is possible to easily convert between the persistence length and statistical segment length when the polymer behaves as a random coil ( $L \gg l_p$ ) because the expression for  $R_g$  of a wormlike chain collapses to:

$$R_g^2 = \frac{1}{3} Ll_p = \frac{1}{3} l_o l_p n \quad (8)$$

and through algebraic manipulation the following expression can be used to convert between  $l_p$  and  $b$ :

$$l_p = \frac{v_m}{v_r} \frac{b^2}{2l_o} \quad (9)$$

where  $v_m$  is the monomer volume and  $v_r$  is the reference volume (chosen to be  $0.1 \text{ nm}^3$ ). Therefore throughout the text both the persistence length and statistical segment length are provided for each model however a gaussian coil is assumed when converting between persistence length and statistical segment length. Since the contour length of the

polymers studied is always much longer than the persistence length, this assumption should be valid.

The characteristic ratio is also a useful parameter in describing the chain shape of these materials and is defined as:

$$C_{\infty} = \frac{\langle R^2 \rangle}{l_o^2 n} = \frac{v_m b^2}{v_r l_o^2} = \frac{2l_p}{l_o} \quad (10)$$

for a Gaussian coil. The characteristic ratio represents the size of a polymer chain, normalized by the size of the polymer chain if each monomer underwent a random walk and therefore can be thought of as the actual polymer chain size compared to the smallest possible size it could occupy if each monomer underwent a new step in a random walk.

### 2.3. Discussion

Representative small angle neutron scattering curves of P3HT in dichlorobenzene (DCB) are shown in Figure 2.3. All polymer samples show similar scattering patterns with slight variations due to changes in molecular weight and persistence length. The scattering intensity scales as  $q^{-1.96 \pm 0.08}$  which indicates that the polymer chain adopts a random coil geometry and is consistent with the conformation of a polymer chain in a theta solvent or a polymer melt. If P3ATs behaved rod-like, the intensity should scale as  $q^{-1}$ . For a two-dimensional random walk the porod scaling is  $q^{-4/3}$ . If DCB was a good solvent and swelled a Gaussian polymer chain, the intensity should scale as  $q^{-5/3}$ . Conversely, if DCB was a poor solvent causing the polymer chains to collapse, the intensity would instead scale as  $q^{-3}$ . The intensity scaling remains  $q^{-2}$  for all solvent and polymer combinations studied and the Debye model, derived for a Gaussian coil, can be fit to a wide region of the scattering pattern. The Kratky plot in Figure 2.3. also shows a scattering pattern consistent with a Gaussian coil conformation. At high  $q$  values the intensity should scale like a rigid rod (as  $q^{-1}$ ) because at high  $q$ , length scales less than the persistence length are being probed. Unfortunately the scattering intensity at high  $q$  was insufficient to analyze due to the low polymer concentration, low scattering contrast and relatively low molecular weight used in these studies.

Polythiophenes (and other conjugated polymers or rod-like polymers) have strong intramolecular interactions and poor solubility often leading to an upturn in scattering at low  $q$  values.<sup>17, 18</sup> This can obscure the scattering from isolated chains and makes it difficult to extract useful chain shape statistics. By using reasonably low molecular weight polymers, low concentrations, and solvents with high P3AT solubility the amount of low- $q$  scattering has been decreased and it is only apparent at the lowest  $q$  values ( $< 0.008 \text{ nm}^{-1}$ ). For these systems it is much more reliable to fit a model to the entire data set than to try to use Guinier's law at low  $q$  to extract the polymer radius of gyration. Guinier analysis does give radius of gyrations consistent with our findings, however since it can be difficult to choose the relevant  $q$ -range this data has not been included.

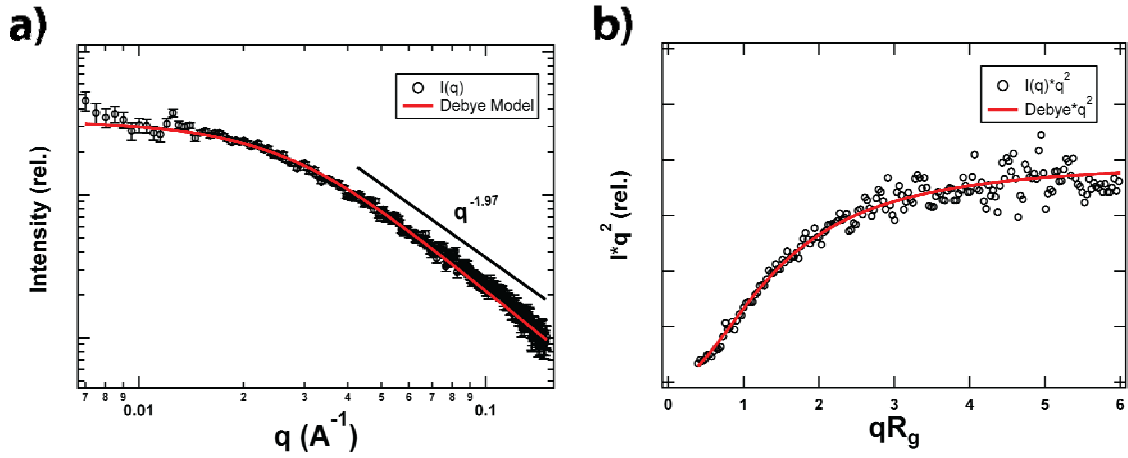


**Figure 2.3. Scattering intensity from P3HT**

a) Small angle neutron scattering (SANS) of P3HT-1 (after incoherent scattering subtraction) in dichlorobenzene shows that P3ATs adopt a random coil chain shape with a scaling of  $I \approx q^{-2}$  over a large region corresponding to a gaussian coil. b) A Kratky plot shows the typical plateau which also indicates a random coil which can be fit using the Debye model.

The standard Debye model assumes monodisperse polymer chains which is a sufficient assumption for P3ATs polymerized using GRIM with polydispersities ranging from 1.05-1.3 for most polymers. As shown in Figure 2.4 and Table 2.2, all models used fit the data quite well however correcting for polydispersity causes subtle changes in the predicted intensity because the range of molecular weights broadens the transition between the low  $q$  plateau ( $\sim 0.01$ - $0.04 \text{ \AA}^{-1}$ ) and the random coil Porod scattering regime at higher  $q$  ( $\sim 0.1$ - $0.2 \text{ \AA}^{-1}$ ). The wormlike chain model results in the highest quality fit because it is able to account for scattering at high  $q$  ( $\sim 0.2 \text{ \AA}^{-1}$ ) by modeling the rod-like nature of the polymer backbone at short length scales. Even though the wormlike chain model fits slightly better than the Debye model, they both provide equally valid information about the polymer chain shape because the Debye model is not derived to fit at high  $q$ . Since the contour length of these polymers is much greater than the persistence length (or statistical segment length), these polymers behave as random coils leading to similar results between the PDI corrected Debye and Worm-like Chain models. Therefore either model can be used to describe the chain shape of these polymers. For the remainder of the discussion, the PDI corrected Worm-like chain model will be used because the model offers more reliable fits since it operates over a larger range of length scales.

Table 2.2 shows that the solvent choice between DCB and toluene does not significantly affect the chain shape. While the solubility of P3EHT and P3DDT is higher in DCB than toluene, both solvents have high polymer solubility and the difference in solvent quality may not be enough to change the chain shape of these materials. The Porod intensity in DCB scales as  $q^{-2.00 \pm 0.09}$  compared to P3ATs in toluene which scale as  $q^{-1.95 \pm 0.07}$ . It is interesting that these materials maintain the same  $q^{-2}$  scaling which indicates that the polymer chains adopt a random coil and not swollen chain architecture. While dichlorobenzene is one of the best solvents that exist for these polymers, it may not have sufficiently favorable interactions to alter the chain conformation which is consistent with what is known about P3AT's strong intermolecular interactions. This is in contrast to polymers in good solvents where solvent-polymer interactions are more favorable than polymer-polymer interactions such that the chain prefers to maximize solvent-polymer contact.

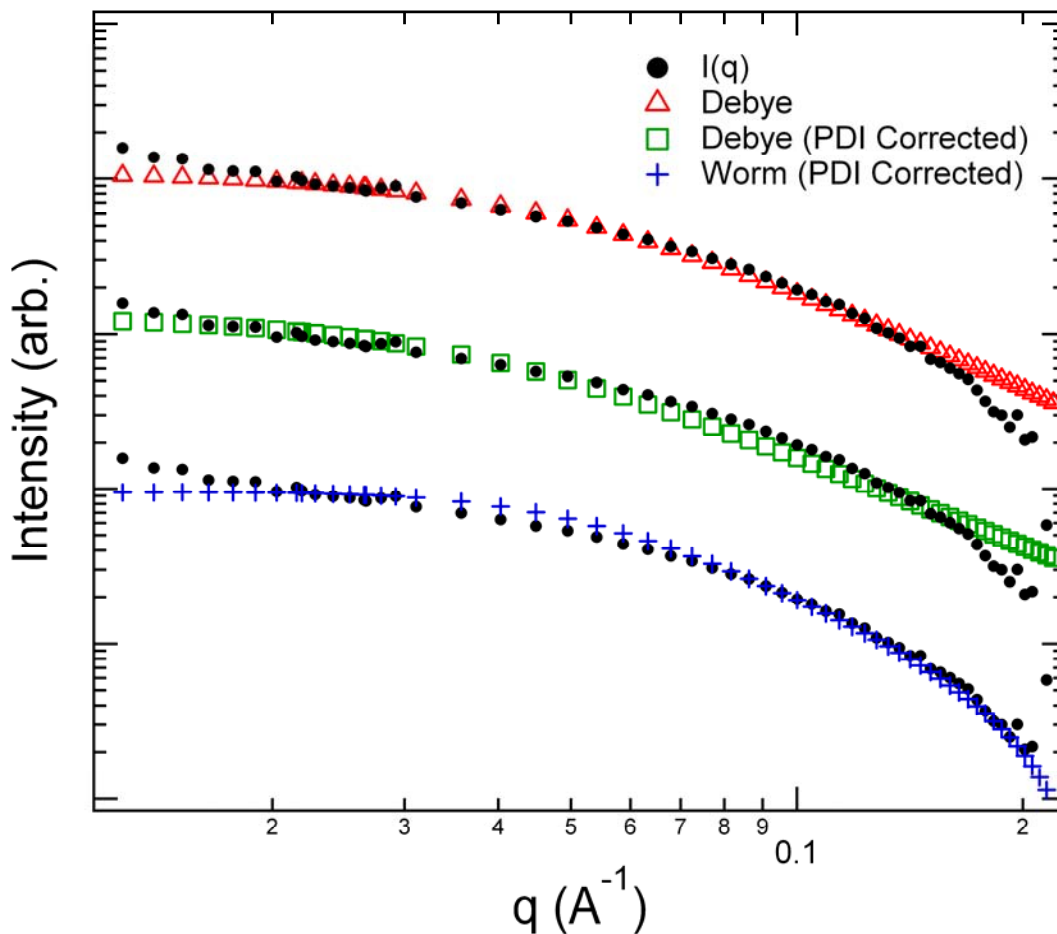


**Figure 2.4. Comparison of models for P3AT SANS**

Scattering from P3EHT-4 can be described well using any of the above models however the worm-like chain model is more consistent at high  $q$ -values where the length scale approaches the persistence length and the polymer no longer behaves like a random coil. Curves are offset to help visualize the quality of fits.

**Table 2.2. Model Comparison of chain shape parameters**

<i>Polymer</i>	<i>Solvent</i>	<i>Debye</i>		<i>Worm-like Chain</i>		
		<i>Debye</i>	<i>Debye</i>	<i>PDI Corrected</i>		
		$b$	$b$	$l_p$	$b$	$l_p$
		(nm)	(nm)	(nm)	(nm)	(nm)
P3HT	DCB	$0.8 \pm 0.1$	$0.9 \pm 0.1$	$3.0 \pm 0.3$	$0.9 \pm 0.5$	$2.9 \pm 0.1$
P3EHT	DCB	$0.8 \pm 0.1$	$0.8 \pm 0.1$	$2.9 \pm 0.2$	$0.8 \pm 0.6$	$3.0 \pm 0.1$
P3EHT	Toluene	$1.2 \pm 0.1$	$0.8 \pm 0.1$	$3.1 \pm 0.2$	$0.9 \pm 0.4$	$3.3 \pm 0.2$
P3DDT	DCB	$0.7 \pm 0.1$	$0.5 \pm 0.1$	$1.1 \pm 0.1$	$0.5 \pm 0.4$	$1.6 \pm 0.1$
P3DDT	Toluene	$0.8 \pm 0.1$	$0.6 \pm 0.1$	$1.4 \pm 0.1$	$0.5 \pm 0.8$	$1.5 \pm 0.1$

**Table 2.3. Comparison of chain shape parameters for different polymers and solvent conditions**

<i>Polymer</i>	<i>Synthetic Route</i>	<i>Solvent</i>	$l_p$ (nm)	$C_\infty$
P3HT	GRIM	DCB	$2.9 \pm 0.1$	$12.1 \pm 1.0$
P3EHT	GRIM	DCB	$3.0 \pm 0.1$	$13.3 \pm 1.0$
P3EHT	GRIM	Toluene	$3.3 \pm 0.2$	$13.4 \pm 1.3$
P3DDT	GRIM	DCB	$1.6 \pm 0.1$	$8.0 \pm 1.3$
P3DDT	GRIM	Toluene	$1.5 \pm 0.1$	$7.2 \pm 1.2$
P3DDT	Rieke	Toluene	$1.5 \pm 0.1$	$7.3 \pm 1.2$
P3HT	Regiorandom Coupling	DCB	$0.9 \pm 0.1$	$4.7 \pm 0.8$
P3HT	Regiorandom Coupling	Toluene	$1.1 \pm 0.4$	$5.4 \pm 2.0$
P3HT	FeCl <sub>3</sub> Oxidation	DCB	$1.4 \pm 0.1$	$7.0 \pm 1.0$
P3EHT	FeCl <sub>3</sub> Oxidation	DCB	$0.8 \pm 0.1$	$3.8 \pm 0.6$

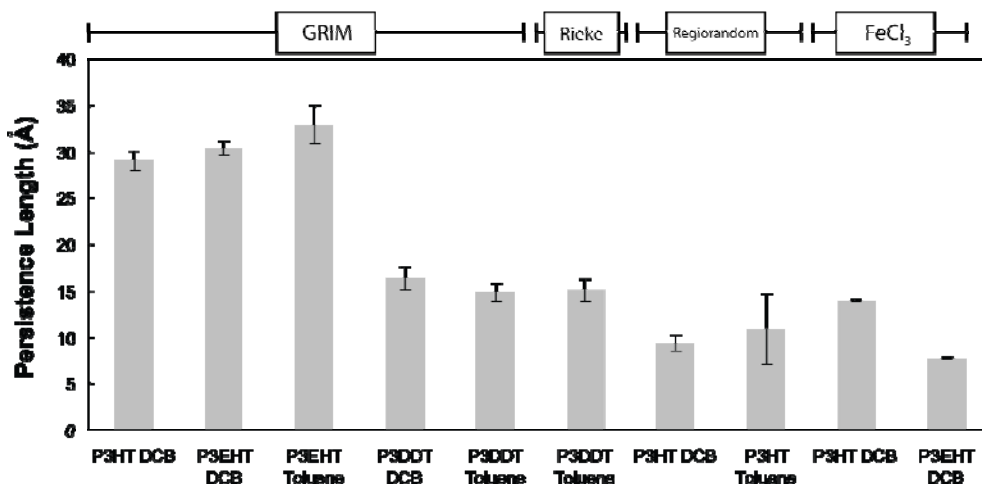


**Figure 2.5. Persistence length of P3ATs**

Comparison of the persistence length from the worm-like chain model shows that P3AT chain shape appears to be a function of sidechain chemistry and regioregularity for the polymers examined.

As seen in Table 2.3 and Figure 2.5, the persistence length of regioregular P3HT and P3EHT is  $3.0 \pm 0.1$  nm. This is significantly longer than the persistence length of a flexible polymer such as polystyrene ( $l_p = 0.92$  nm)<sup>35</sup> or polyisoprene ( $l_p = 0.43$  nm)<sup>36</sup>. The characteristic ratio of these materials is also relatively high ( $\sim 12-14$ ), much greater than polyethylene ( $\sim 6.8$ ), but only slightly more than the characteristic ratio for polystyrene ( $\sim 10.8$ ).<sup>37</sup> It does not appear to affect the chain shape whether P3ATs are synthesized by GRIM or Rieke synthetic routes since both of these methods result in high regioregularity polymers with little to no defects.

There are three major factors that seem to affect the chain shape in these materials: sidechain chemistry, regioregularity and possibly synthetic defects along the backbone. There is a large decrease ( $\sim 50\%$ ) in the persistence length between P3HT or P3EHT and P3DDT. This is likely due to steric interactions between sidechains that causes either backbone torsion and/or a different population between the syn and anti conformations. From previous theoretical studies short sidechains should not dramatically affect the energetics associated with backbone conformations however long sidechains may have an effect on the polymer chain shape.<sup>38, 39</sup> UV-vis absorbance spectra can be used to look at the conjugation length of these materials to try to elucidate which of these effects is more important in these materials. Backbone torsion will result in an increase in the optical band gap (shorter conjugation length) and decreased persistence length. Both the syn and anti conformations are planar and these conformations should maintain conjugation along the backbone so a change in the distribution of syn and anti states can alter the persistence length without affecting the conjugation length. The UV-vis spectrum, shown in Figure 2.8, indicates that P3DDT possesses a conjugation length nearly equal to P3HT. This indicates that the long sidechain may not be causing increased backbone torsion in P3DDT. Instead, the fraction of monomers in the syn conformation may be increased which would lower the persistence length while maintaining a constant conjugation length. The syn conformation may be lower in energy for P3DDT than in P3HT or P3EHT because the syn conformation splays the sidechains apart, possibly increasing the volume of which a sidechain can occupy for very long sidechains. For short sidechains, the syn conformation has more steric hindrances than the anti conformation because the sidechains are closer together and it is the higher energy conformation. Conversely, the conjugation length of P3EHT is slightly shorter than that of P3HT despite the fact that persistence length is unchanged. This indicates that the branched sidechain close to the backbone may lead to a slight increase in backbone torsion. The steric interactions in P3EHT occur close to the polymer backbone and may slightly favor the anti conformation because it is less sterically hindered than the syn conformation for a short bulky sidechain. It is possible that P3EHT could have a slightly higher population of anti conformations but this effect may be offset by the slight increase in backbone torsion resulting in a relatively unchanged persistence length compared to P3HT.

Regioregularity also was observed to dramatically decrease the persistence length of these materials. The persistence length of P3HT was decreased around 67% between highly regioregular P3HT and regiorandom P3HT. Regioregularity has been known to have strong effects on interchain interactions and chain packing affecting properties such

as crystallinity.<sup>5</sup> It also should affect the intrachain interactions by introducing large steric hindrances, possibly causing backbone torsion and a different distribution of syn and anti conformations.<sup>38</sup> The conjugation length of regiorandom P3HT is the lowest of the polymers studied which may suggest that there exists a higher level of backbone torsion in these materials (Figure 2.8).

Finally, the persistence length of P3HT and P3EHT synthesized using the historically relevant FeCl<sub>3</sub> catalyzed reaction is reduced by a similar amount as regiorandom P3HT. This is slightly surprising because these polymers are around 80% regioregular and we may have expected their persistence lengths to be somewhere between that of regioregular and regiorandom P3AT. This synthesis is much less specific than the other synthetic routes studied and can result in polymers which have defects along the chain where the backbone is coupled through the 4 position rather than the 5 position on the thiophene ring.<sup>19,20</sup> These defects could lead to increased steric hindrance or larger effective bond angles consistent with the lower observed conjugation length. It also appears that the branched sidechain of P3EHT leads to a greater decrease in the persistence length than in P3HT when both are synthesized via the FeCl<sub>3</sub> synthetic route but it is unclear if this is due to a difference in intramolecular interactions caused by the sidechain or a change in defect concentration arising during the synthesis of these materials.

The chain shape of polymers can be thought of as depending on the bond angle and degree of backbone torsion between monomers. The chain shape of a polymer can be described using the freely rotating chain model assuming fixed bond angles and no restrictions on torsion angles. The persistence length for a freely rotating chain can be estimated using the following equation:

$$l_p^{FRC} = \frac{l_o}{2} C_\infty^{FRC} = \frac{l_o}{2} \left( \frac{1 - \cos \theta}{1 + \cos \theta} \right) \quad (11)$$

where  $l_o$  is the monomer length (0.39 nm) and  $\theta$  is the bond angle between monomers. For polythiophenes, the bond angle between monomers has been estimated to be 121.1°<sup>40</sup> and leads to a predicted persistence length of 0.61 nm. This estimate is very low and the error in this estimate originates from the fact that polythiophenes have two conformational states that are energetically preferred leading to a planar structure and therefore do not occupy all torsion angles equally.

Instead, the chain shape can be better described using the hindered rotation chain model which can take into account conformations of differing energetics:

$$l_p^{HRC} = \frac{l_o}{2} C_\infty^{HRC} = \frac{l_o}{2} \left( \frac{1 - \langle \cos \phi \rangle}{1 + \langle \cos \phi \rangle} \right) \left( \frac{1 - \cos \theta}{1 + \cos \theta} \right) \quad (12)$$

where  $\theta$  is the bond angle between monomers and  $\phi$  is the torsion angle of rotation about the backbone of a monomer relative to its neighbor as shown in Figure 2.6.<sup>41</sup> For the syn conformation  $\phi = 0^\circ$  and for the anti conformation  $\phi = 180^\circ$ . The energy difference between these states has been calculated theoretically to be around 0.05 eV for a bithiophene molecule.<sup>38-40</sup> To compute the average population as a function of angle, a Boltzmann distribution is assumed. If only the syn or anti conformations are allowed and



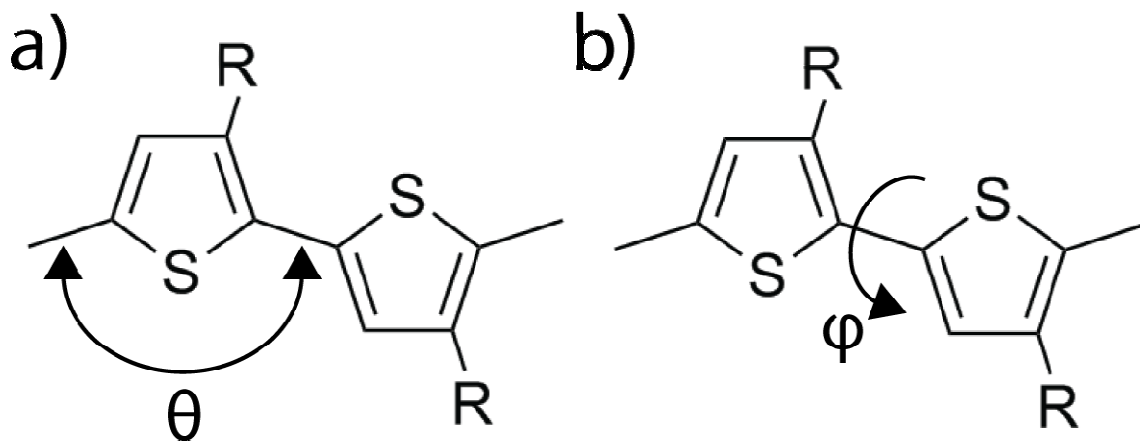


**Figure 2.6. Bond angles of P3ATs**

a) The bond angle ( $\theta$ ) between monomers has been calculated to be around  $121^\circ$  and is assumed to be relatively fixed. The torsion angle ( $\phi$ ) varies between  $0^\circ$  for the syn conformation and  $180^\circ$  for the anti conformation shown above. The torsion angle between monomers can vary from these conformations however this will affect the delocalization of electrons and impact the conjugation length.

no other backbone torsion angles are considered, 86% of the monomers are in the anti conformation at room temperature and P3AT should have a persistence length of 3.8 nm. It is unlikely that backbone torsion is absent because polythiophenes have broad energy wells centered at  $0^\circ$  and  $180^\circ$  and therefore the distribution of backbone torsion should be accounted for. The energy was assumed to scale as the degree of overlap between the p orbitals of the thiophene monomers that should scale roughly as  $\cos^2 \phi$ . The barrier height for rotation of polythiophene has been experimentally and theoretically predicted to be around 0.18 eV.<sup>38, 39, 42</sup> Using this simple model to include the effects of backbone torsion, we estimate the persistence length to be around 3.2 nm which agrees fairly well with our experimental observations. Backbone torsion is important but a smaller effect than the distribution of syn/anti conformations on the persistence length of regioregular P3ATs. Regiorandom P3ATs will have a different energy landscape because of increased steric interactions leading to shorter persistence lengths.<sup>38</sup> While this model can account for the effect of bond angles and backbone torsion between adjacent monomers, it is unable to account for long range interactions such as excluded volume or sterics which may also be important in predicting the chain shape of P3ATs.

If the amount of backbone torsion is increased in P3ATs, the persistence length and conjugation length should decrease. Thermochromism exists in P3ATs and it has been shown that the optical band gap increases as temperature increases.<sup>16, 43</sup> By increasing temperature, the amount of backbone torsion should increase and the distribution of syn and anti conformations along the backbone should also change. Since the difference in energy of the syn and anti conformations is around  $1.8k_B T$  at room temperature, the persistence length of these materials should be relatively strongly temperature-dependent. As shown in Figure 2.7, both the estimated conjugation length and the measured persistence length decrease as temperature is increased, with the measured persistence length decreasing by around 40% between  $40^\circ\text{C}$  and  $160^\circ\text{C}$ . Also presented in Figure 2.7, the decrease is remarkably well described by the hindered rotating chain using no fitting parameters. This suggests that the rotational energetics that describes a bithiophene molecule may translate to P3HT and that the sterics of the hexyl sidechain may not dramatically affect the conformations of this polymer. Instead the energetics related to the delocalization of electrons along the polymer backbone is responsible for its relatively stiff backbone. The temperature dependence of P3ATs with varying sidechains or regioregularity may be different because of the increased steric interactions. This observed temperature dependent behavior is in contrast with most polymer persistence lengths which typically are not strong functions of temperature. In traditional polymers, the difference in energy between the possible conformations is often much less than  $k_B T$  and the energy wells associated with these conformations may be much steeper than P3ATs since the energetics for many polymers are dominated by excluded volume interactions. Polystyrene, for example, shows no change in the chain shape over a similar temperature range because all possible conformations are accessible at room temperature.<sup>44</sup> Interactions between the solvent and polymer chain may also be temperature dependent causing a change in chain shape however the Porod intensity scaling in this study does not change as a function of temperature.

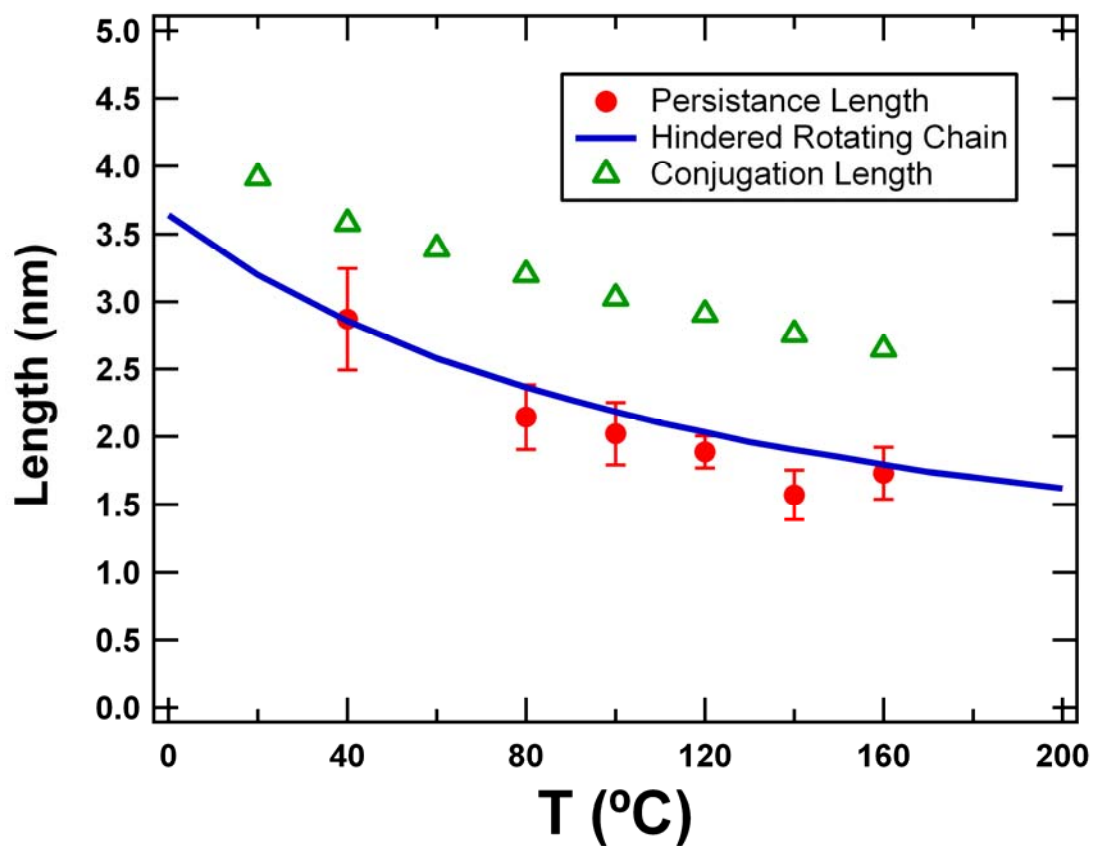


**Figure 2.7. Characteristic lengths of P3ATs as a function of temperature**

The persistence length of P3HT in DCB decreases as a function of temperature. This trend can be predicted using the hindered rotating chain model and energetic predictions from literature. The conjugation length calculated from the optical band gap<sup>12, 45, 46</sup> also decreases as a function of temperature however is always greater than the persistence length.

The decrease in the conjugation length as a function of temperature demonstrates that the backbone torsion increases with temperature. It is not known how the conjugation length is exactly related to the average torsion angle however the persistence length drops by 20% more than the conjugation length between 40°C and 160°C which shows that the persistence length is more sensitive to temperature than the conjugation length in P3HT. While it is clear that the backbone conjugation accounts for strong intramolecular interactions in P3ATs, the measured conjugation length for conjugated polymers is not necessarily a good indicator of the chain stiffness in conjugated polymers. In poly(phenylene vinylene) and polyfluorene the conjugation length is usually less than the persistence length.<sup>8, 11, 12, 47</sup> In these cases the steric interactions make one of the two possible planar conformations very unfavorable resulting in stiff polymers. The electronic structure of these polymers limits the conjugation length of these materials and is dramatically affected by chain stiffness. In P3HT, the opposite trend is observed where the average conjugation length is 3.8 nm which is around 25% higher than the measured persistence length.<sup>12, 45, 46</sup> Furthermore, P3DDT has a similar conjugation length to P3HT but it has a much shorter persistence length. These apparent disagreements can be reconciled by the fact that both the syn and anti conformations preserve the conjugation but do not maintain the spatial backbone correlations. Poly(phenylene vinylene) and polyfluorene only have one planar conformation which is populated to a large extent. This makes the chains very stiff however they possess small degrees of backbone torsion which limits the conjugation length. Polythiophenes also have backbone torsion which limits the conjugation length however have two populated planar states which preserve conjugation leading to a longer persistence length than conjugation length.

Altering the chain shape of P3ATs may have effects on their intermolecular interactions, changing their liquid crystalline behavior and affecting crystallization. In particular, the chain shape of a polymer may impact the morphology of the polymer crystal. P3ATs are well known to crystallize into a fibrillar morphology. The exact reason why P3AT chooses a fibrillic crystal geometry is unclear however the degree of backbone flexibility may allow the polymer chains to loop back into the polymer crystal or bridge fibrils separated by amorphous regions. Stiffer conjugated polymers may adopt different crystalline morphologies more reminiscent of molecular crystals because of their rigid backbones.<sup>48</sup> Increasing the rod-like behavior of P3ATs may lead to liquid crystalline behavior and improved the interchain ordering. It may be possible to increase the persistence length of polythiophenes by fusing rings along the backbone or by increasing the quinodal structure. For example, the fused thiophene rings in poly(2,5-bis(3-alkylthiophen-2-yl)thieno[3,2-b]thiophene) (PBTBT) may lead to its liquid crystalline smectic phase creating a well ordered terraced crystalline morphology which displays very high charge transport.<sup>49, 50</sup> Alternatively, it may also be useful to decrease the persistence length in order to decrease liquid crystalline interactions or improve the mechanical properties of thin films. A decrease in the persistence length may cause a decrease in the liquid crystallinity, making it more processable. Decreased interchain interactions could also change the solubility of the polymer or the solubility of small molecules such as fullerenes within the amorphous phase of the polymer. The persistence length can likely be decreased by changing the heterocycle, leading to a more aromatic electronic structure. The sidechain chemistry or regioregularity also appears to

have a large affect on the persistence length however it is unclear how large of a range the persistence length could be tuned by changing the sidechain or regioregularity and may be accompanied by a decrease in the material properties.

Interchain interactions in the melt may cause deviations from the values derived from dilute solution experiments however theoretically the persistence lengths of polymers in dilute solution should be similar to the persistence lengths calculated in the melt if the polymer solutions are near the theta solvent condition.<sup>44</sup> Efforts were made to study these materials in the melt however low-q scattering prevented analysis even for P3AT samples which were isotropic melts. It is unclear what the source of this large low-q scattering is however it must be caused by correlations over large length scales and probably has origins similar to the low-q scattering seen in rod-like or liquid crystalline polymers.<sup>25</sup>

## 2.4. Conclusions

The chain statistics of P3ATs in solution have been measured using small angle neutron scattering and modeled using the Debye model and the Worm-like chain model. These materials adopt a random coil geometry and have a semiflexible backbone with a persistence length around 3 nm for regioregular P3ATs. The sidechain chemistry, regioregularity and synthetic route can have an impact on the persistence length, decreasing it by as much as ~60 - 70%. Using the known molecular geometry and a simple model for the intramolecular interactions, the persistence length of P3ATs and temperature dependence can be predicted. The flexibility of the backbone arises from the distribution of syn and anti conformations as well as significant backbone torsion in polythiophenes. This results in a longer persistence length than the estimated conjugation length, opposite of many other common conjugated polymers.

## 2.5. Appendix

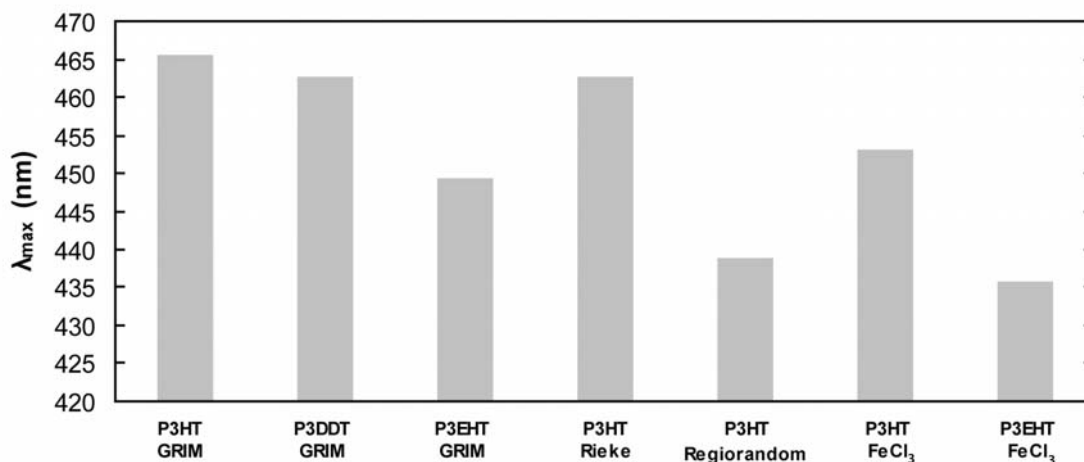


**Figure 2.8. Absorption maxima of polymers studied**

The conjugation length was estimated using correlations developed in literature using the following equation:

$$\frac{1}{n} = -2.537 \frac{1}{E_g} + 1.041 \quad (13)$$

where  $E_g$  (in eV) is the measured optical bandgap and  $n$  is the monomer conjugation number. This can be converted to conjugation length by multiplying by the monomer length. This correlation was obtained from literature and constructed for use with chloroform however UV-vis and SANS in this study used dichlorobenzene. This leads to ~2% higher measured  $\lambda_{max}$  which propagates through the above correlation to over predict the conjugation length by around 1%. When calculating the conjugation length at different temperatures, it is assumed that any changes in the optical band gap were from changes in the conjugation length however complex spectroscopic or electronic phenomena may cause deviations from this analysis.

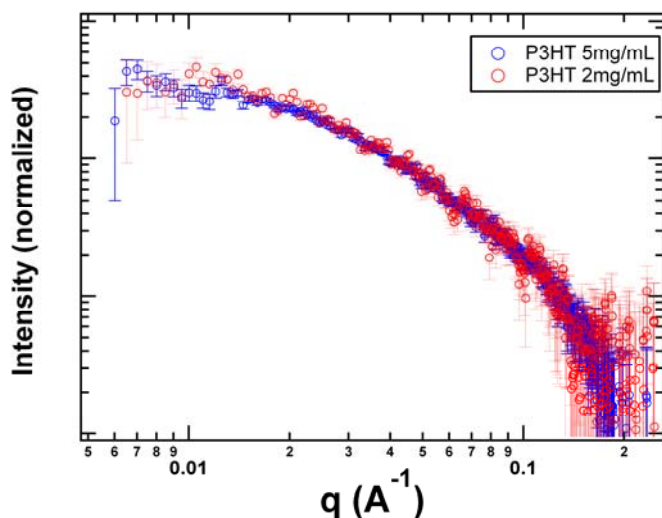


**Figure 2.9. Comparison of P3HT scattering at different concentrations**

Scattering at different concentrations using P3HT-1. No substantial difference or large amount of low  $q$  scattering is observed when the P3AT concentration is  $\leq 5$  mg/mL when normalized for concentration. Concentrations less than 2 mg/mL suffer from poor signal-to-noise and require substantially longer exposure times.

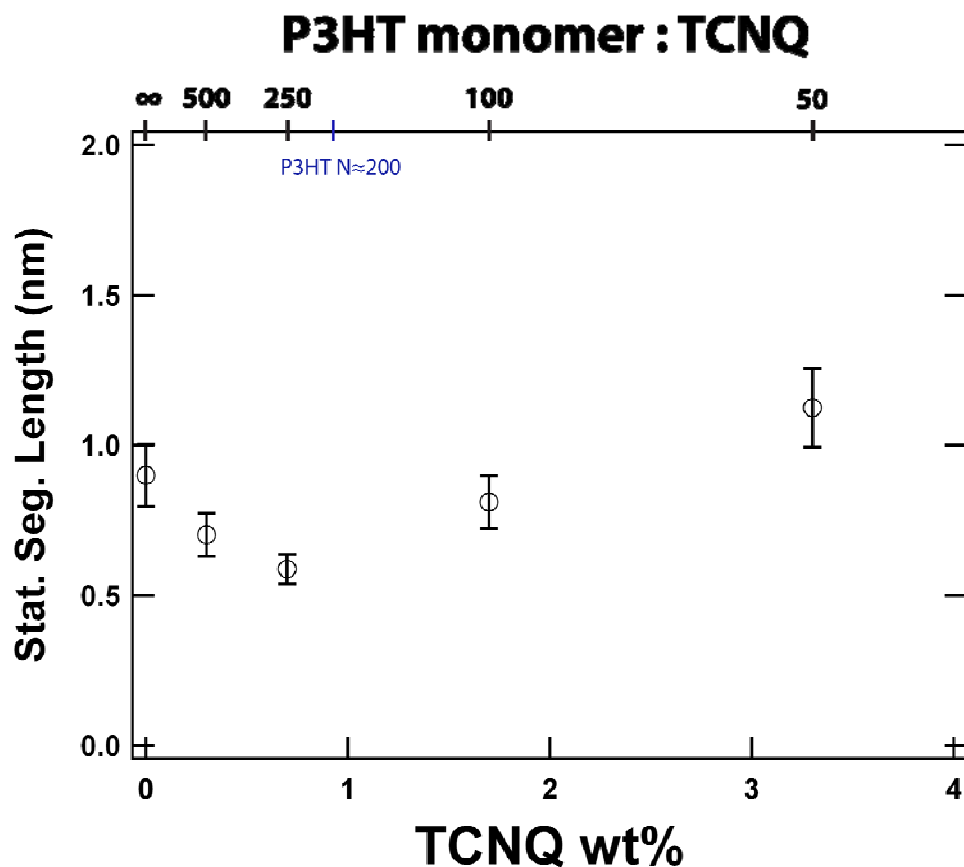


**Figure 2.10. Statistical segment length of P3HT as a function of TCNQ doping concentration**  
 TCNQ and P3HT were dissolved in DCB overnight and held at 60 °C. A slight trend of increasing statistical segment length at higher doping levels may exist however it also appears that the statistical segment length may slightly decrease at low doping levels. There may be an inversion point in this trend around the point where there is 1 TCNQ molecule per polymer chain. It is unclear what the molecular mechanism for this may be. At low doping, the dopant may cause defects along the backbone when on average there is less than one molecule per chain. At higher doping levels, polarons and bipolarons may interact, causing the chain to stiffen. Higher doping levels could not be studied because of polymer aggregation leading to increased low  $q$  scattering and an overprediction of the statistical segment length. Several doping systems were investigated and none produced aggregation-free solutions at high doping concentration. It has also been suggested that doping should lead to stiffer polymer chains<sup>51, 52</sup> and while previous work appears to show a large increase in the persistence length<sup>18</sup>, this work was unable to demonstrate a dramatic increase in the persistence length as a function of doping concentration. It is unclear how aggregation was avoided in previous studies.

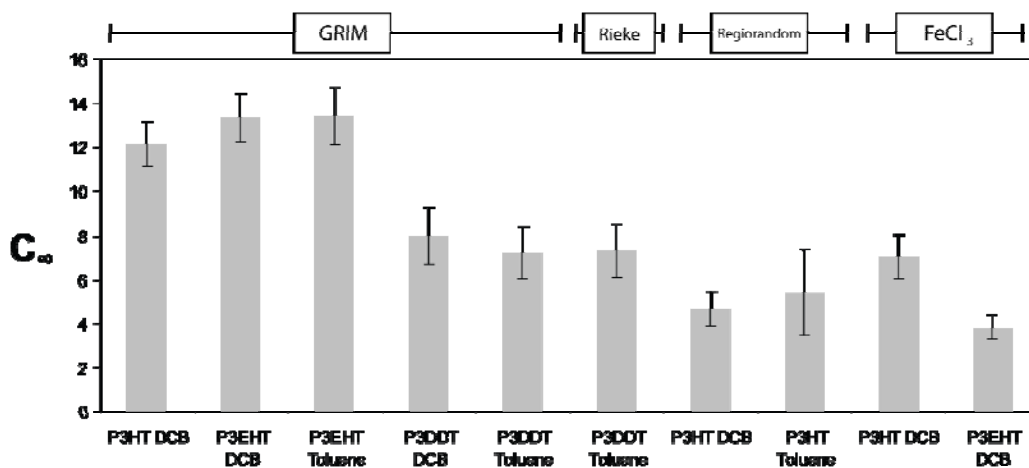


Figure 2.11. Characteristic ratio of P3ATs  
Comparison of the characteristic ratio calculated from the worm-like chain model.

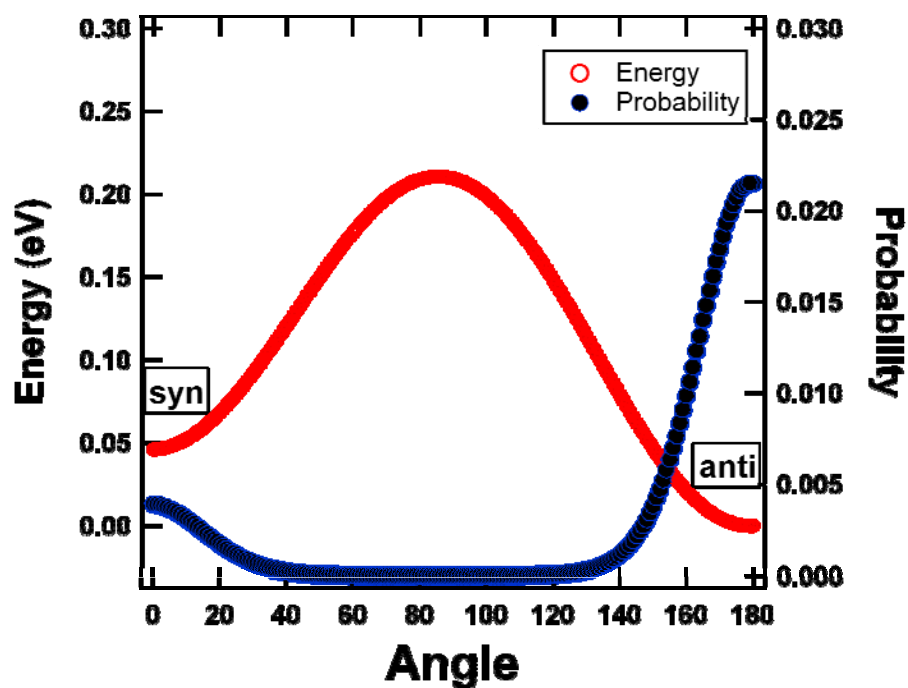


Figure 2.12. Conformation population from Boltzmann model  
Energy as a function of angle which was used in the hindered rotating chain model. Using Boltzmann statistics, the distribution of occupied conformations is included for 40 °C.



## 2.6. Acknowledgments

Research was supported through the DOE-BES LBL Thermoelectrics Program under Contract No. DE-AC02-05CH11231. A portion of this research was performed at Oak Ridge National Laboratory's Spallation Neutron Source, sponsored by the U.S. Department of Energy, Office of Basic Energy Sciences. We would like to thank Shrayesh Patel, Adrienne Rosales, Dr. Hannah Murnen, Prof. Mark Dadmun and Prof. Nitash Balsara for helpful discussions.

## 2.7. References

1. Chow, A. W.; Bitler, S. P.; Penwell, P. E.; Osborne, D. J.; Wolfe, J. F., Synthesis and Solution Properties of Extended Chain Poly(2,6-Benzothiazole) and Poly(2,5-Benzoxazole). *Macromolecules* **1989**, 22, (9), 3514-3520.
2. Yu, L. P.; Bao, Z. N., Conjugated Polymers Exhibiting Liquid Crystallinity. *Advanced Materials* **1994**, 6, (2), 156-159.
3. Olsen, B. D.; Segalman, R. A., Self-assembly of rod-coil block copolymers. *Materials Science & Engineering R-Reports* **2008**, 62, (2), 37-66.
4. Hu, D. H.; Yu, J.; Wong, K.; Bagchi, B.; Rossky, P. J.; Barbara, P. F., Collapse of stiff conjugated polymers with chemical defects into ordered, cylindrical conformations. *Nature* **2000**, 405, (6790), 1030-1033.
5. Snyder, C. R.; Henry, J. S.; DeLongchamp, D. M., Effect of Regioregularity on the Semicrystalline Structure of Poly(3-hexylthiophene). *Macromolecules* **2011**, 44, (18), 7088-7091.
6. Hartmann, L.; Tremel, K.; Uttiya, S.; Crossland, E.; Ludwigs, S.; Kayunkid, N.; Vergnat, C.; Brinkmann, M., 2D Versus 3D Crystalline Order in Thin Films of Regioregular Poly(3-hexylthiophene) Oriented by Mechanical Rubbing and Epitaxy. *Advanced Functional Materials* **2011**, 21, (21), 4047-4057.
7. Gettinger, C. L.; Heeger, A. J.; Drake, J. M.; Pine, D. J., A Photoluminescence Study of Poly(Phenylene Vinylene) Derivatives - the Effect of Intrinsic Persistence Length. *Journal of Chemical Physics* **1994**, 101, (2), 1673-1678.
8. Gettinger, C. L.; Heeger, A. J.; Drake, J. M.; Pine, D. J., The Effect of Intrinsic Rigidity on the Optical-Properties of Ppv Derivatives. *Molecular Crystals and Liquid Crystals Science and Technology Section a-Molecular Crystals and Liquid Crystals* **1994**, 256, 507-512.
9. Adachi, T.; Brazard, J.; Chokshi, P.; Bolinger, J. C.; Ganesan, V.; Barbara, P. F., Highly Ordered Single Conjugated Polymer Chain Rod Morphologies. *Journal of Physical Chemistry C* **2010**, 114, (48), 20896-20902.

10. Hu, D. H.; Yu, J.; Padmanaban, G.; Ramakrishnan, S.; Barbara, P. F., Spatial confinement of exciton transfer and the role of conformational order in organic nanoparticles. *Nano Letters* **2002**, 2, (10), 1121-1124.
11. Fytas, G.; Nothofer, H. G.; Scherf, U.; Vlassopoulos, D.; Meier, G., Structure and dynamics of nondilute polyfluorene solutions. *Macromolecules* **2002**, 35, (2), 481-488.
12. Meier, H.; Stalmach, U.; Kolshorn, H., Effective conjugation length and UV/vis spectra of oligomers. *Acta Polymerica* **1997**, 48, (9), 379-384.
13. Socci, E. P.; Farmer, B. L.; Adams, W. W., Molecular-Dynamics Simulations of a Poly(P-Phenylene) Oligomer. *Journal of Polymer Science Part B-Polymer Physics* **1993**, 31, (13), 1975-1982.
14. Petekidis, G.; Vlassopoulos, D.; Galda, P.; Rehahn, M.; Ballauff, M., Determination of chain conformation of stiff polymers by depolarized Rayleigh scattering in solution. *Macromolecules* **1996**, 29, (27), 8948-8953.
15. Lu, Y. J.; Weers, B.; Stellwagen, N. C., DNA persistence length revisited. *Biopolymers* **2001**, 61, (4), 261-275.
16. Salaneck, W. R.; Inganas, O.; Nilsson, J. O.; Osterholm, J. E.; Themans, B.; Bredas, J. L., Thermochromism in the Poly(3-Alkylthiophene)S - a Study of Conformational Defects by Photoelectron-Spectroscopy. *Synthetic Metals* **1989**, 28, (1-2), C451-C460.
17. Aime, J. P.; Bargain, F.; Schott, M.; Eckhardt, H.; Elsenbaumer, R. L.; Miller, G. G.; McDonnell, M. E.; Zero, K., Structural Study of Conducting Polymers in Solution. *Synthetic Metals* **1989**, 28, (1-2), C407-C417.
18. Aime, J. P.; Bargain, F.; Schott, M.; Eckhardt, H.; Miller, G. G.; Elsenbaumer, R. L., Structural Study of Doped and Undoped Polythiophene in Solution by Small-Angle Neutron-Scattering. *Physical Review Letters* **1989**, 62, (1), 55-58.
19. Anthony, J. E.; Heeney, M.; Ong, B. S., Synthetic aspects of organic semiconductors. *Mrs Bulletin* **2008**, 33, (7), 698-705.
20. Roncali, J., Conjugated Poly(Thiophenes) - Synthesis, Functionalization, and Applications. *Chemical Reviews* **1992**, 92, (4), 711-738.
21. Yamamoto, T.; Komarudin, D.; Arai, M.; Lee, B. L.; Suganuma, H.; Asakawa, N.; Inoue, Y.; Kubota, K.; Sasaki, S.; Fukuda, T.; Matsuda, H., Extensive studies on pi-stacking of poly(3-alkylthiophene-2,5-diyl)s and poly(4-alkylthiazole-2,5-diyl)s by optical spectroscopy, NMR analysis, light scattering analysis, and X-ray crystallography. *Journal of the American Chemical Society* **1998**, 120, (9), 2047-2058.
22. Adachi, T.; Brazard, J.; Ono, R. J.; Hanson, B.; Traub, M. C.; Wu, Z. Q.; Li, Z. C.; Bolinger, J. C.; Ganesan, V.; Bielawski, C. W.; Bout, D. A. V.; Barbara, P. F.,

Regioregularity and Single Polythiophene Chain Conformation. *Journal of Physical Chemistry Letters* **2011**, 2, (12), 1400-1404.

23. He, Z. R.; Yang, X. Z.; Zhao, D. L., Numerical Estimation of Unperturbed Dimensions of Regioirregular Poly(3-Ethylthiophene)S. *Macromolecular Theory and Simulations* **1995**, 4, (2), 277-288.

24. Patel, S. N.; Javier, A. E.; Stone, G. M.; Mullin, S. A.; Balsara, N. P., Simultaneous Conduction of Electronic Charge and Lithium Ions in Block Copolymers. *Acs Nano* **2012**, 6, (2), 1589-1600.

25. Vaia, R. A.; Krishnamoorti, R.; Benner, C.; Trimer, M., Chain conformation of rod-like polymers in the melt: Small-angle neutron scattering of poly(benzoyl paraffenylene). *Journal of Polymer Science Part B-Polymer Physics* **1998**, 36, (13), 2449-2459.

26. Loewe, R. S.; Ewbank, P. C.; Liu, J. S.; Zhai, L.; McCullough, R. D., Regioregular, head-to-tail coupled poly(3-alkylthiophenes) made easy by the GRIM method: Investigation of the reaction and the origin of regioselectivity. *Macromolecules* **2001**, 34, (13), 4324-4333.

27. Loewe, R. S.; Khersonsky, S. M.; McCullough, R. D., A simple method to prepare head-to-tail coupled, regioregular poly(3-alkylthiophenes) using grignard metathesis. *Advanced Materials* **1999**, 11, (3), 250-+.

28. Niemi, V. M.; Knuutila, P.; Osterholm, J. E.; Korvola, J., Polymerization of 3-Alkylthiophenes with FeCl<sub>3</sub>. *Polymer* **1992**, 33, (7), 1559-1562.

29. Debye, P., Molecular-Weight Determination by Light Scattering. *Journal of Physical and Colloid Chemistry* **1947**, 51, (1), 18-32.

30. Kotlarchyk, M.; Chen, S. H., Analysis of Small-Angle Neutron-Scattering Spectra from Polydisperse Interacting Colloids. *Journal of Chemical Physics* **1983**, 79, (5), 2461-2469.

31. Visser, S. A.; Pruckmayr, G.; Cooper, S. L., Small-Angle Neutron-Scattering Analysis of Model Polyurethane Ionomers. *Macromolecules* **1991**, 24, (25), 6769-6775.

32. Sharp, P.; Bloomfield, V., Light Scattering from Wormlike Chains with Excluded Volume Effects. *Biopolymers* **1968**, 6, (8), 1201-&.

33. Tashiro, K.; Ono, K.; Minagawa, Y.; Kobayashi, M.; Kawai, T.; Yoshino, K., Structure and Thermochromic Solid-State Phase-Transition of Poly(3-Alkylthiophene). *Journal of Polymer Science Part B-Polymer Physics* **1991**, 29, (10), 1223-1233.

34. Benoit, H.; Doty, P., Light Scattering from Non-Gaussian Chains. *Journal of Physical Chemistry* **1954**, 57, (9), 958-963.

35. Brulet, A.; Boue, F.; Cotton, J. P., About the experimental determination of the persistence length of wormlike chains of polystyrene. *Journal De Physique II* **1996**, 6, (6), 885-891.
36. Dai, L. M., Random Coils of Polyisoprene in Solution - a Small-Angle X-Ray-Scattering Study. *European Polymer Journal* **1993**, 29, (5), 645-651.
37. Young, R. J.; Lovell, P. A., *Introduction to polymers*. 2nd ed.; Chapman & Hall: London ; New York, 1991; p x, 443 p.
38. Themans, B.; Salaneck, W. R.; Bredas, J. L., Theoretical-Study of the Influence of Thermochromic Effects on the Electronic-Structure of Poly(3-Hexylthiophene). *Synthetic Metals* **1989**, 28, (1-2), C359-C364.
39. Darling, S. B.; Sternberg, M., Importance of Side Chains and Backbone Length in Defect Modeling of Poly(3-alkylthiophenes). *Journal of Physical Chemistry B* **2009**, 113, (18), 6215-6218.
40. Westenhoff, S.; Beenken, W. J. D.; Yartsev, A.; Greenham, N. C., Conformational disorder of conjugated polymers. *Journal of Chemical Physics* **2006**, 125, (15).
41. Flory, P. J., The Configuration of Real Polymer Chains. *Journal of Chemical Physics* **1949**, 17, (3), 303-310.
42. Bucci, P.; Longeri, M.; Veracini, C. A.; Lunazzi, L., Nematic Phase Nuclear Magnetic-Resonance Investigations of Rotational-Isomerism .3. Conformational Preferences and Interconversion Barrier of 2,2'-Bithienyl. *Journal of the American Chemical Society* **1974**, 96, (5), 1305-1309.
43. Salaneck, W. R.; Inganas, O.; Themans, B.; Nilsson, J. O.; Sjogren, B.; Osterholm, J. E.; Bredas, J. L.; Svensson, S., Thermochromism in Poly(3-Hexylthiophene) in the Solid-State - a Spectroscopic Study of Temperature-Dependent Conformational Defects. *Journal of Chemical Physics* **1988**, 89, (8), 4613-4619.
44. Wignall, G. D.; Ballard, D. G. H.; Schelten, J., Measurements of Persistence Length and Temperature-Dependence of Radius of Gyration in Bulk Atactic Polystyrene. *European Polymer Journal* **1974**, 10, (9), 861-865.
45. Tenhoeve, W.; Wynberg, H.; Havinga, E. E.; Meijer, E. W., Substituted Undecithiophenes - the Longest Characterized Oligothiophenes. *Journal of the American Chemical Society* **1991**, 113, (15), 5887-5889.
46. Thienpont, H.; Rikken, G. L. J. A.; Meijer, E. W.; Tenhoeve, W.; Wynberg, H., Saturation of the Hyperpolarizability of Oligothiophenes. *Physical Review Letters* **1990**, 65, (17), 2141-2144.

47. Klaerner, G.; Miller, R. D., Polyfluorene derivatives: Effective conjugation lengths from well-defined oligomers. *Macromolecules* **1998**, 31, (6), 2007-2009.
48. Olsen, B. D.; Jang, S. Y.; Luning, J. M.; Segalman, R. A., Higher order liquid crystalline structure in low-polydispersity DEH-PPV. *Macromolecules* **2006**, 39, (13), 4469-4479.
49. McCulloch, I.; Heeney, M.; Bailey, C.; Genevicius, K.; I, M.; Shkunov, M.; Sparrowe, D.; Tierney, S.; Wagner, R.; Zhang, W. M.; Chabinyc, M. L.; Kline, R. J.; McGehee, M. D.; Toney, M. F., Liquid-crystalline semiconducting polymers with high charge-carrier mobility. *Nature Materials* **2006**, 5, (4), 328-333.
50. DeLongchamp, D. M.; Kline, R. J.; Jung, Y.; Lin, E. K.; Fischer, D. A.; Gundlach, D. J.; Cotts, S. K.; Moad, A. J.; Richter, L. J.; Toney, M. F.; Heeney, M.; McCulloch, I., Molecular basis of mesophase ordering in a thiophene-based copolymer. *Macromolecules* **2008**, 41, (15), 5709-5715.
51. Bredas, J. L.; Chance, R. R.; Silbey, R., Comparative Theoretical-Study of the Doping of Conjugated Polymers - Polarons in Polyacetylene and Polyparaphenylene. *Physical Review B* **1982**, 26, (10), 5843-5854.
52. Nowak, M. J.; Rughooputh, S. D. D. V.; Hotta, S.; Heeger, A. J., Polarons and Bipolarons on a Conducting Polymer in Solution. *Macromolecules* **1987**, 20, (5), 965-968.

### Chapter 3. The Relationship Between Morphology and Performance of Donor Acceptor Rod-Coil Block Copolymers Solar Cells

Reproduced with permission from Bryan McCulloch, Yufei Tao, Suhan Kim and Rachel A. Segalman. *Reproduced by permission of The Royal Society of Chemistry* (<http://pubs.rsc.org/en/content/articlelanding/2009/sm/b907836c>)

Self-assembled functional rod-coil block copolymers (poly(3-hexylthiophene)-b-poly(n-butylacrylate-stat-acrylate perylene)) containing electron donor (poly(3-hexylthiophene)) and acceptor (perylene) moieties were synthesized, characterized, and studied in photovoltaic devices. The block copolymers were synthesized by a combination of the McCullough route towards monodisperse polythiophene, living radical polymerization and “click chemistry”. The nanostructure was tuned via time allowed for self-assembly to control the degree of order. As a result, devices with active layers which were completely disordered (molecularly mixed), contain short range order in which the nanodomains were molecularly pure, but were poorly organized or consisted of cylindrical fibrils with well-organized long range order were compared. Active layers with well formed but poorly organized nanodomains had the highest photovoltaic efficiencies indicating that molecular scale segregation has a significant effect on device performance.

#### 3.1. Introduction

Organic photovoltaic devices are attractive for many energy applications due to their inherently low materials costs, mechanical flexibility, and the promise of scalability to large area, light weight devices.<sup>1</sup> In contrast to many inorganic semiconductors, organic semiconducting materials generate excitons (electron-hole pairs) instead of free charge carriers upon photoexcitation. The exciton binding energy in organic materials exceeds thermal energy at room temperature<sup>2</sup> so the exciton does not separate into free charges spontaneously. Instead, free charge carriers can be formed by creating an interface between a light absorbing electron donating species and an electron accepting material. The donor material has a lower ionization potential and the acceptor material has a larger electron affinity. Ideally, the exciton diffuses to the donor-acceptor (D-A) interface prior to recombination. Then, due to the energy difference between the donor's highest occupied molecular orbital (HOMO) and acceptor's lowest unoccupied molecular orbital (LUMO) energy levels, the electron will be transferred to the acceptor and the hole will reside in the donor. The free charge carriers must then migrate to their respective electrodes to generate a photocurrent before charge recombination occurs.

There are two major bottlenecks in the creation of photocurrent: charge separation and charge transport to the electrodes. In order for an exciton to separate, it must find a D-A

interface before recombination. Generally, even with the prolonged excitonic lifetime in organics, the exciton diffusion length is limited to approximately 10nm, necessitating a 10nm lengthscale of interfaces within the active layer of the device to maximize charge separation.<sup>3, 4, 5</sup> Once separated, the electron and hole must be transported through the acceptor and donor phases (respectively) back to the cathode and anode. These dual requirements suggest optimization through the creation of a bicontinuous morphology where the domain size is on a 10nm lengthscale. Figure 3.1 schematically depicts possible active layer morphologies. The bilayer morphology (Fig. 1a) is commonly achieved by thermal evaporation techniques, generally appropriate for small molecules.<sup>6</sup> This morphology provides the most direct pathway to transport electrons and holes to the electrodes and minimizes the recombination of the free charges, however exciton separation is limited to the small interfacial area. Excitons are only separated within ~10nm of the interface, though the light penetration depth is much greater (~100nm). A bicontinuous morphology with a large amount of interfacial area would be ideal, but is difficult to realize. Structures created by blending of the donor and acceptor components<sup>7</sup> are generally referred to as bulk heterojunction structures (Figure 3.1). The interface morphology in these devices is non-equilibrium, depending on the phase separation of the two components. The casting conditions, thermal histories, and thermodynamic interactions of these components must be tuned to create small lengthscale phase separation and a large amount of internal interfacial area. The morphologies resulting from phase separation are necessarily difficult to tune in terms of connectivity to the electrodes and are subject to Ostwald ripening. Furthermore, even when phase separated two component blends encompass some degree of molecular scale mixing which has unexpected effects on electronic properties.<sup>8</sup> Indeed, studies of the relationship between morphologies in blend structures and photovoltaic performance have only begun to appear in the last few years<sup>9-14</sup> While some of the highest efficiencies to date have been demonstrated in bulk heterojunction devices, optimization generally requires combinatorial processing to achieve optimal morphologies. It is unclear whether this type of processing can be scaled with similar effects.

Block copolymers made by covalently linking distinct chains with electron donor and acceptor properties may be good candidates for solar cell applications due to their ability to self-assemble into structures on the 10nm length scale. Self-assembly in classical block copolymers is a compromise between the immiscibility of the blocks and the penalty associated with stretching a chain across the interface.<sup>15</sup> As a result, the nanodomain size is set by the size of the polymer and not subject to ripening. Furthermore, the shape of the nanodomain can be predicted and is not a result of processing history. Finally, the nanodomains are molecularly pure with mixing of components only occurring in the immediate vicinity of the interface. These effects promise to separate the nanodomain morphology of an active layer from its processing



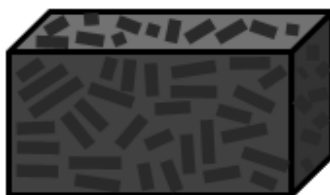
(a) Bilayer morphology



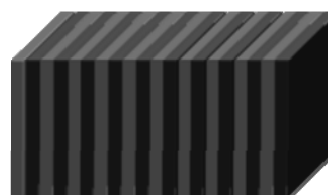
(b) Bulk heterojunction morphology



(c) Disordered structures from hindered block copolymer self-assembly



(d) Poorly organized nanostructures can result from intermediate casting conditions with block copolymers



(e) Block copolymers self-assembled to induce long range order (orientation with respect to substrate requires additional field induced control)

### Figure 3.1. Photovoltaic Morphologies

Numerous active layer morphologies of the electron donating and accepting components have been suggested in the literature. Figures A and B are commonly used bilayer and bulk heterojunction morphologies. Block copolymers can be used to form disordered structures, structures with poor order, or long range ordered structures.



history and provide a chemical purity of domains. These properties are of interest in bulk heterojunction devices.

While a large amount of work has been done to understand classical block copolymer self-assembly, the backbone conjugation that imparts a semiconducting bandgap also creates chain rigidity in the polymer. Chain rigidity introduces liquid crystallinity, an intramolecular interaction not found in classical block copolymers. Additionally, the conformational asymmetry of so-called rod-coil block copolymers provides an additional geometrical constraint. Experimentally, a large number of intriguing phases have been observed<sup>16</sup> including zig-zag, herringbone, and hockey puck phases, as well as cylindrical and spherical phases reminiscent of more classical systems. This phase behavior is the subject of a few recent reviews.<sup>16, 17</sup> The self-assembly of rod-coil block copolymers relies on four thermodynamic parameters: the Flory-Huggins strength of segregation ( $\chi N$ , where  $N$  is the molecular length) which parameterizes the interactions between chemically dissimilar blocks, the Maier-Saupe interaction relating the rod-rod alignment tendency ( $\mu N$ ), the volume fraction of coil ( $\phi_{\text{coil}}$ ) and the geometrical asymmetry of the system ( $v$ )<sup>18-21</sup>. The phase diagram for a model conjugated rod-coil block copolymer system suggests that lamellar phases occur for a much larger range of volume fraction than in the classical block copolymer case<sup>22, 23</sup> though hexagonal<sup>24-26</sup> and spherical<sup>24, 26</sup> phases have been observed under certain circumstances. While classical block copolymers generally form layered morphologies with the long axis parallel to the substrate due to preferential wetting conditions, it appears that the kinetics of rod-coil block copolymer self-assembly can trap a less well ordered morphology with layers arranged both perpendicular and parallel from the substrate.<sup>27, 28</sup>

Several groups have prepared donor-acceptor block copolymers for photovoltaics.<sup>29-33</sup> Novel diblock copolymers consisting of an electron donating poly(alkoxy phenylene) and a coil block with pendant fullerenes demonstrated intriguing device performance, though the self-assembly was kinetically hindered by the presence of the crystallizable fullerene.<sup>29-32</sup> Scherf and coworkers prepared a series of diblock/triblock copolymers with both electron-donor and electron-acceptor blocks, which formed regular nanostructures in thin films.<sup>34-36</sup> The use of pendant donor and acceptor groups on a coil-like polymeric backbone results in polymers that bear more resemblance to classical block copolymers. Thelakkat and coworkers have demonstrated a (poly(bisphenyl-4-vinylphenylamine) - block-poly(perylene diimide acrylate)) in which all of the electronic functionalities are attached as sidegroups.<sup>37-41</sup> Backbone conjugated polymers, such as poly(3-hexyl thiophene) (P3HT), have higher charge mobilities. Recently, block copolymers incorporating poly(3-hexyl thiophene) as the donor material and a hybrid acceptor material made of an acrylate backbone with pendant perylene groups has been synthesized.<sup>42-44</sup> This block copolymer system has shown

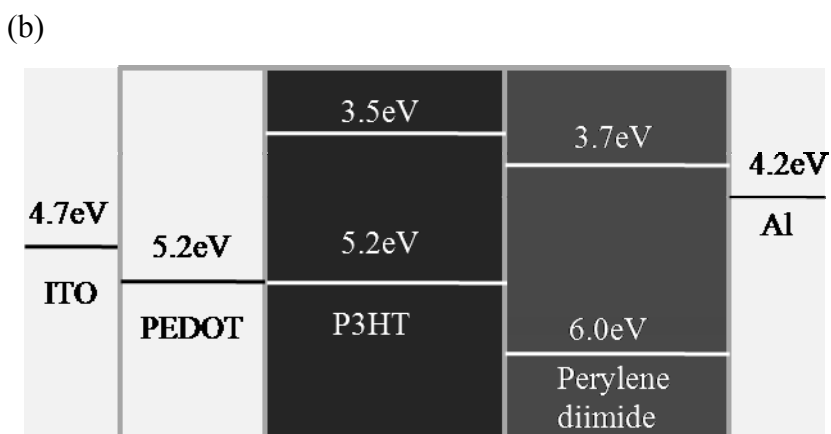
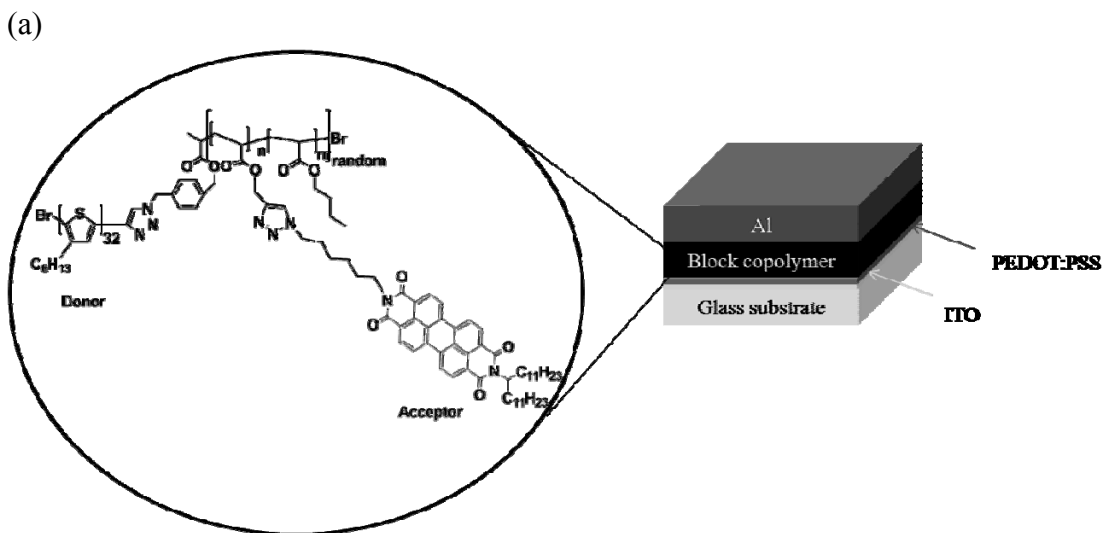


**Figure 3.2. Block Copolymer Photovoltaic Structure**

(a) The structure of a typical block copolymer solar cell fabricated in this study. (b) A schematic showing the energy levels of the components in the device.

improved device performance in comparison to an analogous blend, suggesting that the molecular scale phase separation of a block copolymer is advantageous.

While several donor-acceptor block copolymers have been demonstrated, well organized nanostructures have been slow to appear. If cast quickly from a non-preferential solvent, block copolymers do not have time to self assemble and molecularly mix (Figure 3.1). If cast slowly or annealed above the glass transition temperature for suitable periods of time, the block copolymers may form not only the monodisperse, molecularly pure nanostructures generally associated with block copolymer self-assembly, but these nanostructures will also orient cooperatively to form large grains with long range order. Intermediate conditions allow for the formation of the monodisperse nanodomains, but the system may lack sufficient mobility to form long range, well defined grains (as shown in Figure 3.1). The impact of nanoscale segregation and long range order on device behavior is unclear.

Here, a single active layer photovoltaic device based on poly(3-hexyl thiophene)-*b*-poly(*n*-butyl acrylate-*stat*-acrylate perylene) block copolymer as shown in Figure 3.2 is synthesized, self-assembled, and characterized by constructing photovoltaic devices. Regioregular P3HT is one of the most promising electron donating conjugated polymers with good solubility, environmental stability,<sup>45</sup> high charge carrier mobilities and a low bandgap relative to most conjugated polymers. Perylene diimide derivatives have large molar absorption coefficients, good electron accepting properties<sup>46,47-50</sup> and previous studies suggest good photovoltaic performance both in layered and bulk heterojunction structures<sup>51-56</sup>. We show that the degree of order achieved through self-assembly can be tuned by altering the mobility of the backbone and the time available for self-assembly. We find that while long range ordered self assembly can be achieved, nanostructures consisting of well-defined interfaces but lacking periodic block copolymer structure perform better. The statistical polymerization of the perylene precursor with non-functional butyl acrylate improves chain mobility and the kinetics of self-assembly, but increased amounts of butyl acrylate reduce the performance of the device, as expected. This demonstrates that well controlled domain sizes and a decrease in molecular mixing that is a result of self assembly is advantageous. We postulate that the poor performance of the sample with long range continuity of the nanostructures performs poorly due to the misorientation of these domains resulting in limited charge transport.

## 3.2. Experimental Methods

**3.2.1 General methods.** All reactions were carried out under air free (N<sub>2</sub>) conditions unless otherwise specified. NMR spectra were recorded on Bruker DRX-500. Analytical SEC in THF was performed at 35°C at a nominal flow rate of 1.0 mL/min on a

chromatography line calibrated with linear polystyrene standards. Film thicknesses were determined with a Rudolph Technologies ellipsometer on silicon wafers.

**3.2.2 Materials.** (4-(azidomethyl)phenyl)methanol<sup>57</sup>, 3-(trimethylsilyl)prop-2-ynyl acrylate<sup>58</sup> ethynyl-terminated P3HT (4)<sup>59, 60</sup> and azide substituted asymmetric perylene bisimide (7) were synthesized according to references. All other reagents were obtained from Aldrich and used as received.

Synthesis of 4-(azidomethyl)benzyl 2-bromopropanoate, 1. A solution of (4-(azidomethyl)phenyl)methanol (1.63g, 10 mmol) and Et<sub>3</sub>N (2.1 mL, 15 mmol) in Et<sub>2</sub>O (20 mL) was cooled to 0 °C and a solution of 2-bromopropanoyl bromide (1.61 mL, 15 mmol) was added drop wise over 10 min. The mixture was stirred at 0 °C for 1 hr and then at ambient temperature overnight. The reaction mixture was quenched with 50 mL of water, extracted with ether, and then dried over MgSO<sub>4</sub>. The volatiles were removed under reduced pressure and the crude product was purified by flash chromatography (SiO<sub>2</sub>, R<sub>f</sub>=0.50 Hexane:EtOAc 8:2). Obtained 2.6 g (0.90 mmol, 90%) of (1) as liquid.

<sup>1</sup>H NMR (CDCl<sub>3</sub>) δ: 1.81 (d, *J*=9.0 Hz, 3H, CH<sub>3</sub>-CH<sub>2</sub>), 4.35 (s, 2H, CH<sub>2</sub>-N<sub>3</sub>), 4.41 (q, *J*=7.0 Hz, 2H, CH<sub>2</sub>-Br), 5.20 (d, *J*=4.0 Hz, 2H, CH<sub>2</sub>-O-), 7.31 (d, *J*=7.5 Hz, 2H, Ar), 7.39 (d, *J*=7.5 Hz, 2H, Ar). <sup>13</sup>C NMR (CDCl<sub>3</sub>) δ: 21.57 (1C, CH<sub>3</sub>), 39.86 (1C, CH<sub>2</sub>-Br), 54.37 (1C, CH<sub>2</sub>-N<sub>3</sub>), 67.05 (1C, CH<sub>2</sub>-O-), 128.41 (2C, Ar), 128.59(2C, Ar), 135.66 (1C, C-CH<sub>2</sub>-N<sub>3</sub>), 135.66 (C-CH<sub>2</sub>-O-), 169.97 (1C, C=O).

General polymerization procedure. Synthesis of (3a-c). In a typical experiment, N,N,N',N',N''-pentamethyldiethylenetriamine (PMDTA) ligand (17.3 mg, 0.10 mmol), initiator (1) (29.8 mg, 0.10 mmol), 3-(trimethylsilyl) prop-2-ynyl acrylate (2) (280 mg, 1.5 mmol), n-butyl acrylate (768 mg, 6.0 mmol) and a magnetic stirrer were introduced into a dry 10 mL round-bottom flask. The round flask was subjected to 3 freeze-pump-thaw cycles. CuBr (14.3 mg, 0.1 mmol) catalyst was added into the flask while the contents were in a solid state and deoxygenated by vacuum followed by back filling with nitrogen two times. The flask was placed in an oil bath set at 60 °C for 1 hr, cooled to room temperature, and then aliquots were withdrawn for characterization. Conversions were calculated via <sup>1</sup>H NMR by comparing the integrals of the monomer CH<sub>2</sub>-O- signals (4.77 ppm from 3-(trimethylsilyl) prop-2-ynyl acrylate and 4.15 ppm from n-butyl acrylate) to the peak of polymer CH<sub>2</sub>-O- signals (4.65 ppm from poly (3-(trimethylsilyl) prop-2-ynyl acrylate) and 4.05 ppm from poly( n-butyl acrylate)). The molecular weight of the polymer was calculated by <sup>1</sup>H NMR by comparing the integral of the the peak of polymer CH<sub>2</sub>-O- signals (4.65 ppm from poly (3-(trimethylsilyl) prop-2-ynyl acrylate) and 4.05 ppm from poly( n-butyl acrylate)) to that of the CH<sub>2</sub>-N<sub>3</sub> group connected to the aromatic ring, at 4.35 ppm. Polydispersities were calculated from SEC using polystyrene standards.

3a: conversion: 67% (from NMR). M<sub>n</sub>= 7388 (NMR) M<sub>n</sub>/M<sub>w</sub>=1.22 <sup>1</sup>H NMR (CDCl<sub>3</sub>) δ: 0.18 (s, Si(CH<sub>3</sub>)<sub>3</sub>), 0.95 (s, CH<sub>3</sub>), 1.38 (s, aliphatic H), 1.60-1.73 (m, aliphatic H), 1.93

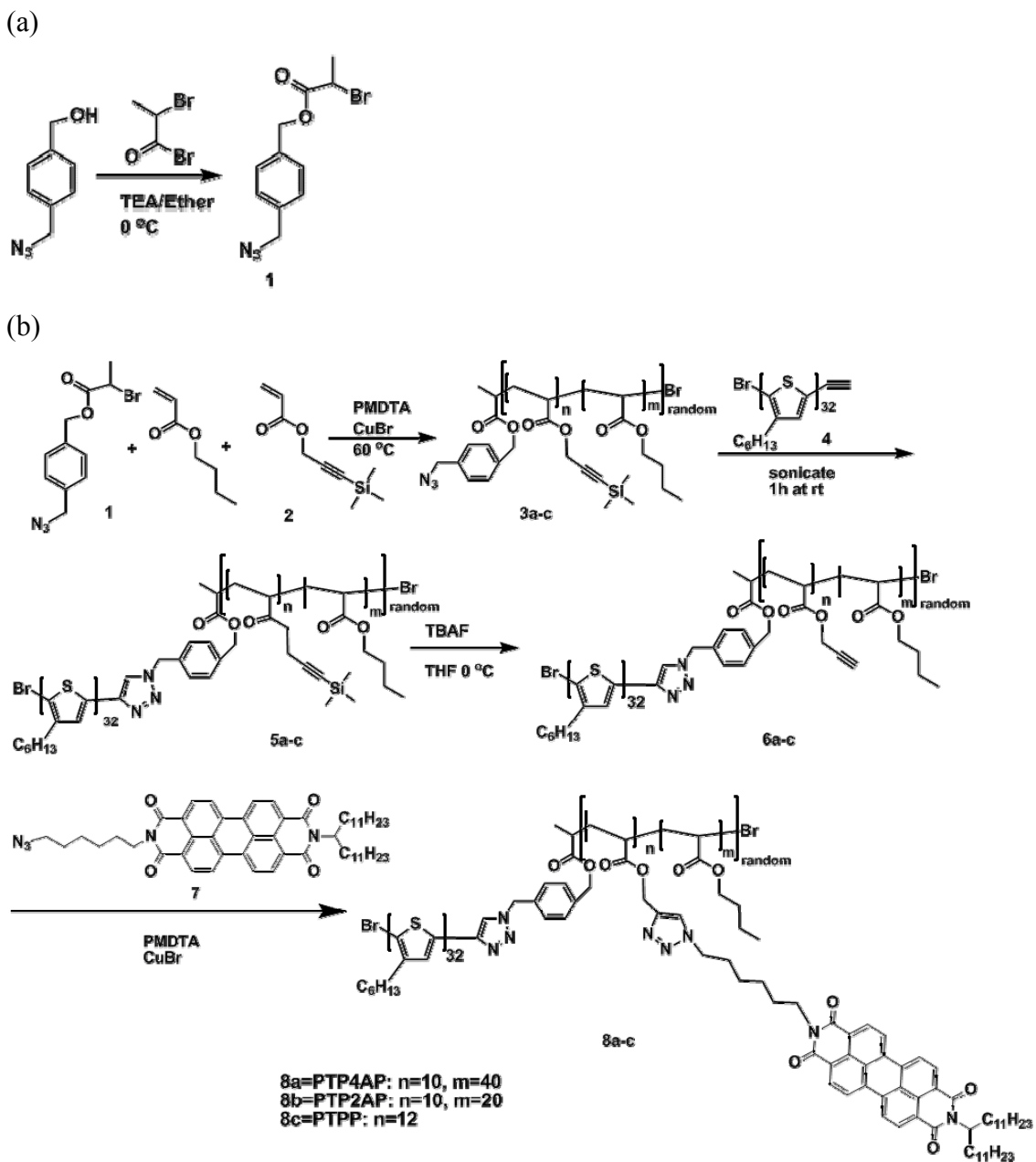


**Figure 3.3. Synthetic Scheme of Block Copolymer**

Synthesis route of the P3HT-*b*-poly(BA-*stat*-PerAcr) block copolymers. BA = *n*-butyl acrylate, PerAcr = acrylate unit with perylene diimide side group.

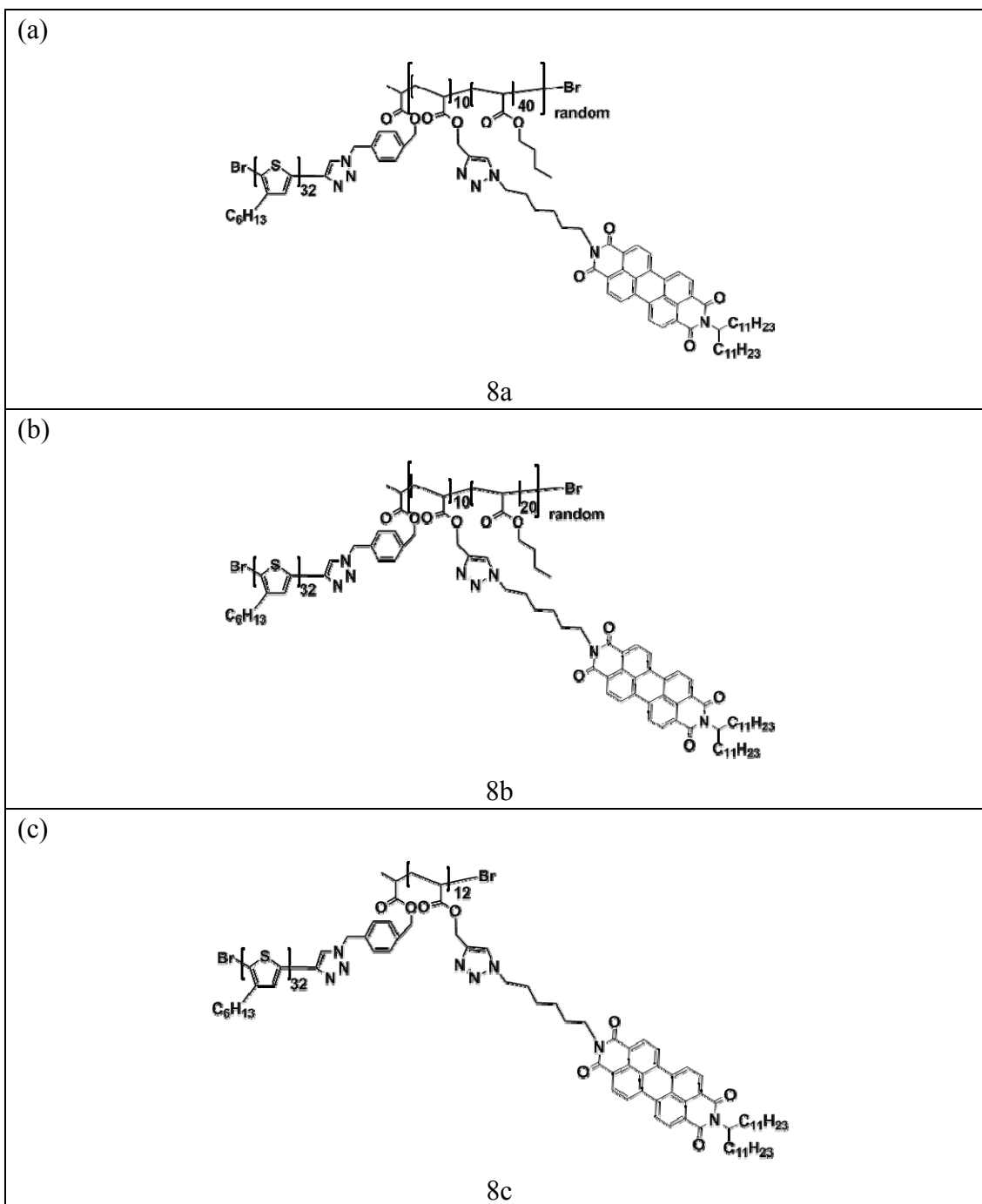


Figure 3.4. Chemical structures for block copolymers

(m, aliphatic H), 2.28-2.41 (m, aliphatic H), 4.05 (s,  $\text{CH}_2\text{-CH}_2\text{-O-}$ ), 4.35 (s,  $\text{CH}_2\text{-N}_3$ ), 4.65 (s,  $\text{C}\equiv\text{C-CH}_2\text{-O-}$ ), 7.32-7.36 (m, aromatic H).

3b: PMDTA (17.3 mg, 0.10 mmol): (1) (29.8 mg, 0.10 mmol): (2) (280 mg, 1.5 mmol): n-butyl acrylate (384 mg, 3.0 mmol): CuBr (14.3 mg, 0.1 mmol). Conversion is 66% (from NMR).  $M_n = 4728$  (NMR)  $M_n/M_w = 1.25$

3c: PMDTA (69.2 mg, 0.40 mmol): (1) (119 mg, 0.40 mmol): (2) (1120 mg, 6 mmol): CuBr (57.2 mg, 0.4 mmol). Conversion is 80% (from NMR).  $M_n = 2542$  (NMR)  $M_n/M_w = 1.32$   $^1\text{H NMR}$  ( $\text{CDCl}_3$ )  $\delta$ : 0.18 (s,  $\text{Si}(\text{CH}_3)_3$ ), 1.60 (s, aliphatic H), 1.73 (s, aliphatic H), 1.93 (s, aliphatic H), 2.41 (s, aliphatic H), 4.35 (s,  $\text{CH}_2\text{-N}_3$ ), 4.65 (s,  $\text{C}\equiv\text{C-CH}_2\text{-O-}$ ), 7.32-7.36 (m, aromatic H).

Synthesis of (5a-c). Without purification of 3a, 200 mg ethynyl-terminated P3HT (4) ( $M_n = 5300$  (NMR),  $M_n/M_w = 1.15$ ) were added into the flask. The round flask was subjected to 3 freeze-pump-thaw cycles before adding 5 mL anhydrous THF and sonicating for 2 hrs. After reaction, the solution was passed through a column of neutral alumina to remove the catalyst. The desired polymer was precipitated by adding methanol solvent to the solution. NMR confirms the quantitative production of the desired block copolymer with a 1,2,3 triazole bridge, as shown in Figure 3.3.

5a:  $M_n = 12600$  (NMR)  $M_n/M_w = 1.23$   $^1\text{H NMR}$  ( $\text{CDCl}_3$ )  $\delta$ : 0.18 (s,  $\text{Si}(\text{CH}_3)_3$ ), 0.91 (m,  $\text{CH}_3$ ), 1.35 (s, aliphatic H), 1.44 (s, aliphatic H), 1.60 (s, aliphatic H), 1.70 (s, aliphatic H), 1.93 (s, aliphatic H), 2.29-2.41 (m, aliphatic H), 2.80 (s, aliphatic H), 4.05 (s,  $\text{CH}_2\text{-CH}_2\text{-O-}$ ), 4.65 (s,  $\text{C}\equiv\text{C-CH}_2\text{-O-}$ ), 6.98 (s, thiophene H) 7.32-7.36 (m, aromatic H).

5b:  $M_n = 10040$  (NMR)  $M_n/M_w = 1.26$

5c:  $M_n = 7845$  (NMR)  $M_n/M_w = 1.33$   $^1\text{H NMR}$  ( $\text{CDCl}_3$ )  $\delta$ : 0.18 (s,  $\text{Si}(\text{CH}_3)_3$ ), 0.91 (s,  $\text{CH}_3$ ), 1.35 (s, aliphatic H), 1.44 (s, aliphatic H), 1.60 (s, aliphatic H), 1.70 (s, aliphatic H), 1.93 (s, aliphatic H), 2.41 (m, aliphatic H), 2.80 (s, aliphatic H), 4.65 (s,  $\text{C}\equiv\text{C-CH}_2\text{-O-}$ ), 6.98 (s, thiophene H) 7.32-7.36 (m, aromatic H).

Synthesis of (6a-c). Polymer 5a (100mg) was dissolved in dry THF (10 mL), bubbled with nitrogen for 10 min, and then cooled to 0 °C. After addition of tetrabutylammonium fluoride (1.0 M, 0.1 mL) to the solution, the mixture was stirred for addition 10 min. The polymer was precipitated in methanol to give 6a.

6a:  $M_n = 11820$  (NMR)  $M_n/M_w = 1.25$   $^1\text{H NMR}$  ( $\text{CDCl}_3$ )  $\delta$ : 0.91 (m,  $\text{CH}_3$ ), 1.35 (s, aliphatic H), 1.44 (s, aliphatic H), 1.60 (s, aliphatic H), 1.70 (s, aliphatic H), 1.93 (s, aliphatic H), 2.29-2.41 (m, aliphatic H), 2.50 (s,  $\text{C}\equiv\text{CH}$ ), 2.80 (s, aliphatic H), 4.05 (s,  $\text{CH}_2\text{-CH}_2\text{-O-}$ ), 4.65 (s,  $\text{C}\equiv\text{C-CH}_2\text{-O-}$ ), 6.98 (s, thiophene H) 7.32-7.36 (m, aromatic H).

6b:  $M_n = 9260$  (NMR)  $M_n/M_w = 1.28$

6c:  $M_n = 6918$  (NMR)  $M_n/M_w = 1.34$   $^1\text{H NMR}$  ( $\text{CDCl}_3$ )  $\delta$ : 0.91 (s,  $\text{CH}_3$ ), 1.35 (s, aliphatic H), 1.44 (s, aliphatic H), 1.60 (s, aliphatic H), 1.70 (s, aliphatic H), 1.93 (s, aliphatic H), 2.41 (m, aliphatic H), 2.50 (s,  $\text{C}\equiv\text{CH}$ ), 2.80 (s, aliphatic H), 4.65 (s,  $\text{C}\equiv\text{C-CH}_2\text{-O-}$ ), 6.98 (s, thiophene H) 7.32-7.36 (m, aromatic H).

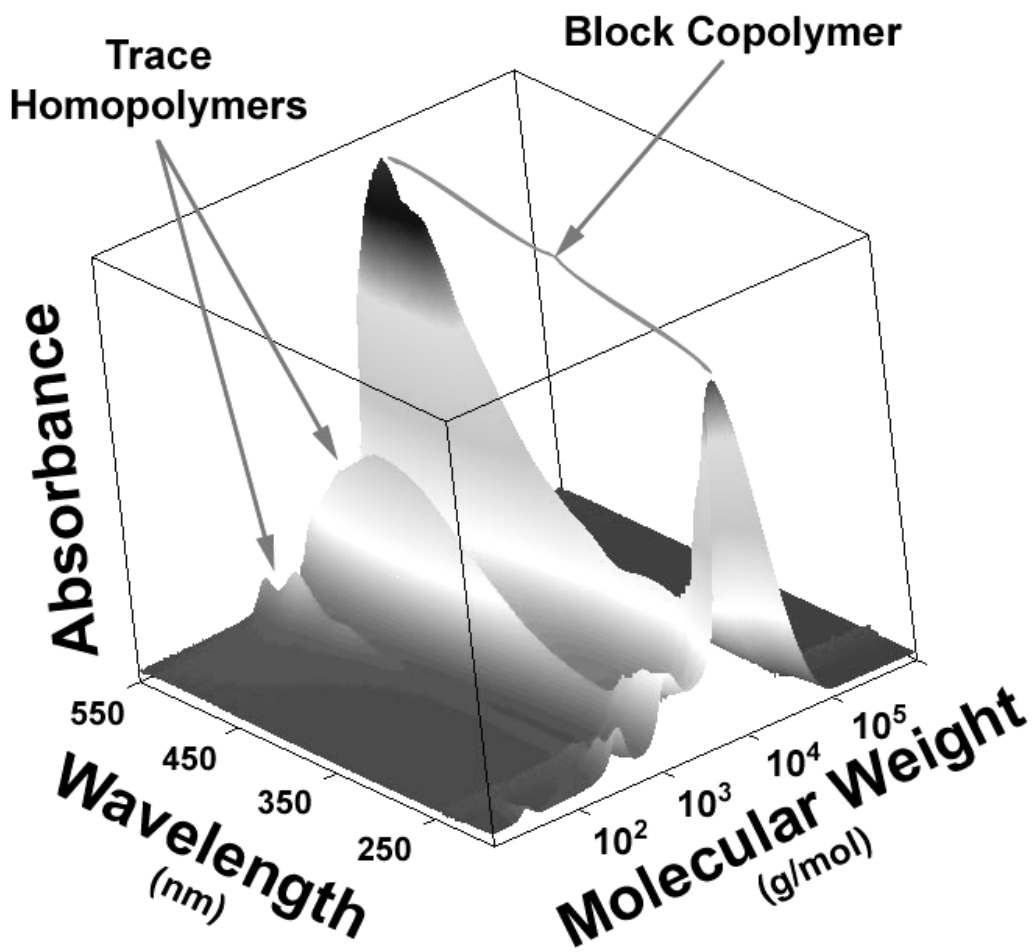


**Figure 3.5. Block Copolymer GPC**

GPC trace of 8a using a UV photodiode array detector showing absorbance intensity versus wavelength and molecular weight indicating the successful coupling of P3HT and a perylene diimide containing polyacrylate. The trace homopolymer P3HT has a molecular weight of ~4,000g/mol and a peak absorption at 453 nm. The block copolymer has an expected molecular weight ~20,000g/mol and narrow polydispersity. This block copolymer also has the expected multiple absorption peaks, including characteristics of both the P3HT block (absorption maximum at 453 nm) as well as perylene diimide (absorption maximum at 485 nm).



**Table 3.1. Block Copolymer Compositions**

polymer	N <sub>perylene</sub>	N <sub>butyl acrylate</sub>	M <sub>n</sub> (NMR)	M <sub>n</sub> /M <sub>w</sub> (SEC)
3a	10	40	7388	1.22
3b	10	20	4728	1.25
3c	12	0	2542	1.32
5a	10	40	12600	1.23
5b	10	20	10040	1.26
5c	12	0	7845	1.33
6a	10	40	11820	1.25
6b	10	20	9260	1.28
6c	12	0	6918	1.34
8a	10	40	20200	1.26
8b	10	20	17640	1.27
8c	12	0	16974	1.26

Synthesis of (8a-c). Polymer 6a (118 mg, 0.01 mmol), CuBr (7.1 mg, 0.05 mmol), and azide substituted asymmetric perylene biimide (7) (125 mg, 0.15 mmol) were introduced into 25 mL round-bottom flask, which was fitted with a stopper. The flask was evacuated and back-filled with dry nitrogen three times. After the evacuating cycles, dry THF (10 mL) and PMDTA (8.6 mg, 0.05 mmol) were added. The reaction mixture was sonicated for 2 h. After reaction, the solution was passed through a column of neutral alumina to remove the catalyst. The desired polymer was precipitated in acetone three times to remove the excess of azide substituted asymmetric perylene bisimide. In order to study the effect of adding butyl acrylate to the backbone of the electron accepting block, the number of perylene units was kept at around 10 to keep the ratio of the donor and acceptor monomer units constant in all samples 8a-c. The ratio of butyl acrylate to perylene was increased from 0 to 4 from 8a to 8c.

8a (PTP4AP):  $M_n = 20200$  (NMR)  $M_n/M_w = 1.26$   $^1\text{H NMR}$  ( $\text{CDCl}_3$ )  $\delta$ : 0.82 (s,  $\text{CH}_3$ ), 0.91 (s,  $\text{CH}_3$ ), 1.19-2.41 (m, aliphatic H), 2.80 (s, aliphatic H), 4.05 (s,  $\text{CH}_2\text{-CH}_2\text{-O-}$ ), 4.65 (s,  $\text{C}\equiv\text{C-CH}_2\text{-O-}$ ), 5.02 (s, aliphatic H), 6.98 (s, thiophene H) 7.32-8.20 (m, aromatic H).

8b (PTP2AP):  $M_n = 17640$  (NMR)  $M_n/M_w = 1.27$

8c (PTPP):  $M_n = 16974$  (NMR)  $M_n/M_w = 1.26$   $^1\text{H NMR}$  ( $\text{CDCl}_3$ )  $\delta$ : 0.82 (s,  $\text{CH}_3$ ), 0.91 (s,  $\text{CH}_3$ ), 1.19-2.41 (m, aliphatic H), 2.80 (s, aliphatic H), 4.65 (s,  $\text{C}\equiv\text{C-CH}_2\text{-O-}$ ), 5.02 (s, aliphatic H), 6.98 (s, thiophene H) 7.32-8.20 (m, aromatic H).

**3.2.3 Devices Fabrication and Measurement.** Prepatterned 150 nm sputtered ITO-coated ( $20\Omega\text{ m}^{-1}$ ) glass substrates were obtained from Thin Film Devices, Inc. The substrates were cleaned by ultrasonication for 20 min in acetone, and then 2% Helmanex soap in water for 20 min. This cleaning was followed by extensive rinsing and then ultrasonication with deionized water and then 2-propanol. A final 10 min oxygen plasma treatment completed the substrate cleaning. A 40 nm thick film of poly(styrenesulfonate)-doped poly(3,4-ethylene dioxythiophene) (PEDOT/PSS) (Baytron-P) was spin-coated onto the cleaned glass/ITO substrate at a rate of 4000 rpm and baked for 1h at  $125^\circ\text{C}$ . All procedures after this point were performed in an inert-atmosphere glove box. For spun cast devices, solutions of block copolymers ( $10\text{ mg mL}^{-1}$  in toluene) were applied to the substrate and spun at 1000 rpm for 60 s. For drop cast devices, solutions of block copolymers ( $0.5\text{ mg mL}^{-1}$  or  $1\text{ mg mL}^{-1}$  in toluene) were used to flood the substrate which was then covered to reduce the evaporation rate of the solvent and allowed to dry. Solvent annealing was accomplished in a saturated vapor environment and upon completion of annealing, the vapor was allowed to flash quickly off of the sample. Contacts on the ITO anode were created by mechanically removing some of the organic film. Substrates were then held under high vacuum ( $10^{-7}$  torr) for 4 hrs to facilitate removal of remaining solvent prior to evaporating 100 nm of Al through a shadow mask at a rate of  $0.1\text{--}0.5\text{ nm s}^{-1}$ . During the evaporation, samples were rotated at 1Hz to ensure even metal deposition. The configuration of the shadow mask afforded eight independent devices on each substrate and one control connection between the Al

and the ITO substrate. Devices were left to cool to room temperature before further processing. Device testing was performed under an argon atmosphere with an oriel xenon arc lamp with an AM 1.5G solar filter. Current–voltage data was measured with a Keithly 236 SMU. Reported efficiencies are averages from all eight devices on each substrate.

**3.2.4 Transmission Electron Microscopy.** Samples for top view transmission electron microscopy (TEM) were prepared by either spin-casting films from toluene solutions ( $10 \text{ mg mL}^{-1}$ ) or drop casting films from toluene solution ( $0.5 \text{ mg mL}^{-1}$  or  $1 \text{ mg mL}^{-1}$ ) onto a silicon wafer covered with a thin layer of PEDOT:PSS to mimic the device conditions. The slow dissolution of PEDOT:PSS in a water bath allowed for the release of the block copolymer films from the silicon wafer. Films were then retrieved on top of 500-mesh copper TEM grids. To create TEM contrast, the P3HT domains were preferentially stained by exposure to  $\text{I}_2$  vapor for 4 hrs or  $\text{RuO}_4$  vapors for 10 minutes. Preference of these stains for P3HT was confirmed via staining and subsequent imaging of large scale blend samples (not shown). TEM images were obtained on a FEI Tecnai 12 (200 kV, bright-field) using the internal charge-coupled device (CCD) camera.

Samples for cross-sectional TEM were prepared by drop casting films from toluene solution ( $0.5 \text{ mg mL}^{-1}$  or  $1 \text{ mg mL}^{-1}$ ) onto a silicon wafer covered with a thin layer of PEDOT:PSS. In this case, the P3HT domains in the films were stained for one day using  $\text{RuO}_4$  vapors to insure even staining throughout the depth of the film. A thin cross-sectional TEM sample of a drop cast film was prepared by the “Shadow Focused Ion Beam” method.<sup>61</sup> TEM images were obtained on a Zeiss LIBRA 200MC (200 kV, bright-field) using the internal charge-coupled device (CCD) camera.

**3.2.5 Atomic Force Microscopy.** Samples for atomic force microscopy (AFM) were prepared by either spin-casting or drop casting polymers from toluene solution onto PEDOT:PSS onto (100) silicon wafers. AFM samples were analyzed on a Digital Instruments MultiMode AFM operating in Tapping Mode<sup>TM</sup>.

### 3.3. Results and Discussion

**3.3.1 Synthesis of Block Copolymers.** Conjugated block copolymers have been previously prepared by either a macroinitiation approach<sup>29, 62</sup> or a coupling approach<sup>63-65</sup>. When the conjugated chain is used as the initiator for the polymerization of a second block (usually via a living polymerization route), controlled polymerization is achievable, but characterization of the molecular weights and chemical integrities of the individual blocks after polymerization is difficult. Furthermore, exposure of the conjugated block to the polymerization conditions of the second block can lead to higher polydispersities, side-reactions, and degradation. By contrast, coupling reactions allow each block to be

synthesized and characterized separately, but a balance must be found in which the coupling reaction is high yield and the resulting block copolymer is easily separable from its constituent homopolymers, but does not result in side-reactions. Here, well defined functional rod-coil block copolymers containing electron donor and acceptor moieties with narrow molecular weight distributions are synthesized by a combination of living free radical polymerization and two “click chemistry” steps as shown in Scheme 1 utilizing the coupling approach.

Atom transfer radical polymerization (ATRP) of a protected alkyne functionalized monomer with an azide end functionalized initiator yielded a monodisperse (PDI~1.2) polymer (3). Click chemistry was then used to couple the P3HT rod (4) to the polyacrylate chain (3). The high efficiency of this coupling reaction allowed for very mild reaction conditions which helped to preserve the chemical integrity of the individual blocks. Care was taken to remove the catalyst and any unreacted azide functionalized P3HT. The alkyne functionalities on the block copolymer were then deprotected to yield a defined number of sites to which further functionalities could be attached(6). In this case, electron acceptors were attached via another click chemistry step.

4-(azidomethyl)benzyl 2-bromopropanoate (1) was chosen as the ATRP initiator. The number average molecular weight ( $M_n$ (NMR)) of the corresponding polymers was determined by using both the benzylic and aromatic protons as internal  $^1\text{H}$  NMR standards. This initiator (1) was prepared in a single step from 4-(azidomethyl)phenylmethanol and 2-bromopropanoyl bromide as shown in Scheme 1a. The homo- and copolymerization of 3-(trimethylsilyl) prop-2-ynyl acrylate (2) and *n*-butyl acrylate with the initiator in the presence of a CuBr/PMDTA31 catalyst yielded good control over the polymer molecular weight and molecular weight distribution (Table 3.1). Adding *n*-butyl acrylate to the polymerization should decrease the glass transition temperature of this block and increase its self-diffusion coefficient. The azide end-group is stable under the ATRP reaction conditions, as verified by comparing the ratios of the aromatic protons to azide connected benzylic protons via  $^1\text{H}$  NMR.

Ethynyl terminated P3HT was prepared according to the McCullough methods<sup>58</sup>. Low polydispersity ethynyl terminated P3HT (4) ( $M_n=5300$  (NMR),  $M_n/M_w=1.15$ ) was synthesized by terminating the P3HT with a Grignard reagent (ethynylmagnesium chloride). Ethynyl terminated P3HT (4) was then added to (3). Since polymer (4) dissolves only very slowly in THF, sonication was used to promote the solubilization. The two polymer building blocks (3 and 4) were coupled via 1,3-dipolar cycloaddition reactions between the azide and alkyne end groups using CuBr and PMDTA<sup>66,67</sup>, forming block copolymer (5). The coupling reactions were finished within 2 hours by monitoring the disappearance of homopolymer (4) with SEC. The block copolymer contains trace amounts of unreacted P3HT homopolymer and acrylate homopolymer which are easily

distinguished from our target block copolymer (Figure 3.3). After the reaction, the polymer solution was filtered through a neutral alumina column twice to remove the copper catalyst. The excess homopolymer (3) and monomers were easily removed by precipitating in methanol.

The trimethylsilyl sidechain protecting group was removed quantitatively using tetrabutylammonium fluoride (TBAF) as verified by  $^1\text{H}$  NMR. Completion of the deprotection was confirmed by the disappearance of  $\text{Si}(\text{CH}_3)_3$  (0.18 ppm) protons and the appearance of  $\text{C}\equiv\text{CH}$  (2.50 ppm) in  $^1\text{H}$  NMR spectra. We also note that if the copper catalyst was not completely removed from polymer (5) after previous reaction steps, coupling reactions in the polymer were observed during deprotection (as seen in SEC). In all of the polymers in this study, great care was taken to remove trace catalyst so that no coupling was apparent.

Azide substituted asymmetric perylene diimide groups (7) were attached to the polyacrylate backbone by click chemistry with  $\text{CuBr}$  as the catalyst in the presence of PMDTA. The success of the click reaction yielding block copolymer (8) was confirmed by the disappearance of  $\text{C}\equiv\text{CH}$  (2.50 ppm) in  $^1\text{H}$  NMR spectra and an expected increase in polymer size observed in SEC. After the reaction, the polymer solution was filtered through neutral alumina column twice to remove the copper catalyst completely. Since (7) is soluble in acetone and (8) is not soluble in acetone, the excess of (7) was removed *via* precipitating from acetone three times. The narrow molecular weight distribution (Table 1) from SEC suggests no crosslinking reactions occurred during the click reaction. UV-Vis spectroscopy indicates that perylene diimide functionalized homopolymer absorbs sharply at 485 nm and P3HT absorbs broadly at 453 nm. Figure 3.3 shows a three dimensional SEC plot showing wavelength, absorbance, and molecular weight from a SEC fitted with a photodiode array detector in its effluent stream. Trace P3HT homopolymer has the expected broad absorbance centered at 453 nm. Only after the coupling with a perylene diimide containing block does the polymer assume a higher molecular weight (20kg/mol) and absorbances at both 485 nm and 453 nm, indicating the successful incorporation of both functionalities onto the polymer chain. Molecular weights found using SEC are determined by using polystyrene calibrations and tend to reflect chain shape rather than the true molecular weight. As a result, molecular weights shown in Table 3.1 are derived by from NMR analysis.

**3.3.2 Self-Assembly of the Bifunctional Block Copolymer.** While block copolymer chemistries improve the efficiency of dissociating excitons, the level of long range ordering of the block copolymer nanostructures is expected to be crucial in optimizing performance. When casting quickly, block copolymers can be prevented from ordering, leading to molecular scale mixing of the two blocks. Casting slightly slower will lead to poor ordering which establishes interfaces between the donor and acceptor but does not

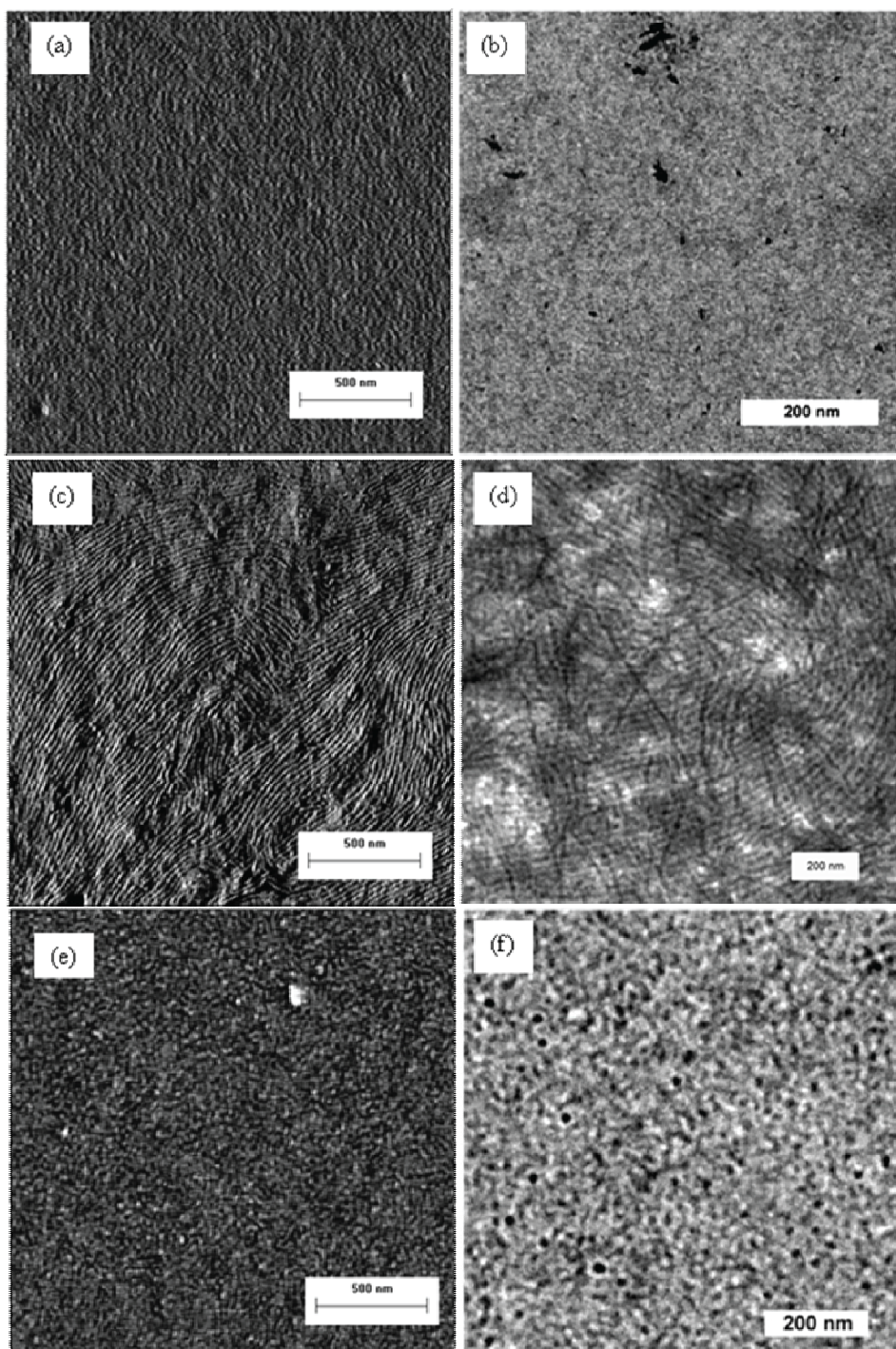


**Figure 3.4. Block Copolymer Nanostructure**

AFM tapping mode phase images and TEM plane view images of P3HT-PTP4AP with (a)(b) disordered structures, (c)(d) long range order, and (e)(f) poorly organized nanostructures. TEM contrast originates from  $I_2$  staining of P3HT. AFM contrast originates from the mechanical property contrast between the blocks.

lead to the long range continuity of the domains. If annealed or cast slowly, block copolymers will self assemble into long range periodic structures. Herein we demonstrate the effect of this variation in self assembly on device performance.

Rod-coil block copolymer 8a (PTP4AP) was chosen to study the effect of long range order on solar cell device performance. Surface chemistries and thermal/solvent histories are well known to influence the detailed order of block copolymers<sup>68</sup>. Care was therefore taken such that all samples studied via AFM and TEM exactly replicated actual devices including the presence of a PEDOT:PSS substrate surface. Disordered, molecularly mixed thin films of block copolymer PTP4AP were prepared by spin coating (rapid drying) PTP4AP solution in toluene onto the PEDOT:PSS passivation layer, as shown in Figure 3.4 (AFM and TEM micrographs showing a lack of nanostructure). The lack of order results from the relatively fast casting of a bulky, kinetically hindered block copolymer. These conditions do not allow for the time and molecular mobility necessary for self-assembly. In order to obtain structures with well defined nanodomains, drop casting and solvent annealing were used to prolong the thin film self-assembly process. A dilute block copolymer PTP4AP ( $0.5 \text{ mg mL}^{-1}$  or  $1 \text{ mg mL}^{-1}$  in toluene) solution was drop casted on PEDOT:PSS. Evaporation of the solvent was slowed by covering the container containing the substrate and liquid film. As shown in Figure 3.4, this casting technique resulted in nanostructures (periodicity = 26.8 nm, as calculated from 2D Fourier transforms of the TEM image) with long range order, stereotypical of either block copolymer self-assembly or P3HT fibril formation.

Electron microscopy samples were obtained by floating the film off of the PEDOT:PSS substrate and picking up the films on a copper grid. The films were then stained with  $\text{I}_2$  or  $\text{RuO}_4$  which makes the P3HT segments appear dark in the TEM (as confirmed via staining of macrophase separated blends). The images in Figure 3.4 show projections through the top plane of the film and indicate that either nanostructured cylinders with long axes parallel to the substrate or lamellae lying perpendicular to the substrate. Cross-sectional transmission electron microscopy studies using focused ion beam etching (FIB) is used to distinguish between these two types of nanostructures. As shown in Figure 3.5, the nanodomains have a circular cross section and appear to lie with their long axes parallel to the substrate. Contrast in the AFM phase images (Fig. 3c) derives from mechanical property difference between the P3HT and polyacrylate blocks in the block copolymers. The polyacrylate regions appear softer and stickier. The characteristic domain spacing of the block copolymer (26.8 nm) is of the same order as the exciton diffusion length, resulting in a promising morphology to efficiently charge separation at the DA interface. Cylindrical nanosegregated morphologies in P3HT containing block copolymers have been attributed to both block copolymer driven self-assembled cylinders<sup>26</sup> and the crystallization of P3HT<sup>69, 70</sup> resulting in cylindrical fibrils. Since both of these phenomena result in structures of similar size and degree of

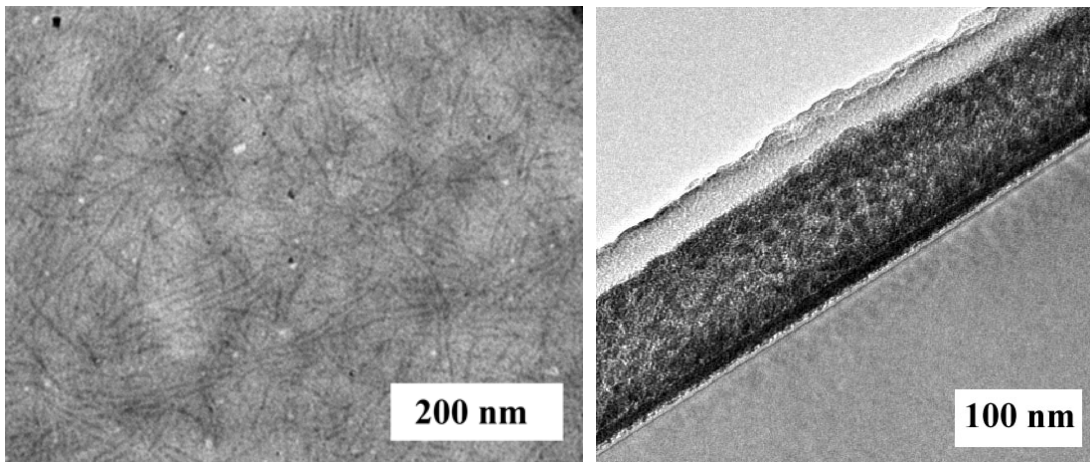


**Figure 3.5. Internal film Morphology**

TEM plane view (a) and cross-sectional (b) images of P3HT-PTP4AP confirming the morphology of long range order samples consist of fibrillic cylinders lying parallel to the surface. Cross-sectional sample were prepared by FIB. Contrast originates from  $\text{RuO}_4$  which is used to stain the P3HT.



long range order, it is not possible to distinguish the driving force for the nanostructures shown here.

Nanostructures with intermediate degrees of order were achieved by spin-coating disordered films and then exposing them to high vapor pressures of a non-selective solvent to impart mobility to the chains. Structures shown in Figures 4e and 4f were fabricated by first spin-coating and then annealing in a saturated vapor of toluene for 12 hrs. The characteristic domain spacing (25.4 nm calculated from fast fourier transform (FFT) analysis of the TEM image) from solvent annealed films is very similar to the drop-cast films but significantly less order is present.

**3.3.3 Device Behavior of Self-Assembled Film.** To evaluate the effect of morphology on device behavior, the casting procedures above were used to fabricate thin film solar cells. As shown in Figure 3.2, the same PEDOT:PSS layer served as the substrate to the block copolymer film, but in this case PEDOT:PSS was stacked on top of the glass/ITO anode. After casting and/or annealing of the block copolymer layer, an aluminum cathode was evaporated onto the film. Devices were then characterized by current-voltage measurements under an illumination of  $100 \text{ mW cm}^{-2}$  (AM 1.5G conditions).

Increases in power conversion efficiencies ( $\eta$ ) are related to increases in the short-circuit current density ( $J_{sc}$ ), the open circuit voltage ( $V_{oc}$ ), and the fill factor (FF). The  $J_{sc}$  is the current value when the solar cell is at zero bias and is related to the amount of absorbed light and charge carrier mobilities of the organic materials. More light absorption and higher mobilities will generate higher  $J_{sc}$  by creating more excitons and transporting the resulting charges more efficiently. The  $V_{oc}$  is the voltage produced when the current in the cell equals zero. It has been suggested that in bulk heterojunction cells, the limited  $V_{oc}$  is related to the energy difference between the HOMO of the donor and the LUMO of the acceptor.<sup>71, 72</sup> The FF is the ratio of the maximum power produced to the product of the short circuit current and the open circuit voltage. Ideally, the fill factor should be unity, but losses due to inefficiencies in charge transport and recombination result in typical values between 0.2~0.7 for organic solar cells. Previous studies suggest that the solar cell device thickness has a strong effect on performance as it can be tuned to optimize both charge transport (important in materials with low charge mobility) and light absorption.<sup>71, 72</sup> The thicknesses in spun-cast devices can be controlled exactly. As a result, the films which were molecularly mixed or poorly organized nanostructures could be prepared over a wide range of thicknesses. For active layers with well formed, but poorly ordered nanostructures, power conversion efficiencies ( $\eta$ ) of the devices increased as film thicknesses increased from 70 nm to 103 nm after which the efficiency became thickness independent indicating that maximum absorption had been reached. This also indicates the device thickness has little effect on

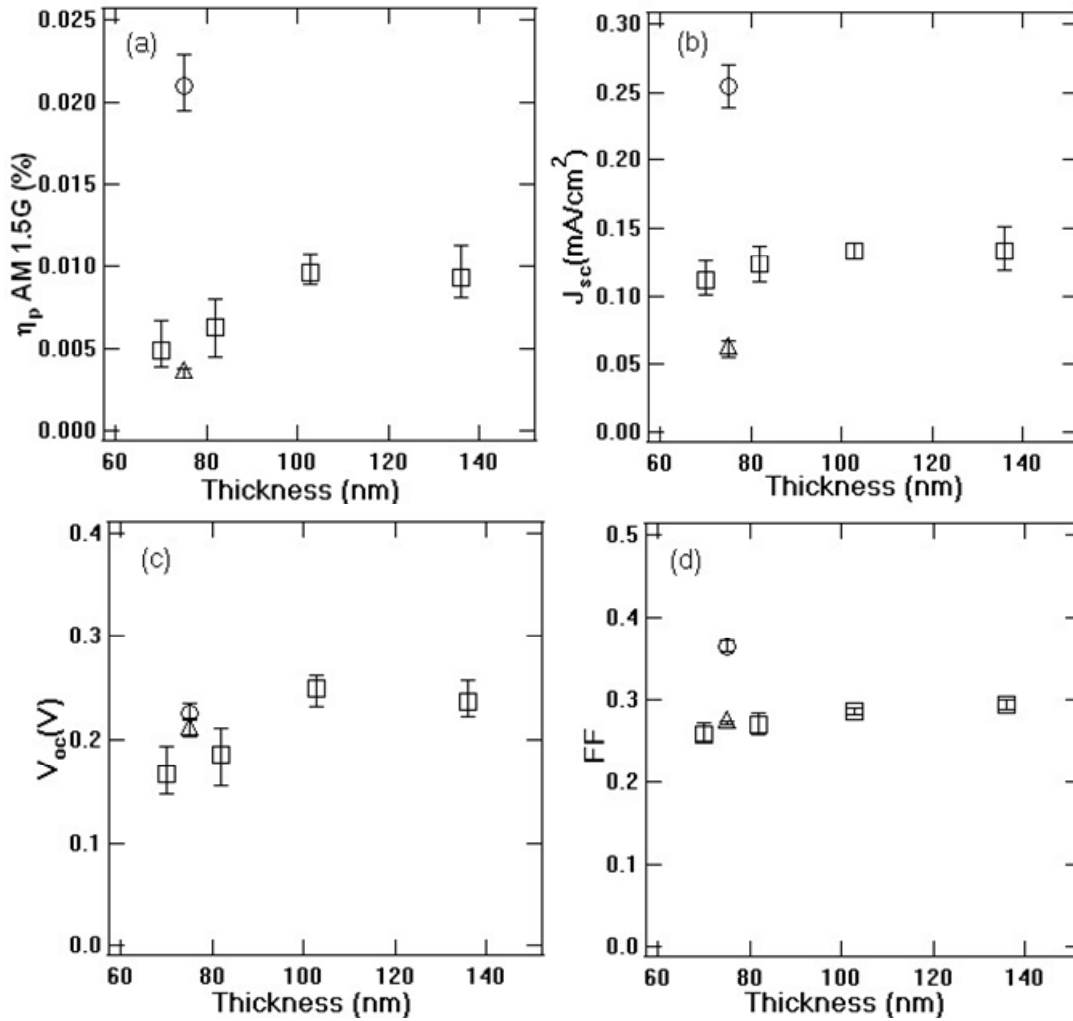


**Figure 3.6. Photovoltaic device performance**

Solar cell devices of PTP4AP  $\Delta$ =disorder,  $\square$ =long range order and  $\circ$ =poorly organized nanostructures. In all cases, the sample with poorly organized nanostructure shows increased power conversion efficiency (a), short-circuit current density (b), open circuit voltage (c), and fill factor (d) under AM 1.5, 100 mV cm<sup>-2</sup> conditions.

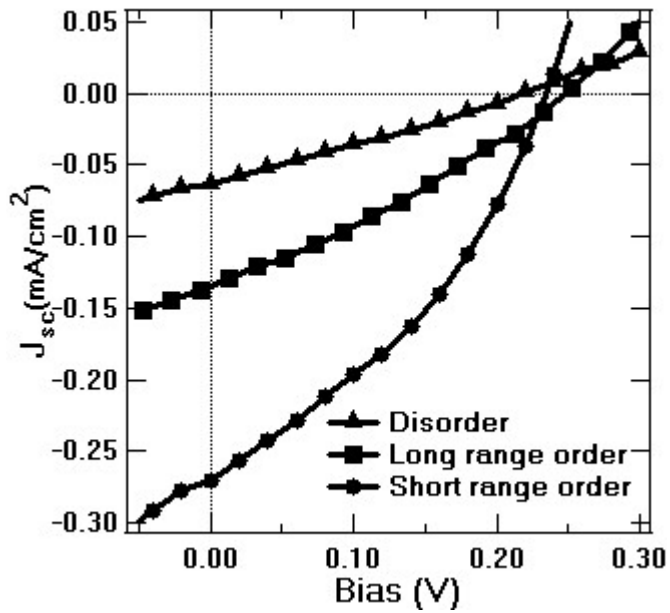


**Figure 3.7. Effect of ordering on efficiency**

Plot of current density versus voltage for photovoltaics devices constructed from PTP4AP under different prepared conditions. ▲ = disorder structures, ■ = long range order nanostructures, ● = poorly organized nanostructures. The solar cell devices with poorly organized nanostructures show the best device performance.

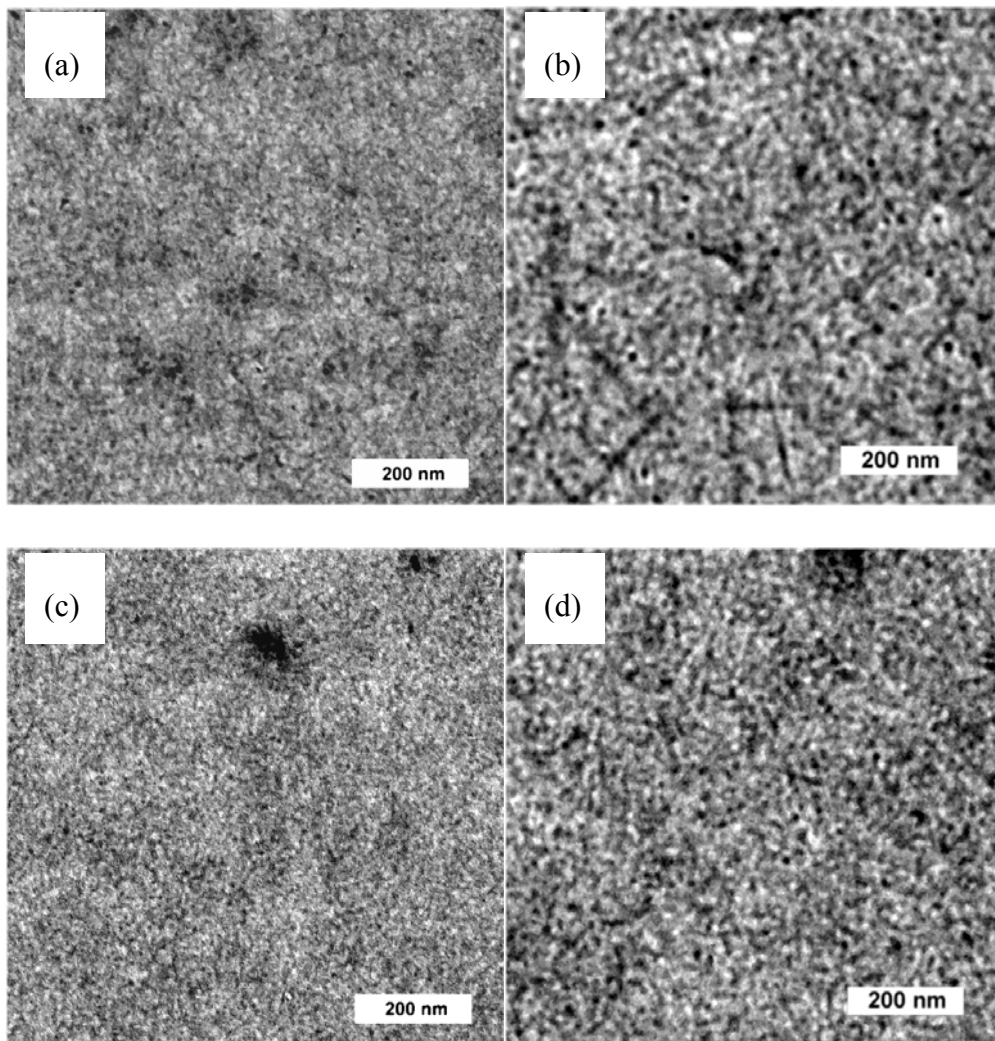


**Figure 3.8. Effect of butyl acrylate on morphology**

Poorly organized nanostructures of block copolymer with varying fractions of low glass transition (plasticizing) butyl acrylate after solvent annealed in toluene. (a) PTP2AP, (c) PTPP for 0h, (b) PTP2AP for 12h, and (d) PTPP for 24h.

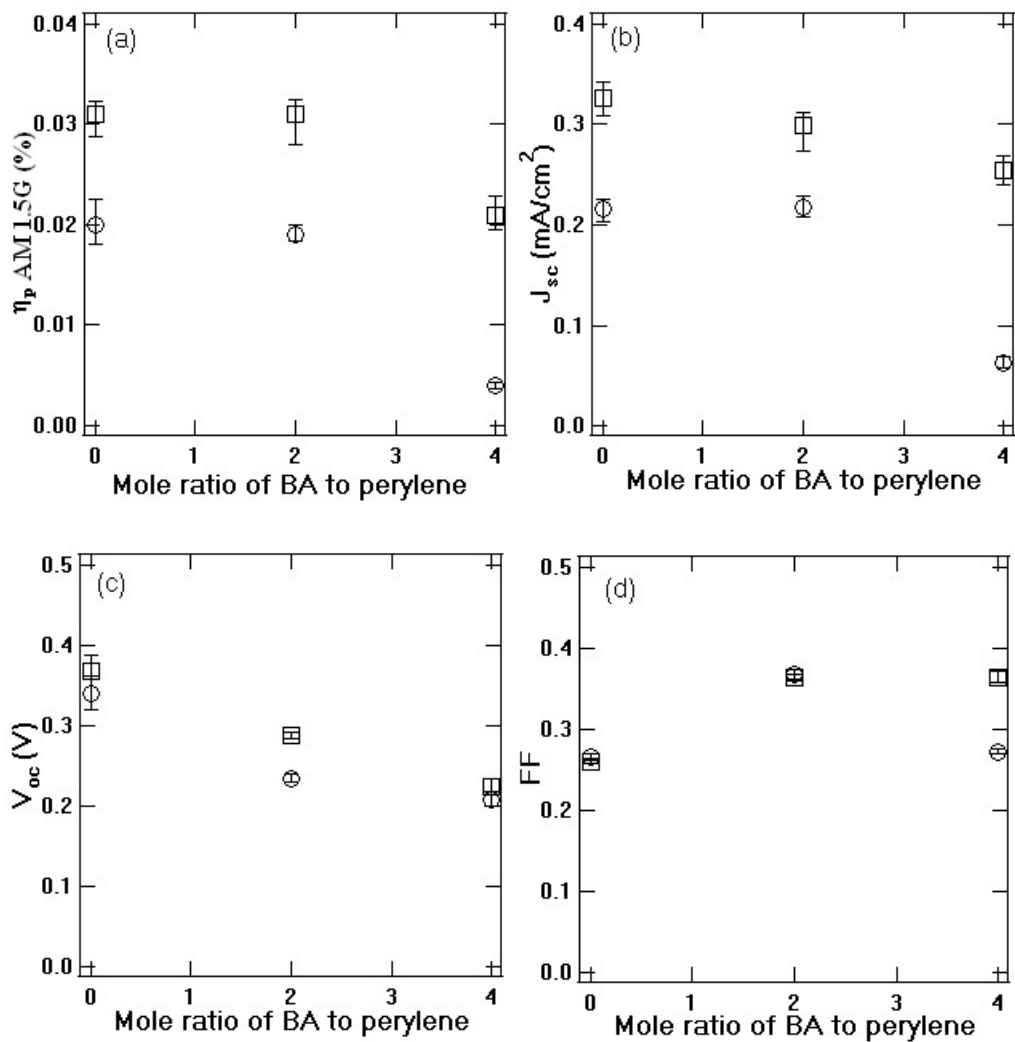


**Figure 3.9. Effect of butyl acrylate on device performance**

Solar cell devices made by from block copolymer as a function of mole ratio of  $N_{\text{perylene}}$  and  $N_{\text{butyl acrylate}}$ . (a) Variation of power conversion efficiency, (b) short-circuit current density, (c) voltage, and (d) fill factor under AM 1.5, 100 mV cm<sup>-2</sup> conditions. ○=disorder □=poor order.

the charge transport efficiency in the thickness ranged studied. In comparison, molecularly mixed active layers had lower  $J_{sc}$ 's indicating that the formation of well defined, but poorly organized nanostructures results in improved charge carrier mobilities. As expected, the  $V_{oc}$ 's and FF were similar in the two devices.

As shown in Figure 3.6, we find that charge mobility improves when going from a molecularly mixed to a well-defined but poorly organized nanostructure. The structure with truly long-range order, reminiscent of classical block copolymers behaves worse than the poorly organized sample. We postulate that this difference is related to the detailed morphology and particularly the orientation of the anisotropic structures in the well ordered sample. While these cylindrical nanostructures are well defined, they lie with their long axis parallel to the electrodes which does not allow for efficient charge transport throughout the device.

The enhancements seen in the  $J_{sc}$  and FF for the poorly organized nanostructures suggest that this morphology results in better hole and electron transport. TEM micrographs (Fig. 3f) indicate that this nanostructure's lack of organization may result in a lack of directionality in the morphology which leads to improved charge transport pathways. In comparison, the cylindrical structure is aligned with its long axes running parallel to the electrodes. It appears likely that this orientation is detrimental, particularly to hole transport (P3HT is on the inside of the cylinders). Many techniques exist to control nanodomain orientation within block copolymer thin films and it is clear that the use of these techniques could be advantageous to device performance<sup>68</sup>

**3.3.4 The Effect of Chemical Structure.** It is possible that the presence of bulky, crystalline perylene diimide results in decreased chain mobility and therefore poor self-assembly. Butyl acrylate was co-polymerized with the precursor for the perylene diimide segments to improve chain mobility. Clearly the incorporation of this insulating monomer will affect charge mobility so the amount of butyl acrylate was optimized to both allow for both optimal self-assembly into ordered structures while still allowing charge transport. Here, the block copolymer was varied so as to keep the number of perylene diimide groups per chain ( $N_{\text{perylene}}$ ) constant while varying their spacing by inserting more or fewer butyl acrylate groups along the chain, as shown in Scheme 2.

Similar to the previously discussed PTP4AP, block copolymers with less butyl acrylate ( PTP2AP and PPTP) show no nanophase segregation when films are spin cast from toluene(Fig. 8a,c). After solvent annealing in toluene, they all show poorly organized nanostructures (Fig. 8b,d) and have very similar morphologies to PTP4AP. As expected, large amounts of insulating butyl acrylate monomer is detrimental to device performance (particularly efficiency and  $J_{sc}$ ), but this effect tapers off at lower ratios around 2:1 butyl acrylate to perylene diimide ratio. This indicates that an optimum may

exist in which some butyl acrylate may be added to improve self-assembly without damaging device performance. In each case, the self-assembled (poorly ordered) device showed superior performance compared to the disordered system.

### 3.4. Conclusions

The synthesis of well defined functional rod-coil block copolymers P3HT-b-poly(BA-stat-PerAcr) containing electron donor (P3HT) and acceptor (perylene) moieties with narrow molecular weight distributions has been demonstrated. The block copolymer PTP4AP forms disordered structures, poorly organized nanostructures and long range ordered nanostructures depending on the time allowed for self-assembly. Samples with well defined interfaces but poorly organized nanostructures had significantly improved device performances. Samples with long range nanostructure formed cylindrical fibrils and performed poorly because the long axis of the nanostructure ran parallel to the electrodes, limiting charge transport. It should be possible to increase the device efficiency by orienting the long range block copolymer structure perpendicular to the electrodes. Chain mobility can be increased in to enhance self assembly by incorporating plasticizing butyl acrylate groups into the perylene domain in the block copolymer with relatively little affect on device performance.

### 3.5. Acknowledgments

We gratefully acknowledge support from the Department of Energy Office of Basic Energy Sciences (DOE-BES) through the Plastic Electronics Program at Lawrence Berkeley National Lab (LBNL). We thank the Alivisatos group at UC Berkeley and the National Center for Electron Microscopy (NCEM) for assistance and use of instrumentation employed in this study.

### 3.6. References

1. Brabec, C. J.; Sariciftci, N. S.; Hummelen, J. C., Plastic solar cells. *Advanced Functional Materials* **2001**, 11, (1), 15-26.
2. Bredas, J. L.; Cornil, J.; Heeger, A. J., The exciton binding energy in luminescent conjugated polymers. *Advanced Materials* **1996**, 8, (5), 447-&.
3. Milner, R. G.; Arias, A. C.; Stevenson, R.; Mackenzie, J. D.; Richards, D.; Friend, R. H.; Kang, D. J.; Blamire, M., Phase separation in polyfluorene blends investigated with complementary scanning probe microscopies. *Materials Science and Technology* **2002**, 18, (7), 759-762.

4. Voigt, M.; Chappell, J.; Rowson, T.; Cadby, A.; Geoghegan, M.; Jones, R. A. L.; Lidzey, D. G., The interplay between the optical and electronic properties of light-emitting-diode applicable conjugated polymer blends and their phase-separated morphology. *Organic Electronics* **2005**, 6, (1), 35-45.
5. Higgins, A. M.; Martin, S. J.; Thompson, R. L.; Chappell, J.; Voigt, M.; Lidzey, D. G.; Jones, R. A. L.; Geoghegan, M., Surface segregation and self-stratification in blends of spin-cast polyfluorene derivatives. *Journal of Physics-Condensed Matter* **2005**, 17, (8), 1319-1328.
6. Tang, C. W., 2-Layer Organic Photovoltaic Cell. *Applied Physics Letters* **1986**, 48, (2), 183-185.
7. Yu, G.; Gao, J.; Hummelen, J. C.; Wudl, F.; Heeger, A. J., Polymer Photovoltaic Cells - Enhanced Efficiencies Via a Network of Internal Donor-Acceptor Heterojunctions. *Science* **1995**, 270, (5243), 1789-1791.
8. Bull, T. A.; Pingree, L. S. C.; Jenekhe, S. A.; Ginger, D. S.; Luscombe, C. K., The Role of Mesoscopic PCBM Crystallites in Solvent Vapor Annealed Copolymer Solar Cells. *ACS Nano* **2009**, 3, (3), 627-636.
9. Shaheen, S. E.; Brabec, C. J.; Sariciftci, N. S.; Padinger, F.; Fromherz, T.; Hummelen, J. C., 2.5% efficient organic plastic solar cells. *Applied Physics Letters* **2001**, 78, (6), 841-843.
10. Chirvase, D.; Parisi, J.; Hummelen, J. C.; Dyakonov, V., Influence of nanomorphology on the photovoltaic action of polymer-fullerene composites. *Nanotechnology* **2004**, 15, (9), 1317-1323.
11. Hoppe, H.; Niggemann, M.; Winder, C.; Kraut, J.; Hiesgen, R.; Hinsch, A.; Meissner, D.; Sariciftci, N. S., Nanoscale morphology of conjugated polymer/fullerene-based bulk-heterojunction solar cells. *Advanced Functional Materials* **2004**, 14, (10), 1005-1011.
12. Ma, W. L.; Yang, C. Y.; Gong, X.; Lee, K.; Heeger, A. J., Thermally stable, efficient polymer solar cells with nanoscale control of the interpenetrating network morphology. *Advanced Functional Materials* **2005**, 15, (10), 1617-1622.
13. Yang, X. N.; Loos, J.; Veenstra, S. C.; Verhees, W. J. H.; Wienk, M. M.; Kroon, J. M.; Michels, M. A. J.; Janssen, R. A. J., Nanoscale morphology of high-performance polymer solar cells. *Nano Letters* **2005**, 5, (4), 579-583.



14. Hoppe, H.; Sariciftci, N. S., Morphology of polymer/fullerene bulk heterojunction solar cells. *Journal of Materials Chemistry* **2006**, 16, (1), 45-61.
15. Bates, F. S.; Fredrickson, G. H., Block copolymers - Designer soft materials. *Physics Today* **1999**, 52, (2), 32-38.
16. Olsen, B. D.; Segalman, R. A., Self-assembly of rod-coil block copolymers. *Materials Science & Engineering R-Reports* **2008**, 62, (2), 37-66.
17. Lee, M.; Cho, B. K.; Zin, W. C., Supramolecular structures from rod-coil block copolymers. *Chemical Reviews* **2001**, 101, (12), 3869-3892.
18. Pryamitsyn, V.; Ganesan, V., Self-assembly of rod-coil block copolymers. *Journal of Chemical Physics* **2004**, 120, (12), 5824-5838.
19. Reenders, M.; ten Brinke, G., Compositional and orientational ordering in rod-coil diblock copolymer melts. *Macromolecules* **2002**, 35, (8), 3266-3280.
20. Holyst, R.; Schick, M., Correlations in a Rigid - Flexible Diblock Copolymer System. *Journal of Chemical Physics* **1992**, 96, (1), 730-740.
21. Williams, D. R. M.; Fredrickson, G. H., Cylindrical Micelles in Rigid-Flexible Diblock Copolymers. *Macromolecules* **1992**, 25, (13), 3561-3568.
22. Olsen, B. D.; Segalman, R. A., Structure and thermodynamics of weakly segregated rod-coil block copolymers. *Macromolecules* **2005**, 38, (24), 10127-10137.
23. Olsen, B. D.; Shah, M.; Ganesan, V.; Segalman, R. A., Universalization of the phase diagram for a model rod-coil diblock copolymer. *Macromolecules* **2008**, 41, (18), 6809-6817.
24. Sary, N.; Rubatat, L.; Brochon, C.; Hadziioannou, G.; Ruokolainen, J.; Mezzenga, R., Self-assembly of poly(diethylhexyloxy-p-phenylenevinylene)-b-poly(4-vinylpyridine) rod-coil block copolymer systems. *Macromolecules* **2007**, 40, (19), 6990-6997.
25. Olsen, B. D.; Segalman, R. A., Nonlamellar phases in asymmetric rod-coil block copolymers at increased segregation strengths. *Macromolecules* **2007**, 40, (19), 6922-6929.
26. Dai, C. A.; Yen, W. C.; Lee, Y. H.; Ho, C. C.; Su, W. F., Facile synthesis of well-defined block copolymers containing regioregular poly(3-hexyl thiophene) via anionic macroinitiation method and their self-assembly behavior. *Journal of the American Chemical Society* **2007**, 129, (36), 11036-+.

27. Olsen, B. D.; Toney, M. F.; Segalman, R. A., Square Grains in Asymmetric Rod-Coil Block Copolymers. *Langmuir* **2008**, 24, (5), 1604-1607.
28. Olsen, B. D.; Li, X. F.; Wang, J.; Segalman, R. A., Thin film structure of symmetric rod-coil block copolymers. *Macromolecules* **2007**, 40, (9), 3287-3295.
29. de Boer, B.; Stalmach, U.; van Hutten, P. F.; Melzer, C.; Krasnikov, V. V.; Hadziioannou, G., Supramolecular self-assembly and opto-electronic properties of semiconducting block copolymers. *Polymer* **2001**, 42, (21), 9097-9109.
30. Barrau, S.; Heiser, T.; Richard, F.; Brochon, C.; Ngov, C.; van de Wetering, K.; Hadziioannou, G.; Anokhin, D. V.; Ivanov, D. A., Self-assembling of novel fullerene-grafted donor-acceptor rod-coil block copolymers. *Macromolecules* **2008**, 41, (7), 2701-2710.
31. Heiser, T.; Adamopoulos, G.; Brinkmann, M.; Giovanella, U.; Ould-Saad, S.; Brochon, C.; van de Wetering, K.; Hadziioannou, G., Nanostructure of self-assembled rod-coil block copolymer films for photovoltaic applications. *Thin Solid Films* **2006**, 511, 219-223.
32. Van De Wetering, K.; Brochon, C.; Ngov, C.; Hadziioannou, G., Design and synthesis of a low band gap conjugated macroinitiator: Toward rod-coil donor-acceptor block copolymers. *Macromolecules* **2006**, 39, (13), 4289-4297.
33. van der Veen, M. H.; de Boer, B.; Stalmach, U.; van de wetering, K. I.; Hadziioannou, G., Donor-acceptor diblock copolymers based on PPV and C-60: Synthesis, thermal properties, and morphology. *Macromolecules* **2004**, 37, (10), 3673-3684.
34. Guntner, R.; Asawapirom, U.; Forster, M.; Schmitt, C.; Stiller, B.; Tiersch, B.; Falcou, A.; Nothofer, H. G.; Scherf, U., Conjugated polyfluorene/polyaniline block copolymers - improved synthesis and nanostructure formation. *Thin Solid Films* **2002**, 417, (1-2), 1-6.
35. Asawapirom, U.; Guntner, R.; Forster, M.; Scherf, U., Semiconducting block copolymers - synthesis and nanostructure formation. *Thin Solid Films* **2005**, 477, (1-2), 48-52.
36. Tu, G. L.; Li, H. B.; Forster, M.; Heiderhoff, R.; Balk, L. J.; Scherf, U., Conjugated triblock copolymers containing both electron-donor and electron-acceptor blocks. *Macromolecules* **2006**, 39, (13), 4327-4331.
37. Lindner, S. M.; Thelakkat, M., Nanostructures of n-type organic semiconductor in a p-type matrix via self-assembly of block copolymers. *Macromolecules* **2004**, 37, (24), 8832-8835.

38. Lindner, S. M.; Huttner, S.; Chiche, A.; Thelakkat, M.; Krausch, G., Charge separation at self-assembled nanostructured bulk interface in block copolymers. *Angewandte Chemie-International Edition* **2006**, 45, (20), 3364-3368.
39. Sommer, M.; Thelakkat, M., Synthesis, characterization and application of donor-acceptor block copolymers in nanostructured bulk heterojunction solar cells. *European Physical Journal-Applied Physics* **2006**, 36, (3), 245-249.
40. Lindner, S. M.; Kaufmann, N.; Thelakkat, M., Nanostructured semiconductor block copolymers: pi-pi Stacking, optical and electrochemical properties. *Organic Electronics* **2007**, 8, (1), 69-75.
41. Sommer, M.; Lindner, S. M.; Thelakkat, M., Microphase-separated donor-acceptor diblock copolymers: Influence of HOMO energy levels and morphology on polymer solar cells. *Advanced Functional Materials* **2007**, 17, (9), 1493-1500.
42. Sommer, M.; Lang, A. S.; Thelakkat, M., Crystalline-crystalline donor-acceptor block copolymers. *Angewandte Chemie-International Edition* **2008**, 47, (41), 7901-7904.
43. Michael Sommer, Andreas S. L. M. T., Crystalline-Crystalline Donor-Acceptor Block Copolymers13. *Angewandte Chemie International Edition* **2008**, 47, (41), 7901-7904.
44. Zhang, Q.; Cirpan, A.; Russell, T. P.; Emrick, T., Donor&#x2212;Acceptor Poly(thiophene-block-perylene diimide) Copolymers: Synthesis and Solar Cell Fabrication. *Macromolecules* 0, (0).
45. Siringhaus, H.; Brown, P. J.; Friend, R. H.; Nielsen, M. M.; Bechgaard, K.; Langeveld-Voss, B. M. W.; Spiering, A. J. H.; Janssen, R. A. J.; Meijer, E. W.; Herwig, P.; de Leeuw, D. M., Two-dimensional charge transport in self-organized, high-mobility conjugated polymers. *Nature* **1999**, 401, (6754), 685-688.
46. Sommer, M.; Huttner, S.; Wunder, S.; Thelakkat, M., Electron-Conducting Block Copolymers: Morphological, Optical, and Electronic Properties. *Advanced Materials* **2008**, 9999, 1-5.
47. Nakamura, J.; Yokoe, C.; Murata, K.; Takahashi, K., Efficient organic solar cells by penetration of conjugated polymers into perylene pigments. *Journal of Applied Physics* **2004**, 96, (11), 6878-6883.
48. de Bettignies, R.; Nicolas, Y.; Blanchard, P.; Levillain, E.; Nunzi, J. M.; Roncali, J., Planarized star-shaped oligothiophenes as a new class of organic semiconductors for heterojunction solar cells. *Advanced Materials* **2003**, 15, (22), 1939-+.

49. Breeze, A. J.; Salomon, A.; Ginley, D. S.; Gregg, B. A.; Tillmann, H.; Horhold, H. H., Polymer-perylene diimide heterojunction solar cells. *Applied Physics Letters* **2002**, 81, (16), 3085-3087.
50. Kim, J. Y.; Bard, A. J., Organic donor/acceptor heterojunction photovoltaic devices based on zinc phthalocyanine and a liquid crystalline perylene diimide. *Chemical Physics Letters* **2004**, 383, (1-2), 11-15.
51. Dittmer, J. J.; Marseglia, E. A.; Friend, R. H., Electron trapping in dye/polymer blend photovoltaic cells. *Advanced Materials* **2000**, 12, (17), 1270-+.
52. Neuteboom, E. E.; Meskers, S. C. J.; van Hal, P. A.; van Duren, J. K. J.; Meijer, E. W.; Janssen, R. A. J.; Dupin, H.; Pourtois, G.; Cornil, J.; Lazzaroni, R.; Bredas, J. L.; Beljonne, D., Alternating oligo(p-phenylene vinylene)-perylene bisimide copolymers: Synthesis, photophysics, and photovoltaic properties of a new class of donor-acceptor materials. *Journal of the American Chemical Society* **2003**, 125, (28), 8625-8638.
53. Liu, Y.; Yang, C. H.; Li, Y. J.; Li, Y. L.; Wang, S.; Zhuang, J. P.; Liu, H. B.; Wang, N.; He, X. R.; Li, Y. F.; Zhu, D. B., Synthesis and photovoltaic characteristics of novel copolymers containing poly(phenylenevinylene) and triphenylamine moieties connected at 1,7 bay positions of perylene bisimide. *Macromolecules* **2005**, 38, (3), 716-721.
54. Shin, W. S.; Jeong, H. H.; Kim, M. K.; Jin, S. H.; Kim, M. R.; Lee, J. K.; Lee, J. W.; Gal, Y. S., Effects of functional groups at perylene diimide derivatives on organic photovoltaic device application. *Journal of Materials Chemistry* **2006**, 16, (4), 384-390.
55. Shin, W. S.; Jung, H. H.; Kim, M. K.; Kim, M. R.; Kim, M. K.; Naidu, B. V. K.; Jin, S. H.; Lee, J. K.; Lee, J. W.; Gal, Y. S., Photovoltaic properties of N-pyrrolidinyl substituted perylenebis(dicarboximide) derivatives. *Molecular Crystals and Liquid Crystals* **2007**, 462, 59-66.
56. Li, J. L.; Dierschke, F.; Wu, J. S.; Grimsdale, A. C.; Mullen, K., Poly(2,7-carbazole) and perylene tetracarboxydiimide: a promising donor/acceptor pair for polymer solar cells. *Journal of Materials Chemistry* **2006**, 16, (1), 96-100.
57. Ladmiral, V.; Mantovani, G.; Clarkson, G. J.; Cauet, S.; Irwin, J. L.; Haddleton, D. M., Synthesis of neoglycopolymers by a combination of "click chemistry" and living radical polymerization. *Journal of the American Chemical Society* **2006**, 128, (14), 4823-4830.
58. Jeffries-El, M.; Sauve, G.; McCullough, R. D., Facile synthesis of end-functionalized regioregular poly(3-alkylthiophene)s via modified Grignard metathesis reaction. *Macromolecules* **2005**, 38, (25), 10346-10352.

59. Langhals, H.; Saulich, S., Bichromophoric perylene derivatives: energy transfer from non-fluorescent chromophores. *Chemistry-a European Journal* **2002**, 8, (24), 5630-5643.
60. Kaiser, H.; Lindner, J.; Langhals, H., Synthesis of Nonsymmetrically Substituted Perylene Fluorescent Dyes. *Chemische Berichte* **1991**, 124, (3), 529-535.
61. MJ Park, S. K., AM Minor, A Hexemer, NP Balsara, Control of Domain Orientation in Block Copolymer Electrolyte Membranes at the Interface with Humid Air. *Advanced Materials* **2009**, 21, (2), 203-208.
62. Stalmach, U.; de Boer, B.; Videlot, C.; van Hutten, P. F.; Hadziioannou, G., Semiconducting diblock copolymers synthesized by means of controlled radical polymerization techniques. *Journal of the American Chemical Society* **2000**, 122, (23), 5464-5472.
63. Matyjaszewski, K.; Xia, J. H., Atom transfer radical polymerization. *Chemical Reviews* **2001**, 101, (9), 2921-2990.
64. Francke, V.; Rader, H. J.; Geerts, Y.; Mullen, K., Synthesis and characterization of a poly(para-phenyleneethynylene)-block-poly(ethylene oxide) rod-coil block copolymer. *Macromolecular Rapid Communications* **1998**, 19, (6), 275-281.
65. Iovu, M. C.; Jeffries-El, M.; Zhang, R.; Kowalewski, T.; McCullough, R. D., Conducting block copolymer nanowires containing regioregular poly(3-hexylthiophene) and polystyrene. *Journal of Macromolecular Science Part a-Pure and Applied Chemistry* **2006**, 43, (12), 1991-2000.
66. Rostovtsev, V. V.; Green, L. G.; Fokin, V. V.; Sharpless, K. B., A stepwise Huisgen cycloaddition process: Copper(I)-catalyzed regioselective "ligation" of azides and terminal alkynes. *Angewandte Chemie-International Edition* **2002**, 41, (14), 2596-+.
67. Opsteen, J. A.; van Hest, J. C. M., Modular synthesis of block copolymers via cycloaddition of terminal azide and alkyne functionalized polymers. *Chemical Communications* **2005**, (1), 57-59.
68. Segalman, R. A., Patterning with block copolymer thin films. *Materials Science & Engineering R-Reports* **2005**, 48, (6), 191-226.
69. Craley, C. R.; Zhang, R.; Kowalewski, T.; McCullough, R. D.; Stefan, M. C., Regioregular Poly(3-hexylthiophene) in a Novel Conducting Amphiphilic Block Copolymer. *Macromolecular Rapid Communications* **2009**, 30, (1), 11-16.
70. Singh, K. A.; Sauve, G.; Zhang, R.; Kowalewski, T.; McCullough, R. D.; Porter, L. M., Dependence of field-effect mobility and contact resistance on nanostructure in

regioregular poly(3-hexylthiophene) thin film transistors. *Applied Physics Letters* **2008**, 92, (26), 263303.

71. Li, G.; Shrotriya, V.; Yao, Y.; Yang, Y., Investigation of annealing effects and film thickness dependence of polymer solar cells based on poly(3-hexylthiophene). *Journal of Applied Physics* **2005**, 98, (4), -.

72. Sievers, D. W.; Shrotriya, V.; Yang, Y., Modeling optical effects and thickness dependent current in polymer bulk-heterojunction solar cells. *Journal of Applied Physics* **2006**, 100, (11), -.

## Chapter 4. Increased Order-Disorder Transition Temperature for a Rod-Coil Block Copolymer in the Presence of a Magnetic Field

Reproduced with permission from Bryan McCulloch, Giuseppe Portale, Wim Bras and Rachel A. Segalman. *Reproduced by permission of the American Chemical Society* (<http://pubs.acs.org/doi/abs/10.1021/ma201093r>)

The magnetic field alignment of main-chain liquid crystalline block copolymers is strongly dependent on processing history with the highest degree of alignment obtained by cooling from the disordered state through the microphase order-disorder transition (ODT) in the presence of the field. By using *in situ* small angle X-ray scattering in 2 Tesla and 7 Tesla magnetic fields, an increase in the order-disorder transition temperature ( $T_{\text{ODT}}$ ) with increasing applied magnetic field strength was observed. This observation is important to the understanding of liquid crystalline block copolymer alignment as it suggests the coupling between the long range liquid crystalline and block copolymer ordering may act together, dramatically affecting the phase behavior of these materials in the presence of a magnetic field.

### 4.1 Introduction

Block copolymers, capable of self-assembling on the 10 nm lengthscale, are of interest for a broad range of applications including ion transport, nanolithography and optoelectronics, many of which require tunable, periodic and aligned structures.<sup>1</sup> While electric field, shear, and surface induced alignment have all been used to control nanostructure orientation and long range order in classical polymer systems, all these techniques require restrictive geometries and direct contact with the block copolymer surface in order to achieve alignment. Nanostructured conjugated polymers are of interest for photovoltaic applications and previous work demonstrates that these materials may be aligned via magnetic fields<sup>2</sup>. In order to optimize the performance of these materials, alignment of the nanostructure is important to improve properties such as charge transport in these devices. Magnetic alignment offers unique advantages because it may be carried out without direct contact with the sample enabling efficient processing techniques while still obtaining highly aligned materials.

Liquid crystalline molecules, including many conjugated polymers, are often highly anisotropic leading to an inherent magnetic anisotropy which allows them to be easily aligned even in relatively modest magnetic fields. Since the magnetic susceptibility of a single molecule is low, typically magnetic alignment of liquid crystals requires that the magnetic field acting on the director of a large liquid crystalline domain made up of many ordered molecules to overcome thermal fluctuations. By utilizing a block copolymer with a conjugated, rigid (rod-like) moiety, molecular anisotropy is introduced into one of the block copolymer domains and an anisotropic magnetic susceptibility can be achieved in the material which produces a driving force for alignment in a magnetic field. For a rod-coil block copolymer, the backbone of the main chain rod-like polymer aligns parallel to the applied field, forcing the block copolymer interface to be perpendicular to the field.<sup>2</sup> Similarly, magnetic alignment is possible in

polymers with liquid crystalline mesogen sidechains leading to interfaces parallel to the field, however, this can lead to multiple degenerate orientations which satisfy the alignment conditions.<sup>3-8</sup> It has been shown by rotating the sample within the magnetic field this degeneracy can be broken resulting in highly aligned lamellar samples.<sup>9</sup>

While alignment of a smectic liquid crystalline phase for either sidechain or main chain liquid crystalline block copolymers is possible, typically alignment within the nematic phase produces a higher degree of alignment and requires lower fields since the nematic phase contains only orientational order, intramolecular interactions are diminished and the system has increased mobility. Previous work using liquid crystalline main chain rod-coil block copolymers has shown that annealing in the isotropic or nematic phase increases the order parameter 2 to 3 times greater than that for samples annealed only in smectic phase.<sup>2</sup> Additional work has shown aligned samples can be annealed in the smectic phase outside of a magnetic field and preserve much of their original orientation.<sup>10</sup> Osuji and coworkers have used a side chain liquid crystalline block copolymer where lithium ion conducting poly(ethylene oxide) cylinders were aligned, optimizing the ionic transport in a polymer electrolyte membrane and were able to show that the transport within the polymer membrane was improved ten-fold over the randomly oriented morphology.<sup>4, 11</sup> In the above studies, the highest degrees of order were achieved by cooling from above both the point at which the block copolymer chains become miscible (block copolymer microphase order-disorder transition temperature ( $T_{ODT}$ )).<sup>2, 7</sup> It has been postulated that by cooling from above these transition temperatures, kinetic trapping can be prevented by aligning block copolymer domains as they nucleate and grow. While it has not been previously observed, it is clear that the presence of the field may affect the transition temperatures by modulating both block copolymer interactions and providing an exterior directionality to the liquid crystal.

The effect of fields on the order-disorder transition temperature has been explored in the similar but more classical case of insulating coil-coil block copolymers in electric fields. In most cases the electric field is thought to act on the difference in the dielectric constants of the two block copolymer domains, resulting in a minimum energy when the block copolymer interfaces are oriented parallel to the electric field.<sup>12</sup> Unfortunately the difference in the dielectric constant of most block copolymer systems is relatively low requiring high electric fields which are often near the dielectric breakdown threshold of the polymer. Since the dielectric contrast between polymers is relatively small, it has been shown that the salt concentration within the polymer can increase the driving force for alignment lowering the required field strength and increasing the degree of alignment even when only trace levels of salts are present making electric field alignment sensitive to synthetic and processing conditions.<sup>13</sup> It has been predicted that the presence of an electric field may favor mixing of the block copolymer domains, causing a decrease in the  $T_{ODT}$ <sup>14, 15</sup> while others have predicted an increase in the  $T_{ODT}$  because the electric field will reduce fluctuations, stabilizing the ordered phase.<sup>16</sup> Recently, experiments have shown a small decrease in the  $T_{ODT}$  which may confirm that electric fields favor mixing near the ODT.<sup>17</sup> All of these predictions and observations also show the effect of applying an electric field on the  $T_{ODT}$  for most polymer systems should be rather small ( $\sim 2$  °C). While electric field alignment and magnetic field alignment of block



copolymers appear similar, they interact with the polymer in fundamentally different ways potentially resulting in different behavior. Liquid crystalline block copolymers lack any driving force for increased mixing at high magnetic fields and therefore we would not expect the  $T_{ODT}$  to decrease when a magnetic field is applied.

Here we show using in-situ small angle X-ray scattering (SAXS) that a magnetic field can significantly alter the thermodynamics of a main chain liquid crystalline rod-coil block copolymers. The presence of a magnetic field increases the order-disorder transition temperature substantially and can have major implications on optimizing the alignment of these materials. The magnetic field couples to the rod-like liquid crystalline block stabilizing the ordered phase. In addition the lamellar block copolymer microstructure enhances the smectic ordering leading to a much larger increase in the  $T_{ODT}$  than would be expected. Since obtaining highly aligned block copolymer structures using magnetic fields relies on accessing a disordered phase, the fact that the  $T_{ODT}$  may be dramatically increased by the presence of a magnetic field shows we must understand the *in situ* phase behavior in order to intelligently optimize alignment procedures.

## 4.2. Experimental Section

Poly(2,5-di(2'-ethylhexyloxy)-1,4-phenylene vinylene)-*b*-polyisoprene diblock copolymers (PPV-PI) were synthesized as previously described.<sup>18</sup> This study focuses on a particular polymer with total molecular weight ( $M_N$ ) of 12 kg/mol, PDI of 1.10 and polyisoprene volume fraction of 70% as this polymer has been previously shown to demonstrate a lamellar phase (Figure 4.1) with an accessible microphase order-disorder temperature.<sup>19, 20</sup> Molecular characterization including GPC and NMR were used to confirm the block copolymer molecular weight, composition and lack of residual homopolymer. Small angle x-ray scattering and polarized optical microscopy (POM) were used to quantify the zero-field block copolymer order-disorder transition temperature ( $T_{ODT}$ ) and liquid crystalline nematic-isotropic transition temperature ( $T_{NI}$ ).

At room temperature the PPV domain of the block copolymer is crystalline and upon melting at 60 °C, the block copolymer lamellae contain liquid crystalline smectic ordered rods. As the temperature is increased, the system undergoes a simultaneous block copolymer order-disorder transition and liquid crystalline smectic-nematic transition where the rods and coils become miscible and the PPV rods lose translational order while retaining orientational order. The block copolymer phase separation in this system is dominated by liquid crystalline interactions because the rod-rod interactions, as parameterized by a Maier-Saupe parameter ( $\mu_N$ ), are much stronger than the Flory-Huggins interaction between the blocks ( $\chi_N$ ).<sup>20</sup> Further heating above the nematic-isotropic transition results in a second transition to an isotropic system with no block copolymer or liquid crystalline order.

The microphase order-disorder transition temperature ( $T_{ODT}$ ) can be quantified by the simultaneous disappearance of higher order peaks and a dramatic decrease in the intensity of the primary peak of the azimuthally integrated SAXS images. The discontinuity in the primary peak intensity is apparent when the inverse primary peak

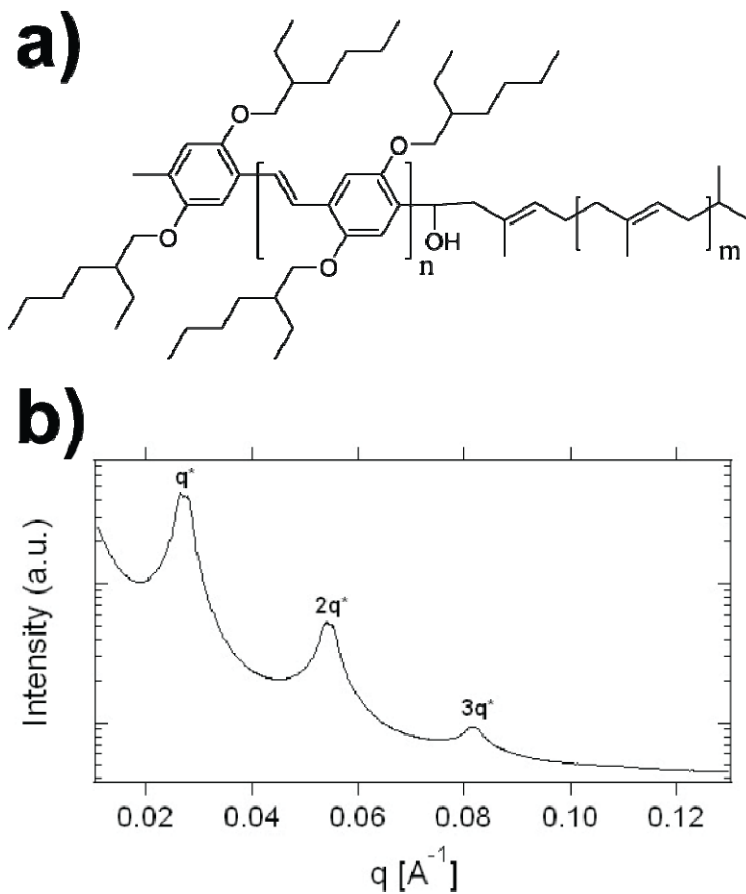


**Figure 4.1. Chemical structure and morphology**

a) Chemical structure of the model rod-coil block copolymer, PPV-PI, with easily accessible phase transitions and an anisotropic magnetic susceptibility, which self assembles into b) lamellae without the presence of any magnetic field confirmed by the multiple integer peak spacing shown in the SAXS spectrum.

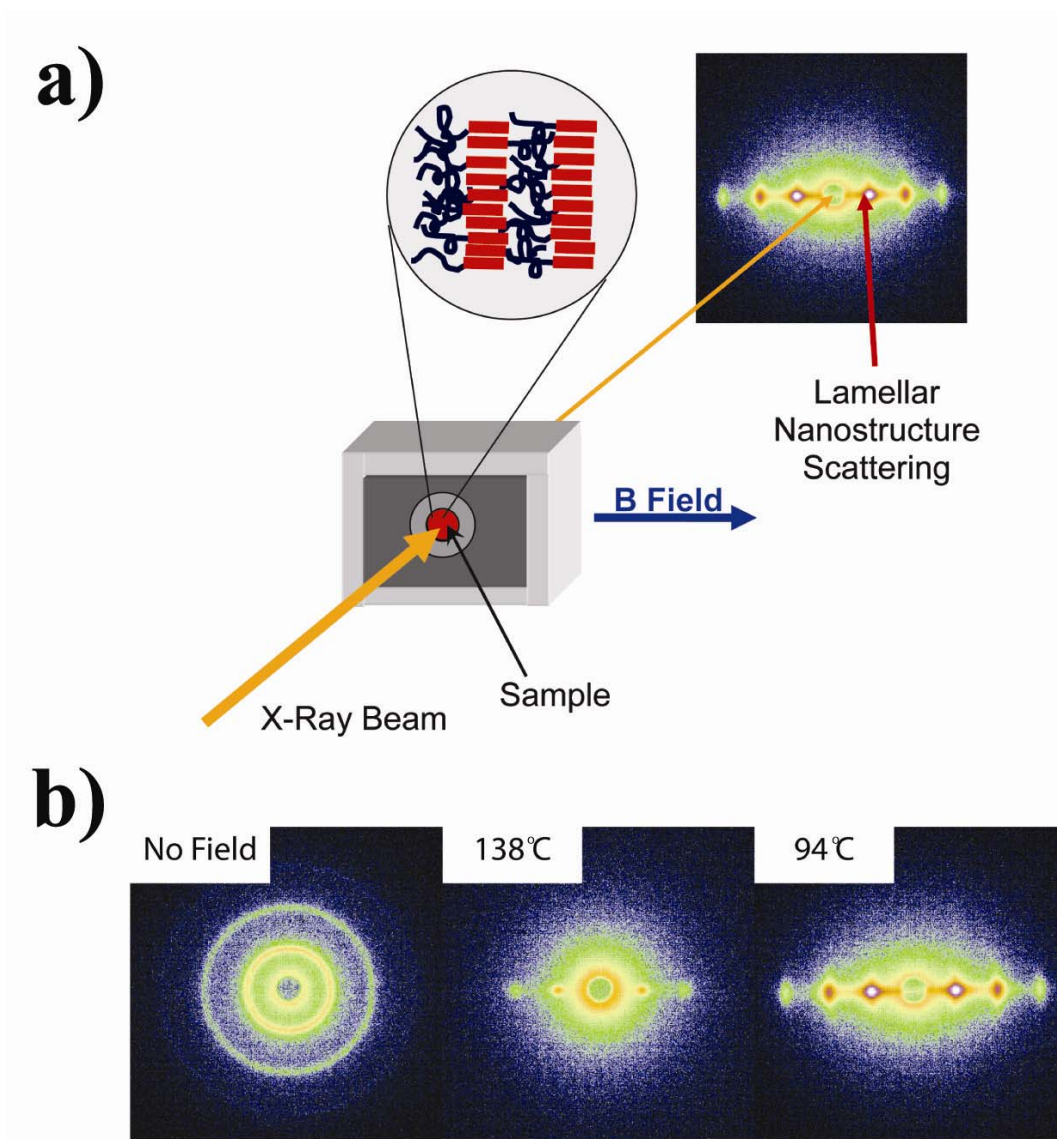


**Figure 4.2. Experimental setup for in situ SAXS**

a) In the presence of a magnetic field the lamellar structure of a main chain liquid crystalline block copolymer will align perpendicular to the field as the conjugated polymer lie parallel to the field. b) The 2D SAXS images taken using a 7 T magnetic field show a high degree of alignment indicated by the sharp peaks parallel to the applied field.

intensity is plotted vs. inverse temperature. Disordered block copolymers are expected to produce a weak primary peak due to correlations caused by joining two distinct polymer chains to form a block copolymer however this block copolymer system has very low chemical contrast so the intensity of the primary peak above the ODT quickly is overwhelmed by noise limiting the number of points above the ODT.<sup>18</sup> For the block copolymer used in these studies, the  $T_{\text{ODT}}$  was measured to be  $115 \pm 2$  °C using SAXS and the nematic-isotropic transition was measured to be  $140 \pm 5$  °C using polarized optical microscopy.

After purification, polymer samples were prepared for x-ray analysis by placing polymer within an aluminum washer and then sealing between two Kapton windows. As shown in Figure 4.2, the sample stage was designed so that in all experiments the magnetic field was applied perpendicular to the X-ray axis. Synchrotron small angle X-ray scattering (SAXS) measurements were performed at the DUBBLE BM26B beamline at the European Synchrotron Radiation Facility (ESRF, Grenoble, France).<sup>21</sup> At ESRF, in-situ SAXS was performed within a 7 T split coil magnet allowing for real-time understanding of order transitions.<sup>22</sup> A separate set of samples were aligned within a 2 T permanent magnet using in-situ SAXS at beamline 7.3.3 at the Advanced Light Source (ALS, Berkeley, USA).<sup>23</sup> Prior to data analysis, background scattering was subtracted from the data and normalized to account for variations in the beam intensity.

To determine the  $T_{\text{ODT}}$  in the presence of a magnetic field, polymer samples were sealed and placed within a home built sample holder which was continuously purged with nitrogen. Samples were annealed at 140 °C (above the zero field  $T_{\text{ODT}}$  and  $T_{\text{NI}}$ ) outside of the magnetic field so that initially each sample was unaligned. The samples were then cooled and inserted into the magnetic field. The temperature of the sample was then increased stepwise and held at each temperature for at least 10 minutes to insure thermal equilibrium was reached. After the  $T_{\text{ODT}}$  was reached, the sample was cooled and held for at least 10 minutes at each temperature step. The temperature scans were repeated multiple times and for a fixed magnetic field strength, the  $T_{\text{ODT}}$  stayed constant upon heating or cooling for all heating scans. No difference in the  $T_{\text{ODT}}$  was observed whether the sample was initially aligned or unaligned before the temperature scan. These results indicate that any change in the transition temperature is not controlled by kinetic factors and is not the result of radiation damage.

### 4.3. Results and Discussion

SAXS allows for the *in-situ* detection of lamellar block copolymer alignment in the presence of a magnetic field and the ability to probe the effects of magnetic field perturbations on rod-coil block copolymer self-assembly. Upon heating an unoriented sample within a magnetic field to an appropriate temperature, the polymer quickly reaches a highly aligned state (Figure 4.2). When a 2 T magnetic field was used, the block copolymer lamellar order persists past the ex-situ  $T_{\text{ODT}}$  of  $115 \pm 2$  °C and disorders above  $120 \pm 3$  °C. This deviation of the  $T_{\text{ODT}}$  appears to be field-strength dependant and is significantly more dramatic at higher field, with order persisting until  $147 \pm 3$  °C at 7 T, as shown in Figure 4.3. The order-disorder transition for this system is determined using

the 1D azimuthally integrated SAXS profile which shows a dramatic decrease in the primary peak intensity and a loss of higher order peaks near the order-disorder transition (Figure 4.4). The  $T_{ODT}$  at 7 T is significantly higher than either the ex-situ  $T_{ODT}$  or  $T_{NI}$  suggesting that the block copolymer and liquid crystalline interactions are strongly affected by the presence of the field. Since the samples heated from a highly aligned state or cooled from an unaligned state display the same  $T_{ODT}$ , it appears that the increase in  $T_{ODT}$  results from a stabilization of the lamellar morphology induced by the magnetic field at higher temperatures, perhaps resulting from favorable enthalpic interactions created by the coupling between the aligned liquid crystalline PPV domains and the magnetic field.

While magnetic fields have not been shown to affect classical coil-coil block copolymer transitions, they have been shown to alter the transition temperature of liquid crystalline systems.<sup>24, 25</sup> Since the liquid crystalline interactions are strong in this block copolymer system compared to the Flory-Huggins block copolymer interactions<sup>20</sup>, the block copolymer morphology is dominated by the rod-like moiety's liquid crystalline behavior. This suggests that the order-disorder transition of the block copolymer may in fact be dominated by the liquid crystalline smectic-nematic transition. Therefore, the change in the transition temperature can be described by accounting for the difference in magnetic susceptibility of liquid crystalline phases.<sup>25</sup> The deviation in the smectic-nematic transition of small molecule liquid crystals follows theoretical predictions in that it scales quadratically with magnetic field strength leading to much larger deviations at high field strengths via the following equation

$$\Delta T_{ODT} = \frac{T_{ODT}(H=0)}{2Q}(\chi_S - \chi_N)H^2 \quad (1)$$

where  $\Delta T_{ODT}$  is the increase in the smectic-nematic transition temperature and is a function of the original smectic-nematic transition temperature with no magnetic field ( $T_{ODT}(H=0)$ ), the difference in magnetic susceptibility between the smectic and nematic phases ( $\chi_S - \chi_N$ ), the magnetic field strength (H) and the latent heat of the transition (Q). The difference between the smectic and nematic phases is positive because coupling between orientational and positional order in a smectic phase increases the liquid crystalline ordering; this results in a higher magnetic susceptibility compared to the nematic phase.<sup>26</sup> It has been shown that the smectic-nematic transition for small molecule liquid crystals should increase slightly in the presence of a magnetic field because the absolute magnitude of magnetic susceptibility should be higher in the more highly ordered smectic phase however the effect in these systems is small with the smectic-nematic transition is increasing by less than 1 °C. The cause of the large increase in the  $T_{ODT}$  in our block copolymer system ( $\Delta T_{ODT} \sim 30$  °C) is not completely understood however it may result from several factors since the magnetic susceptibilities for each phase are not known and the latent heat of the smectic-nematic transition is too small to observe with conventional techniques.

While we do see much greater deviations at high field, the absolute change in the smectic-nematic transition of the block copolymer system is orders of magnitude higher than previously studied small molecule liquid crystals. It is unlikely that differences in the magnetic susceptibility and latent heat of the transition between previously studied

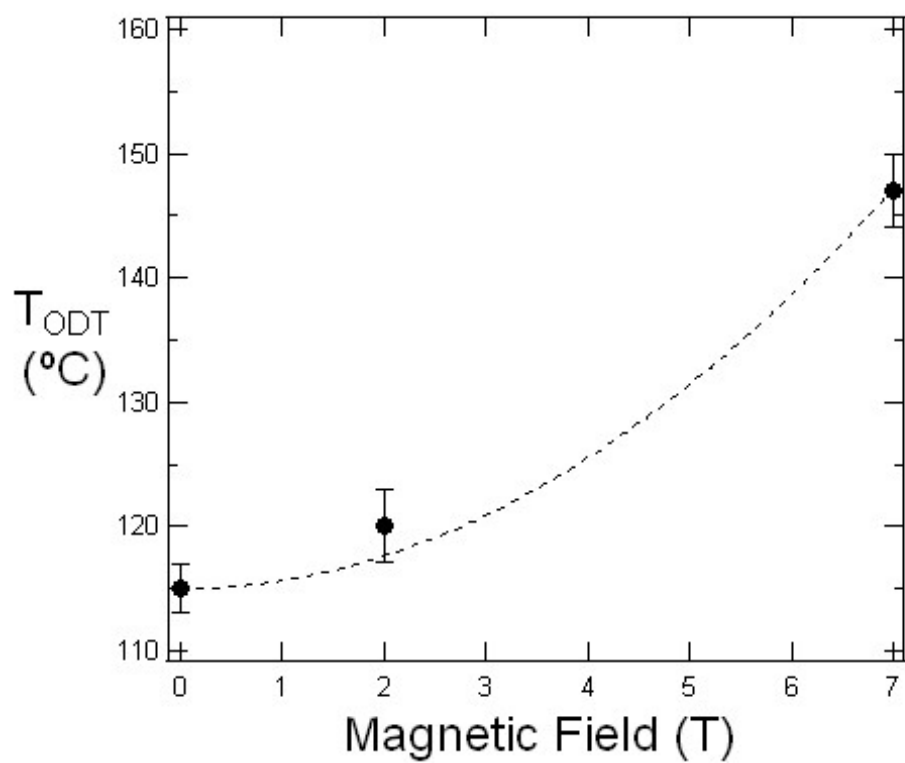


**Figure 4.3. Increased order-disorder transition temperature**

*In situ* small angle X-ray scattering was used to quantify the order-disorder transition temperature ( $T_{ODT}$ ) as a function of magnetic field strength. The  $T_{ODT}$  increases strongly as a function of magnetic field strength.

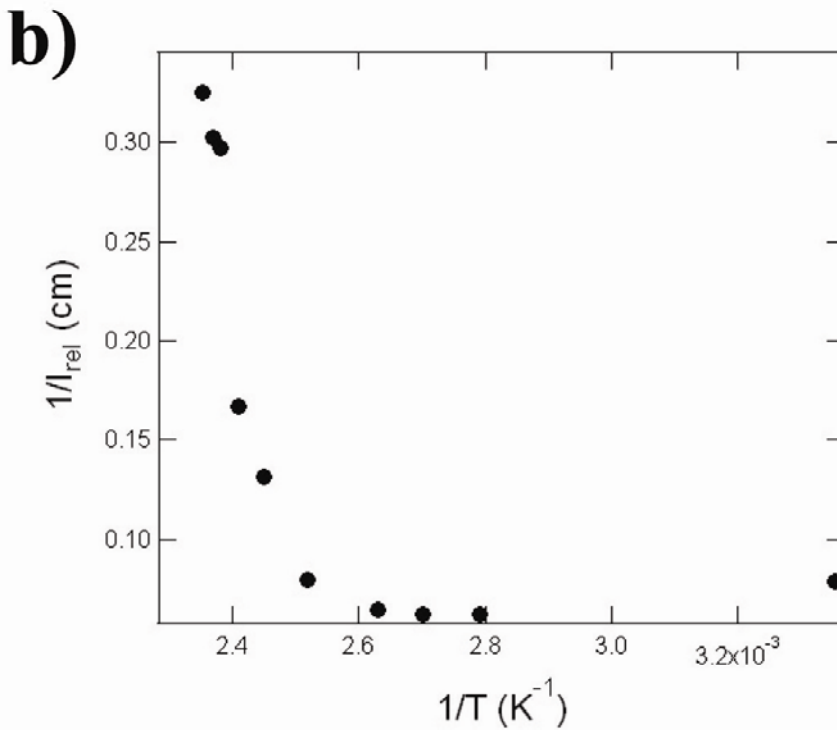
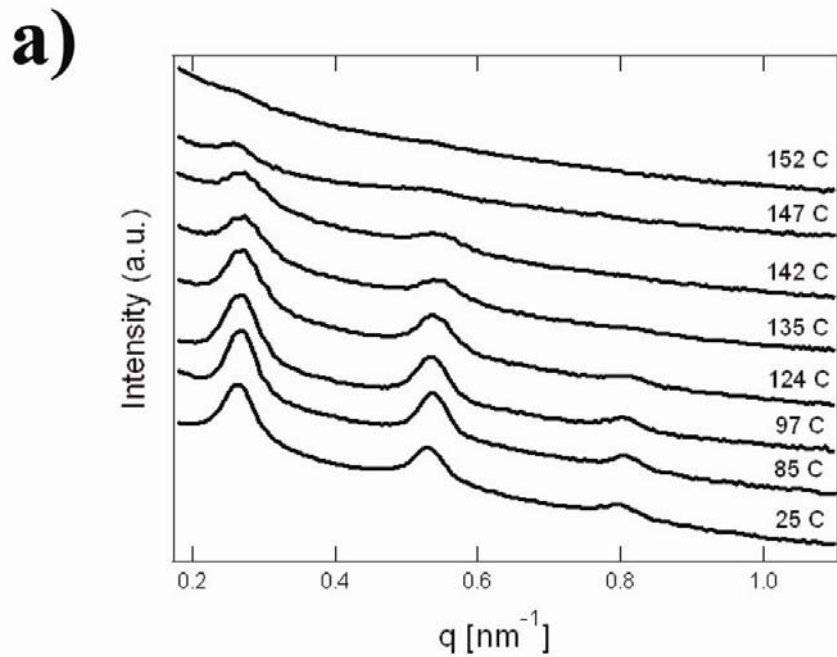


**Figure 4.4. Distinguishing an order-disorder transition**

a) Azimuthally integrated scattering intensity of PPV-PI under a 7T magnetic field as a function of temperature. The integer multiples of  $q^*$  demonstrate that the block copolymer self assembles into a lamellar morphology. b) An order-disorder transition temperature is confirmed by plotting the inverse of the primary peak intensity versus inverse temperature and locating the discontinuity in the curve which coincides with a disappearance of the higher order reflections.

small molecules and this block copolymer system can fully account for the large increase in the  $T_{ODT}$ . The lamellar block copolymer morphology improves the liquid crystalline order of the smectic phase by pinning the PPV chain ends to the block copolymer interface which further increases the difference in the magnetic susceptibility between the smectic and nematic phases. The alignment in the liquid crystalline domains also reduces fluctuations in the system stabilizing the lamellar block copolymer phase at higher temperatures. Therefore, it appears that the coupling between the liquid crystalline moieties and the magnetic field along with the substantially increased ordering in the smectic phase compared to the nematic phase caused by the block copolymer microphase separation likely leads to the dramatic increase in the  $T_{ODT}$ .

#### **4.4. Conclusions**

For the first time, magnetic fields have been shown to have a strong effect on the order-disorder transition temperature ( $T_{ODT}$ ) of a liquid crystalline rod-coil block copolymer. The polymer thermodynamics have been studied as a function of temperature and magnetic field strength using *in-situ* small angle X-ray scattering. In a 2 T magnetic field we observe a 5 °C increase in the  $T_{ODT}$  and for fields as high as 7 T we observe an increase in the  $T_{ODT}$  of 32 °C showing that both the block copolymer and liquid crystalline transitions of the material are affected. The magnetic susceptibility of the liquid crystalline rod-like domain leads to alignment and also causes the  $T_{ODT}$  to increase as a function of magnetic field strength. This work could be used toward understanding how to optimize alignment procedures since magnetic alignment has been shown to be extremely dependent on the processing parameters (temperature, time, etc.) and especially the location of the  $T_{ODT}$ .



## 4.5. Appendix

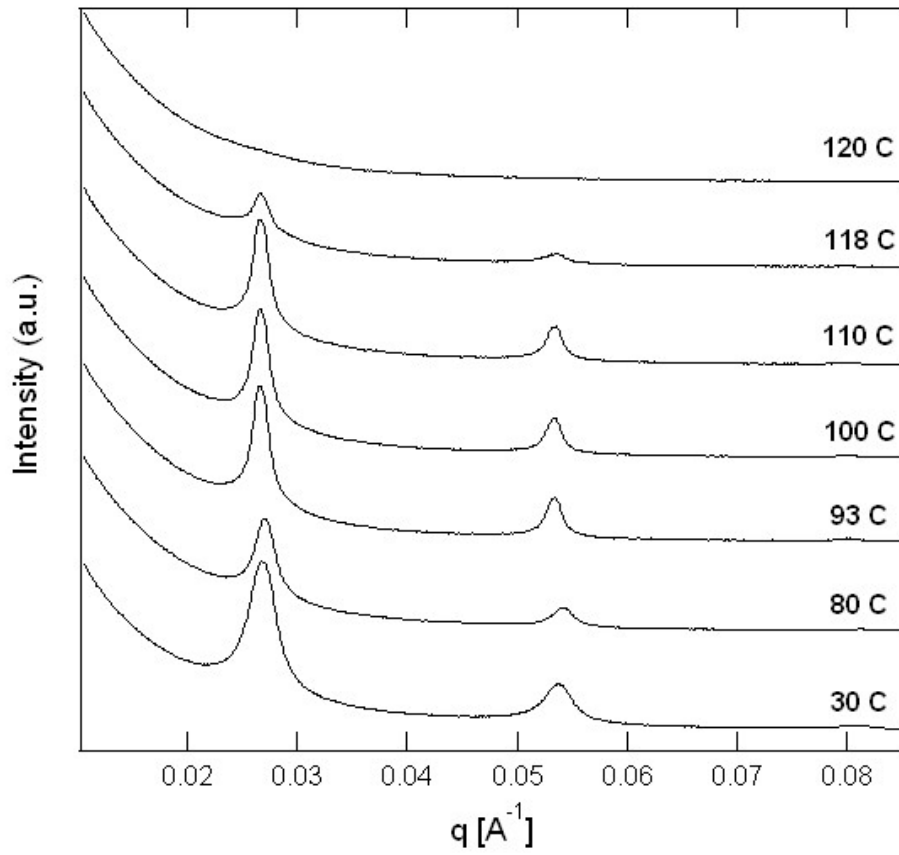


**Figure 4.5. Order-disorder transition in a 2T magnetic field**

Azimuthally integrated scattering intensity of PPV-PI under a 2 T magnetic field as a function of temperature. Upon heating a reversible order-disorder transition is reached at 120 °C which is identified by a dramatic decrease in the primary peak intensity and a loss of higher order peaks.

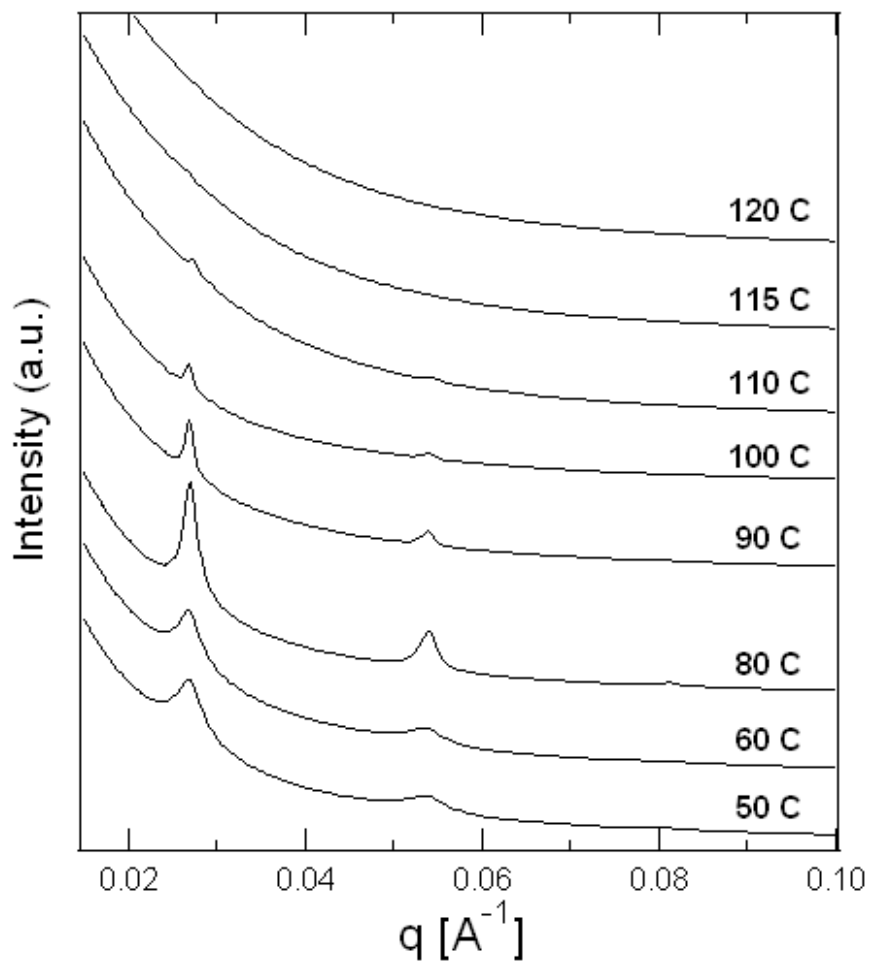


**Figure 4.6. Order-disorder transition outside of a magnetic field**

Azimuthally integrated scattering intensity of PPV-PI without the presence of a magnetic field as a function of temperature. Upon heating a reversible order-disorder transition is reached at 115 °C which is identified by a dramatic decrease in the primary peak intensity and a loss of higher order peaks.

## 4.6. Acknowledgments

Research was supported through the DOE-BES Plastic Electronics Program by the U.S. Department of Energy, Office of Basic Energy Sciences, Division of Materials Sciences and Engineering under Contract No. DE-AC02-05CH11231. BM gratefully acknowledges partial support via the Dow Advanced Materials Fellowship. We thank Dr. Alex Hexemer and Dr. Tanmoy Maiti for their assistance with X-ray scattering studies which were carried out at the Advanced Light Source (ALS) on beamline 7.3.3. The Advanced Light Source is supported by the Director, Office of Science, Office of Basic Energy Sciences, of the U.S. Department of Energy under Contract No. DE-AC02-05CH11231. In-situ small angle X-ray scattering was performed at the European Synchrotron Radiation Facility on beamline BM26B DUBBLE and the Netherlands Organization for Scientific Research (NWO) is thanked for making the beam time available. We also thank Dr. Brad Olson and Dr. Young Rae Hong for helpful discussions.

## 4.7. References

1. Segalman, R. A., Patterning with block copolymer thin films. *Materials Science & Engineering R-Reports* **2005**, *48*, (6), 191-226.
2. Tao, Y. F.; Zohar, H.; Olsen, B. D.; Segalman, R. A., Hierarchical nanostructure control in rod-coil block copolymers with magnetic fields. *Nano Letters* **2007**, *7*, (9), 2742-2746.
3. Gopinadhan, M.; Beach, E. S.; Anastas, P. T.; Osuji, C. O., Smectic Demixing in the Phase Behavior and Self-Assembly of a Hydrogen-Bonded Polymer with Mesogenic Side Chains. *Macromolecules* **2010**, *43*, (16), 6646-6654.
4. Gopinadhan, M.; Majewski, P. W.; Osuji, C. O., Facile Alignment of Amorphous Poly(ethylene oxide) Microdomains in a Liquid Crystalline Block Copolymer Using Magnetic Fields: Toward Ordered Electrolyte Membranes. *Macromolecules* **2010**, *43*, (7), 3286-3293.
5. Hamley, I. W.; Castelletto, V.; Lu, Z. B.; Imrie, C. T.; Itoh, T.; Al-Hussein, M., Interplay between smectic ordering and microphase separation in a series of side-group liquid-crystal block copolymers. *Macromolecules* **2004**, *37*, (13), 4798-4807.
6. Majewski, P. W.; Gopinadhan, M.; Jang, W. S.; Lutkenhaus, J. L.; Osuji, C. O., Anisotropic Ionic Conductivity in Block Copolymer Membranes by Magnetic Field Alignment. *Journal of the American Chemical Society* **2010**, *132*, (49), 17516-17522.
7. Osuji, C.; Ferreira, P. J.; Mao, G. P.; Ober, C. K.; Vander Sande, J. B.; Thomas, E. L., Alignment of self-assembled hierarchical microstructure in liquid crystalline diblock copolymers using high magnetic fields. *Macromolecules* **2004**, *37*, (26), 9903-9908.

8. Majewski, P. W.; Osuji, C. O., Non-degenerate magnetic alignment of self-assembled mesophases. *Soft Matter* **2009**, 5, (18), 3417-3421.
9. Osuji, C. O.; Majewski, P. W., Controlled Alignment of Lamellar Lyotropic Mesophases by Rotation in a Magnetic Field. *Langmuir* **2010**, 26, (11), 8737-8742.
10. Segalman, R. A.; Olsen, B. D.; Gu, X.; Hexemer, A.; Gann, E., Liquid Crystalline Orientation of Rod Blocks within Lamellar Nanostructures from Rod Coil Diblock Copolymers. *Macromolecules* **2010**, 43, (16), 6531-6534.
11. Osuji, C. O.; Majewski, P. W.; Gopinadhan, M.; Jang, W. S.; Lutkenhaus, J. L., Anisotropic Ionic Conductivity in Block Copolymer Membranes by Magnetic Field Alignment. *Journal of the American Chemical Society* **2010**, 132, (49), 17516-17522.
12. Amundson, K.; Helfand, E.; Quan, X.; Smith, S. D., Alignment of Lamellar Block-Copolymer Microstructure in an Electric-Field .1. Alignment Kinetics. *Macromolecules* **1993**, 26, (11), 2698-2703.
13. Xu, T.; Goldbach, J. T.; Leiston-Belanger, J.; Russell, T. P., Effect of ionic impurities on the electric field alignment of diblock copolymer thin films. *Colloid and Polymer Science* **2004**, 282, (8), 927-931.
14. Lin, C. Y.; Schick, M.; Andelman, D., Structural changes of diblock copolymer melts due to an external electric field: A self-consistent-field theory study. *Macromolecules* **2005**, 38, (13), 5766-5773.
15. Amundson, K.; Helfand, E.; Quan, X. N.; Hudson, S. D.; Smith, S. D., Alignment of Lamellar Block-Copolymer Microstructure in an Electric-Field .2. Mechanisms of Alignment. *Macromolecules* **1994**, 27, (22), 6559-6570.
16. Stepanow, S.; Gunkel, I.; Thurn-Albrecht, T.; Trimper, S., Fluctuation effects in the theory of microphase separation of diblock copolymers in the presence of an electric field. *Macromolecules* **2007**, 40, (6), 2186-2191.
17. Boker, A.; Schoberth, H. G.; Schmidt, K.; Schindler, K. A., Shifting the Order-Disorder Transition Temperature of Block Copolymer Systems with Electric Fields. *Macromolecules* **2009**, 42, (10), 3433-3436.
18. Olsen, B. D.; Segalman, R. A., Structure and thermodynamics of weakly segregated rod-coil block copolymers. *Macromolecules* **2005**, 38, (24), 10127-10137.
19. Olsen, B. D.; Segalman, R. A., Nonlamellar phases in asymmetric rod-coil block copolymers at increased segregation strengths. *Macromolecules* **2007**, 40, (19), 6922-6929.
20. Olsen, B. D.; Shah, M.; Ganesan, V.; Segalman, R. A., Universalization of the phase diagram for a model rod-coil diblock copolymer. *Macromolecules* **2008**, 41, (18), 6809-6817.

21. Bras, W.; Dolbnya, I. P.; Detollenaere, D.; van Tol, R.; Malfois, M.; Greaves, G. N.; Ryan, A. J.; Heeley, E., Recent experiments on a combined small-angle/wide-angle X-ray scattering beam line at the ESRF. *Journal of Applied Crystallography* **2003**, *36*, 791-794.
22. Bras, W.; Emsley, J. W.; Levine, Y. K.; Luckhurst, G. R.; Seddon, J. M.; Timimi, B. A., Field-induced alignment of a smectic-A phase: A time-resolved x-ray diffraction investigation. *Journal of Chemical Physics* **2004**, *121*, (9), 4397-4413.
23. Hexemer, A.; Bras, W.; Glossinger, J.; Schaible, E.; Gann, E.; Kirian, R.; MacDowell, A.; Church, M.; Rude, B.; Padmore, H., A SAXS/WAXS/GISAXS Beamline with Multilayer Monochromator. *Journal of Physics: Conference Series* **2010**, *247*, (1).
24. Sakamoto, A.; Yoshino, K.; Kubo, U.; Inuishi, Y., Effects of Magnetic-Field on Phase-Transition Temperature between Smectic-a and Nematic States. *Japanese Journal of Applied Physics* **1976**, *15*, (3), 545-546.
25. Rosenblatt, C., Magnetic-Field Dependence of the Nematic-Isotropic Transition-Temperature. *Physical Review A* **1981**, *24*, (4), 2236-2238.
26. Gennes, P.-G. d., *The physics of liquid crystals*. Clarendon Press: Oxford [Eng.], 1974; p xi, 333 p.

## Chapter 5. Dynamics of Magnetic Alignment in Rod-Coil Block Copolymers

The dynamics associated with magnetic field alignment of a model rod-coil block copolymer poly(2,5-di(2'-ethylhexyloxy)-1,4-phenylene vinylene)-b-polyisoprene (PPV-PI) have been investigated using a combination of time resolved *in situ* small angle x-ray scattering and TEM. Alignment is observed over a wide range of field strengths (0.2-7T) however the highest field strengths studied produce the highest degree of alignment. Experiments examining alignment of a disordered sample, cooled into the ordered state in the presence of a magnetic field, show that a majority of alignment occurs during the process of nucleation and growth. At longer times defect annihilation and grain rotation progress more slowly, however, are necessary in producing extremely highly aligned samples. At the highest field strength, due to the increased  $T_{ODT}$ , selective ordering is likely observed at temperatures near the order-disorder transition leading to nucleation of aligned block copolymer grains resulting in faster and a higher degree of alignment. Additionally, at these high field strengths the alignment process appears to have a more complex defect production and removal process than at low field strengths. At low field strengths isotropic nucleation occurs and then preferential growth of aligned block copolymer grains are primarily responsible for alignment. Finally, an optimum alignment temperature is observed where the thermodynamic driving force for alignment, thermal disordering processes and the kinetic effects governing block copolymer growth and defect removal are balanced.

### 5.1. Introduction

Self-assembled block copolymer nanostructures have been of interest for a wide variety of applications due to their highly tunable functionality, morphologies and domain sizes. While these thermodynamically stable structures are precisely ordered at the nanometer length scale, a macroscopic polymer sample is typically made up of isotropically oriented block copolymer grains. Alignment of anisotropic block copolymer structures such as lamellae and cylinders is needed to enable patterning techniques such as nanolithography<sup>1</sup> or for optimizing properties such as ion or electron transport through the block copolymer nanostructure. Many different alignment techniques have been previously investigated using shear,<sup>2,3</sup> electric fields<sup>4,5</sup> or surface functionalization<sup>6,7</sup> however magnetic field alignment offers two major advantages. First, samples can be aligned without making contact with the material, making it ideal for many applications. Secondly, arbitrary alignment orientations can be achieved by changing the field direction relative to the sample geometry, which can be challenging to achieve using other techniques. Unfortunately most block copolymers do not respond to the application of a magnetic field because they have a very low anisotropy in their magnetic susceptibility requiring impractically high field strengths for alignment. Crystalline or liquid crystalline moieties are incorporated into the block copolymer in order to increase the anisotropy of the magnetic susceptibility of block copolymers.<sup>8-13</sup> Liquid crystalline materials are highly anisotropic in shape and many have been shown to have sufficient anisotropy in their magnetic susceptibility enabling magnetic alignment using moderate field strengths. Interestingly, the anisotropy of the magnetic susceptibility of a single liquid crystalline molecule is too small to align in a magnetic field because the thermal

energy is much greater than the free energy from alignment.<sup>14</sup> The strong liquid crystalline interactions in these materials cause the formation of large grains where the molecular axis are collectively oriented, increasing the free energy of alignment of these large grains. Therefore in these materials alignment is better thought of as alignment of large grains and not as alignment of single molecules. There are two commonly used methods to introduce these liquid crystalline properties into a block copolymer. Small molecule liquid crystals can be attached pendant to the chain of one of the blocks of the block copolymer or one of the blocks can be replaced with a rod-like liquid crystalline polymer. Pendant liquid crystalline block copolymers have been used extensively by several groups to achieve highly aligned samples<sup>8, 9, 12, 13, 15, 16</sup> and have also been expanded to include systems where small molecule liquid crystals are hydrogen bonded to the polymer backbone.<sup>17</sup> Since these techniques align the liquid crystalline molecules attached pendant to the polymer backbone and does not align the block copolymer structure directly there may be degeneracy in the aligned morphology, however, this can be overcome by rotating the sample in the field yielding highly aligned samples.<sup>18</sup> Alignment in these systems has been applied to nanostructured polymer membranes for ion transport showing that alignment can improve transport by an order of magnitude by decreasing the impact of tortuosity and grain boundaries.<sup>10</sup>

Liquid crystallinity can also be introduced in block copolymers by replacing one of the blocks with a rod-like liquid crystalline polymer.<sup>19</sup> By using a conjugated polymer as the rod-like block, magnetic alignment can be used as a pathway to optimize charge transport in optoelectronic systems. Alignment of conjugated polymers in devices such as organic transistors, light emitting diodes or photovoltaics is critical in optimizing device performance because the charge transport in these systems can vary several orders of magnitude since charges travel much faster along the chain or  $\pi$  stack axis.<sup>20, 21</sup> Light absorbance and photoluminescence are also affected by chain orientation which can be used to enhance light absorption or enable properties such as polarized light emission.<sup>22</sup> Work done by Tao et al. has shown that the rod-coil block copolymer poly(2,5-di(2'-ethylhexyloxy)-1,4-phenylene vinylene)-b-polyisoprene (PPV-PI) can be aligned to a very high degree in a 9T magnetic field.<sup>11</sup> In this system, the rod-like conjugated polymer backbone aligns parallel to the magnetic field, templating the block copolymer nanostructure perpendicular to the field. Since the block copolymer backbone is directly aligned, there exists no degeneracy in the alignment direction.

While it has been shown that these liquid crystalline block copolymers align in a magnetic field, the mechanisms which control the alignment process and the final degree of order are still unclear. In order to achieve the highest degrees of alignment it is typically necessary to begin with a sample in the disordered state. In some systems it is possible to align the liquid crystalline moieties while the block copolymer is disordered if there exists a nematic or smectic liquid crystalline phase above the order-disorder transition temperature ( $T_{ODT}$ ). In other systems the liquid crystalline phase can not be aligned above the  $T_{ODT}$  either because there is no liquid crystalline ordering above the  $T_{ODT}$ . The anisotropy in the magnetic susceptibility or the liquid crystalline coherence volume above the  $T_{ODT}$  may also be insufficient to produce alignment. In either case, slowly cooling the block copolymer from an isotropic and disordered state into an

ordered state has been used to optimize alignment. For either case, starting in a disordered state with no liquid crystalline or block copolymer ordering kinetically trapped defects are minimized and the final observed alignment is typically optimized.

Alignment can first occur during the process of nucleation and growth as microphase separation occurs for a block copolymer transitioning from a disordered state to an ordered state. Isotropic nucleation should normally occur because the free energy gain from alignment should be very small for small block copolymer nuclei compared to the driving force for demixing. Nucleation of aligned block copolymer grains may occur at very high field strengths, for materials with highly anisotropic magnetic susceptibility or very near the  $T_{ODT}$  where the free energy driving force for phase separation is similar to the free energy gain for aligning block copolymer nuclei. Another pathway for aligned nucleation is a process we refer to as selective ordering, occurring near the  $T_{ODT}$  where aligned nuclei are stable and unaligned nuclei are unstable. This may occur if the  $T_{ODT}$  is higher for block copolymer grains which are aligned with the field. Alignment can also occur during the growth phase through preferential growth of aligned block copolymer grains. If the free energy of alignment is sufficient, the rate of growth should be higher for aligned block copolymer grains. Additionally, the growth of aligned block copolymer grains should be more selective at high temperatures near the  $T_{ODT}$  because the free energy gain from alignment relative to the driving force for microphase separation is greater. While it appears that both aligned nucleation and preferential growth are more likely to lead to highly aligned samples at higher temperatures near the  $T_{ODT}$ , the increased thermal energy leads to smaller grain sizes and stronger thermal fluctuations which may limit the degree of alignment near the  $T_{ODT}$ .

It may not be possible to reach a disordered phase for all block copolymer chemistries or molecular weights depending on the strength of segregation so it is important to understand alignment in systems where nucleation and growth is not the dominant alignment pathway. Nucleation and growth of aligned grains can still occur in an ordered sample slightly below the  $T_{ODT}$  where fluctuations can temporarily disorder small regions of the block copolymer structure. Further from the  $T_{ODT}$ , grain rotation becomes the primary mechanism which can lead to large increases in alignment in an ordered block copolymer. The speed of this process depends on the driving force for alignment (field strength, grain size, anisotropy of magnetic susceptibility) and resisting friction force related to the viscosity and grain size of the block copolymer melt. This process is complex because in an ordered block copolymer melt, cooperative motion may take place between block copolymer grains during rotation. Therefore, during grain rotation defects and grain boundaries may be produced and possibly limit the degree of grain rotation which occurs. Shear alignment of block copolymer has been extensively studied and observed similar alignment mechanisms and the degree of alignment is also limited by the presence of grain boundaries.<sup>23, 24</sup> Grain boundaries between aligned grains are minimized as all block copolymer grains eventually have similar orientations. Alignment is also enhanced by mechanisms which lead to defect annihilation, removing dislocations and disclinations. The driving force for removal of these defects should be relatively low because these defects only lead to a small region which is slightly misaligned with the field however annealing within a magnetic field should slowly



remove these defects until thermal fluctuations limit the degree of order in the system. At higher temperatures, increased chain diffusion and fluctuations may increase the defect annihilation rate however at high temperatures the strength of segregation decreases, leading to the presence of defects as the equilibrium long range order of the system decreases.

Recent work by Osuji and coworkers suggests that alignment of pendant liquid crystalline block copolymers primarily occurs during nucleation and growth of weakly aligned block copolymer grains and annealing below the  $T_{ODT}$  may lead to slow rotation of block copolymer grains.<sup>25</sup> Electric field block copolymer alignment has also observed the importance of nucleation and growth as well as grain rotation<sup>26-29</sup> during the alignment process. A third process, termed selective melting, has been discussed where near the  $T_{ODT}$  unaligned block copolymer grains should be less stable than ordered block copolymer grains giving rise to another mechanism by which highly aligned block copolymer nanostructures can be created.<sup>30-32</sup> Selective melting arises because the  $T_{ODT}$  is depressed for unaligned grains in an electric field. This is analogous to selective ordering where the  $T_{ODT}$  may be increased in a magnetic field for aligned grains. Both selective melting and selective ordering occur in systems where the phase behavior is strongly influenced by the presence of a field and have not been observed to exist in every block copolymer system.

In this work we take advantage of *in situ* small angle x-ray scattering (SAXS) and TEM of quenched samples to study the relative importance of these mechanisms on the alignment of rod-coil block copolymers. The dynamics of the alignment process have been studied as a function of field strength and temperature. The initial state of the sample is shown to have large impact on final degree of alignment obtained and also affects the dominant pathways of alignment. When samples are cooled from the disordered phase to an ordered phase in the presence of the magnetic field, alignment was observed to occur very quickly. At high field strengths, selective ordering occurring near the ODT leads to aligned nucleation and growth producing highly aligned samples over the time scale of minutes while at lower field strengths isotropic nucleation and preferential growth is the dominate mechanism of alignment. In order to produce highly aligned block copolymer samples it is necessary to anneal these samples in a magnetic field, allowing slower processes such as grain rotation and defect annihilation to occur. Alignment procedure, time, temperature, and field strength all have a strong impact on the final degree of alignment and by understanding the alignment processes we can optimize the alignment of these block copolymer systems.

## 5.2. Experimental Section

PPV-PI block copolymer synthesis has previously been described.<sup>19</sup> This study has used a block copolymer with a number-average molecular weight ( $M_N$ ) of 12 kg/mol, PDI of 1.10 and polyisoprene volume fraction of 70%. This block copolymer self assembles into a lamellar morphology (Figure 5.1) and has previously been shown to have accessible transition temperatures.<sup>33</sup> Molecular characterization including GPC and NMR were used to confirm the block copolymer molecular weight, composition and lack

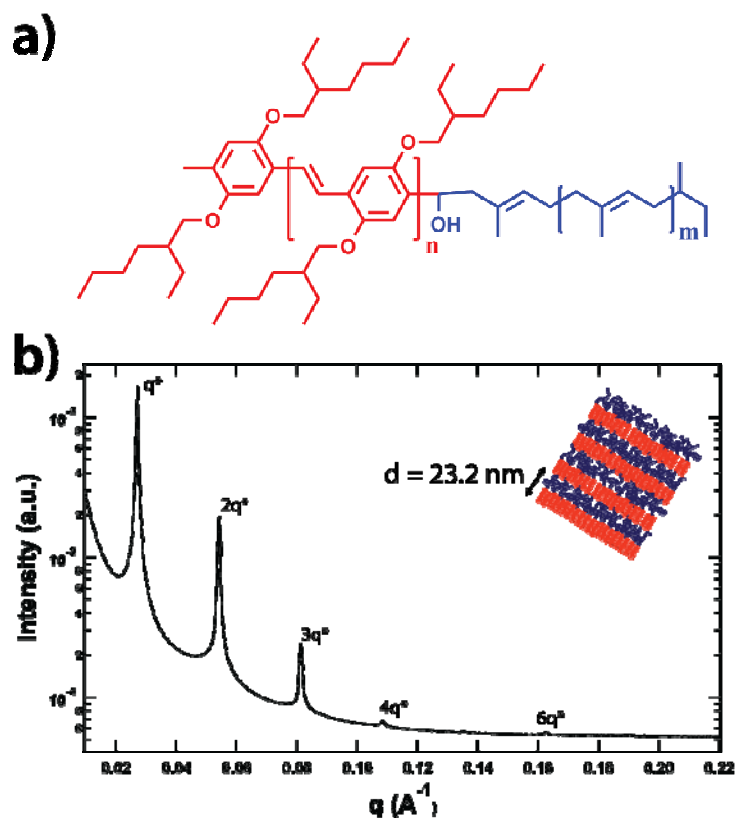


**Figure 5.1. PPV-PI chemical structure and morphology**

a) Chemical structure of PPV-b-PI, a model rod-coil block copolymer having easily accessible phase transitions and an anisotropic magnetic susceptibility. b) This polymer self assembles into lamellae confirmed by the multiple integer peak spacing shown by SAXS.

of residual homopolymer. Small angle x-ray scattering and polarized optical microscopy (POM) were used to quantify the zero-field block copolymer order-disorder transition temperature ( $T_{\text{ODT}}$ ) and liquid crystalline nematic-isotropic transition temperature ( $T_{\text{NI}}$ ).

At room temperature PPV is semicrystalline and melts around 60°C. Above this, the block copolymer lamellae contain PPV with smectic liquid crystalline ordering. As the temperature is increased, the system reaches a simultaneous block copolymer order-disorder transition ( $T_{\text{ODT}}$ ) and liquid crystalline smectic-nematic transition. The simultaneous order-disorder transition and liquid crystalline transition is caused by the dominant liquid crystalline interactions. In this block copolymer system the rod-rod interactions, as parameterized by a Maier-Saupe parameter ( $\mu\text{N}$ ), are much stronger than the Flory-Huggins interaction between the blocks ( $\chi\text{N}$ ).<sup>34</sup> Heating above the nematic-isotropic transition produces a system with no block copolymer or liquid crystalline order. For the block copolymer used in these studies, in the absence of a magnetic field the  $T_{\text{ODT}}$  was measured to be  $115 \pm 2$  °C using SAXS and the nematic-isotropic transition was measured to be  $140 \pm 5$  °C using polarized optical microscopy. Previous work has shown that the  $T_{\text{ODT}}$  of this block copolymer increases in the presence of a large magnetic field to  $120 \pm 5$  °C in a 2T magnetic field and  $147 \pm 5$  °C in a 7T magnetic field.<sup>33</sup>

*In situ* small angle x-ray scattering experiments were performed by placing polymer within a 1mm thick aluminum washer and then sealing between two Kapton sheets. As shown in Figure 5.2, the sample stage was designed so that in all experiments the magnetic field was applied perpendicular to the x-ray axis. Synchrotron small angle x-ray scattering (SAXS) measurements were performed at the DUBBLE BM26B beamline at the European Synchrotron Radiation Facility (ESRF, Grenoble, France).<sup>35</sup> At ESRF, *in situ* SAXS was performed within a 7 T split coil magnet.<sup>36</sup> A separate set of experiments were performed using a 2 T permanent magnet at beamline 7.3.3 at the Advanced Light Source (ALS, Berkeley, USA).<sup>37</sup> Finally, experiments at low fields (0.20 T and 0.39 T) were performed at beamline 1-4 at the Stanford Linear Accelerator Center using small permanent magnets (SSRL, Menlo Park, USA). Prior to data analysis, background scattering was subtracted from the data and normalized to account for variations in the beam intensity. In this work an orientation parameter used to quantify alignment will be defined as:

$$\langle P_2 \rangle = \frac{3\langle \cos^2 \phi \rangle - 1}{2} \quad (1)$$

and

$$\langle \cos^2 \phi \rangle = \frac{\int_0^{2\pi} I(\phi) \cos^2 \phi |\sin \phi| d\phi}{\int_0^{2\pi} I(\phi) |\sin \phi| d\phi} \quad (2)$$

where  $\phi$  is the azimuthal angle between the  $q^*$  peak of the block copolymer and the direction of alignment. A perfectly aligned block copolymer gives  $\langle P_2 \rangle = 1$  and a randomly oriented block copolymer should have  $\langle P_2 \rangle \approx 0$ .

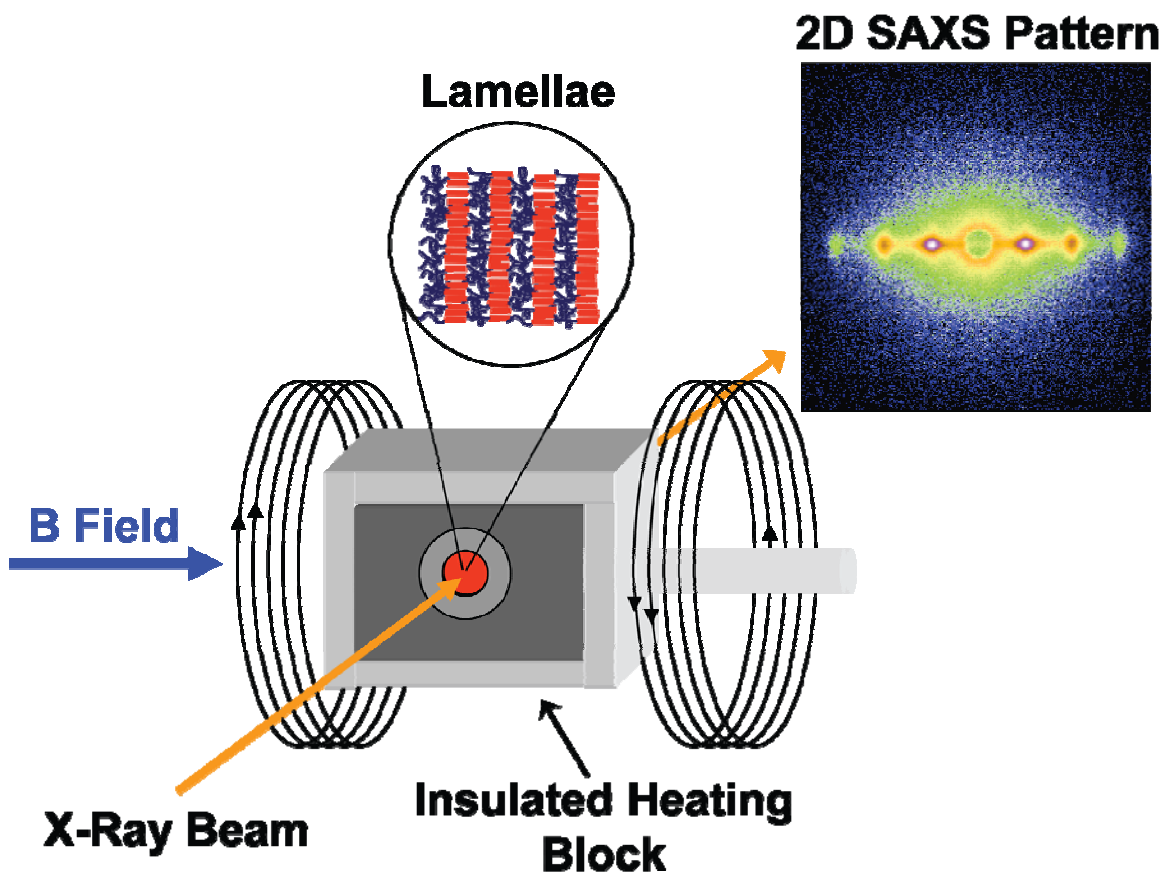


**Figure 5.2. In situ SAXS used for studying magnetic alignment**

In the presence of a magnetic field the lamellar block copolymer nanostructure will align perpendicular to the field because the rod-like conjugated polymer lie parallel to the field. The 2D SAXS images taken using a 7T magnetic field at 100°C shows a high degree of alignment indicated by spots parallel to the applied field.

Transmission electron microscopy (TEM) was also used to examine the block copolymer nanostructure. While this technique is not as useful in quantifying the degree of alignment in these block copolymers because of the relatively small sample volume probed ( $\sim 1 \mu\text{m}^3$ ) compared to SAXS which can probe an average of many block copolymer grains over a much larger volume ( $\sim 1 \text{mm}^3$ ), TEM is most useful in examining a real space image of the block copolymer structure giving information about the arrangement of block copolymer grains and nature of defect structures. Bulk samples for TEM were prepared by quickly quenching aligned samples at specific time points in liquid nitrogen and then immediately crosslinking by exposing to sulfur monochloride vapors in an enclosed vessel. Crosslinking was confirmed to not affect the block copolymer ordering or alignment however it does result in a domain size swelling of around 20%.<sup>11</sup> After the samples were sufficiently crosslinked, excess sulfur monochloride was removed under a nitrogen purge. Samples were embedded in epoxy and microtomed with a diamond knife to 100 nm in thickness. Osmium tetroxide vapors were used to stain the remaining double bonds in the polyisoprene block making these domains appear dark in TEM. TEM imaging was conducted on a JEOL JEM-2100 microscope at an operating voltage of 200 kV.

### 5.3. Results and Discussion

Highly aligned PPV-PI block copolymer samples can be created by slowly cooling from the ordered state in the presence of a magnetic field. As shown in Figure 5.3, the 2D SAXS pattern of a sample slowly cooled in a 6T magnet shows strong alignment indicated by strong arcs parallel to the magnetic field direction. TEM also shows a highly aligned lamellar nanostructure aligned over the entire observed area of the sample; however, as seen in Figure 5.3 there are some regions where small defects in the structure exist. As seen in Figure 5.4, it is also possible to achieve alignment over a wide range of field strengths. At high field strengths the maximum degree of alignment approaches a fully aligned sample. Alignment is also possible in this system using much lower field strengths than previously studied for the magnetic field alignment of block copolymers. This is likely due to the low viscosity, reducing kinetic trapping at low field strengths. The anisotropy in the magnetic susceptibility may also be unusually high, consistent with other observed behaviors such as its elevated  $T_{\text{ODT}}$  at high magnetic field strengths.<sup>33</sup> It appears that the minimum field strength for alignment is around 0.1 T, representing the field strength where the free energy for alignment is roughly equal to the thermal energy. Below this field strength, thermal fluctuations will dominate and alignment should not occur. While it has been shown in previous work that PPV-PI can be nearly perfectly aligned using magnetic fields, it is unclear how the alignment procedure affects the mechanisms important to block copolymer alignment.

The alignment process is most easily understood when carried out at low field strengths because the alignment rate is relatively slow and aligned grains are less likely to interact. By starting with a disordered initial state, many kinetically trapped defect structures are avoided. The sample is held at 150°C and then quickly cooled to 100°C while in a 0.39T magnetic field. As seen in Figure 5.5, the order parameter quickly increases over the course of 1 hour. Wide angle x-ray scattering shows that the liquid

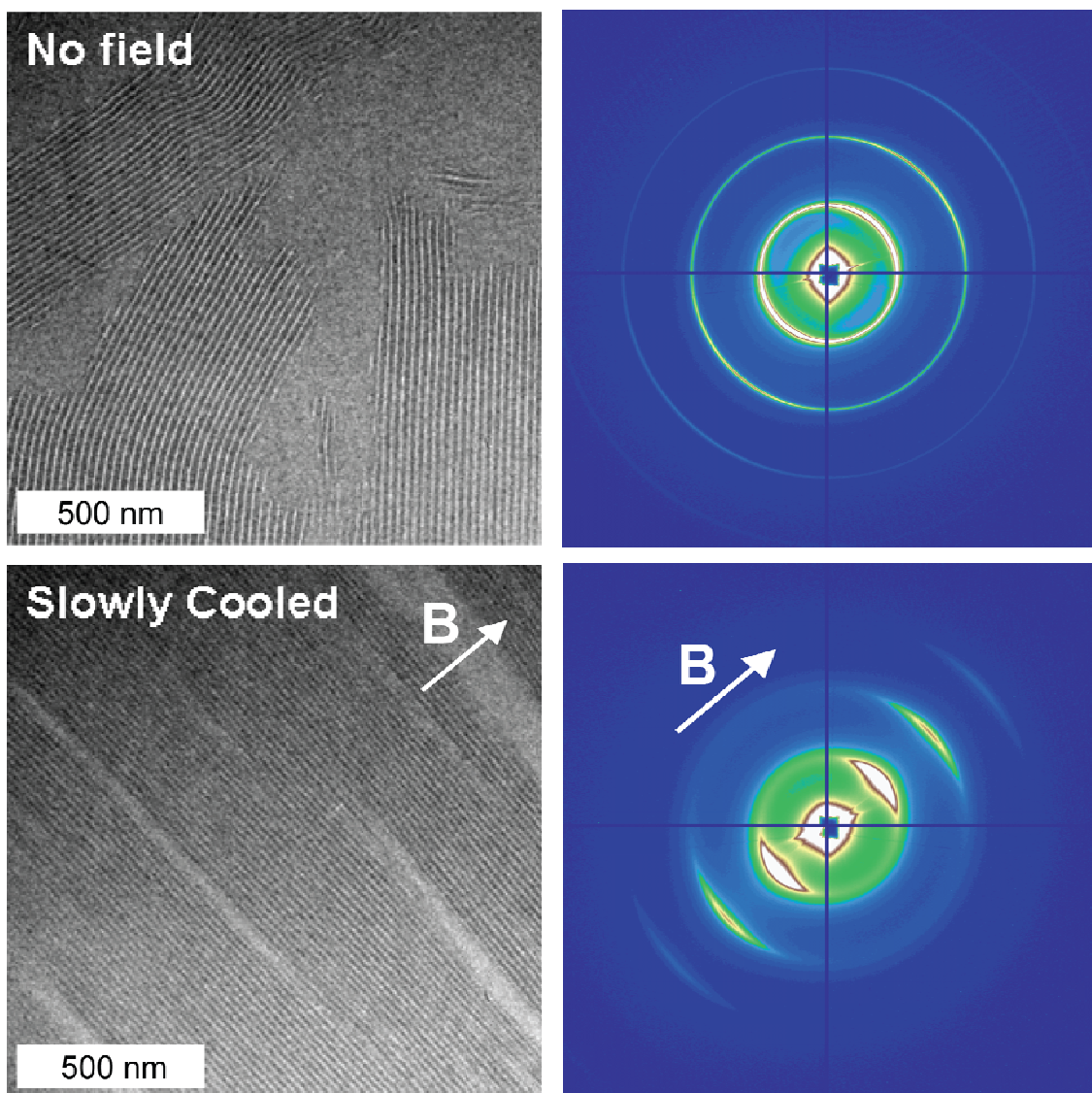


**Figure 5.3. Magnetic alignment of PPV-PI block copolymers**

Isotropically orientated lamellae are observed when the polymer is annealed below the order-disorder transition in the absence of a magnetic field. The block copolymer can achieve a high degree of alignment if cooled in the presence of a field from the disordered state to the ordered state. The highly aligned block copolymer TEM micrograph and SAXS pattern were obtained by cooling the polymer sample in the presence of a 6T magnetic field.

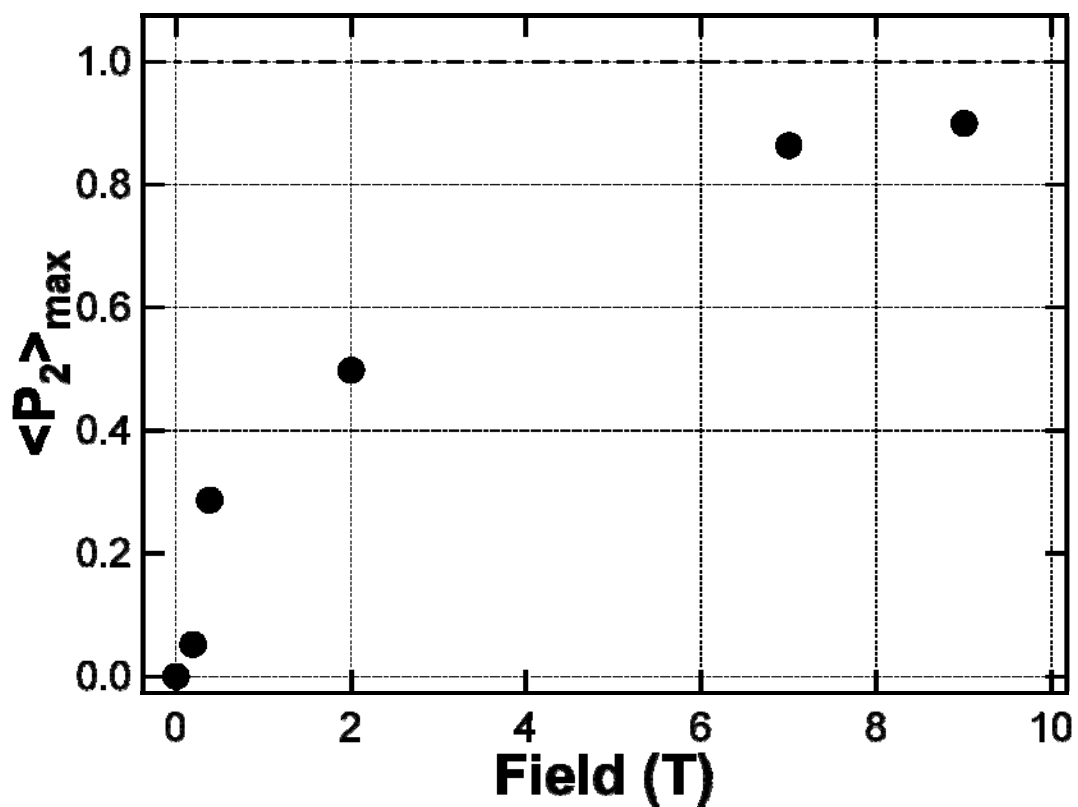


**Figure 5.4. Maximum observed alignment as a function of field strength**

The maximum order parameter observed increases as a function of field strength and asymptotes at high field strength. The minimum field strength for alignment appears to be around 0.1T, much lower than many other systems.

crystalline rod-like domains do not align in the nematic phase and only begin to align below the  $T_{ODT}$  in the smectic phase when the block copolymer is also ordered. After 1 hour, the rate of alignment decreases drastically however alignment continues to increase over the period of several hours. The average scattering intensity and the scattering intensity along the magnetic field both increase quickly until around 2 hours have elapsed. After 2 hours, the average intensity stops changing however the intensity along the direction of the magnetic field continues to slowly increase, similar to the order parameter. At short times, less than 2 hours, nucleation and growth occurs as the block copolymer transitions from the disordered to ordered state and alignment occurs quickly during this period. Nucleation should be isotropic because very small block copolymer grains do not have a sufficient free energy driving force to align. TEM micrographs in Figure 5.5, taken after 5 minutes of alignment, do appear to show very small isotropically oriented block copolymer grains. Instead, it appears that aligned grains preferentially grow in the magnetic field. The favorable free energy of alignment may increase the growth rate of an aligned block copolymer grain compared to an unaligned grain. After 30 minutes, TEM micrographs show large aligned block copolymer grains surrounded by regions with small unoriented block copolymer grains. Block copolymer grains aligned with the magnetic field show very anisotropic growth because the surface energies of rod-coil block copolymer grains are inherently anisotropic. The aligned block copolymer grains continue to grow, however, at around 2 hours the sample is fully ordered and there is a transition to much slower pathways associated with chain diffusion along grain boundaries and grain rotation. After 12 hours, there exists some very large aligned block copolymer grains however much of the sample still exists as small unaligned block copolymer grains. Longer alignment times increase the degree of alignment however at these low field strengths the alignment is limited both kinetically and thermodynamically because the free energy gain from alignment is close to the thermal energy available to the system. At low fields when cooling from the disordered state, it appears alignment is dominated by preferential growth of aligned block copolymer grains occurring at early times during the process of nucleation and growth. At longer times, alignment slows but continues by further increasing the size of these aligned block copolymer grains through either grain boundary diffusion or grain rotation.

The final degree of alignment at low field strengths is limited and in order to obtain higher degrees of alignment, higher field strengths are needed. To study the alignment at higher field strengths, *in situ* SAXS experiments have been performed using a 7T magnet where the sample initially was held at 150°C and then quickly cooled to 100°C. Initially the sample is nearly completely isotropic as shown in Figure 5.6. The block copolymer  $q^*$  peak is not visible due to the low inherent x-ray scattering contrast of PPV-PI.<sup>34</sup> Within minutes after cooling the sample below the  $T_{ODT}$  (147°C at 7T) the sample becomes very highly aligned. After around 7 minutes the aligned structure appears to be partially disrupted and off-axis peaks appear. At longer times these off-axis peaks decrease in intensity and a highly aligned sample is recovered. Interestingly only two-fold symmetry is observed in these off-axis peaks which is unusual because the system should be symmetric about the magnetic field direction and four-fold symmetry should be produced by any off-axis peaks. When the experiment is repeated, similar two-fold symmetry of the off-axis peaks is observed however the angle of the off-axis peaks seems to randomly choose between clockwise or counterclockwise rotation. This seems



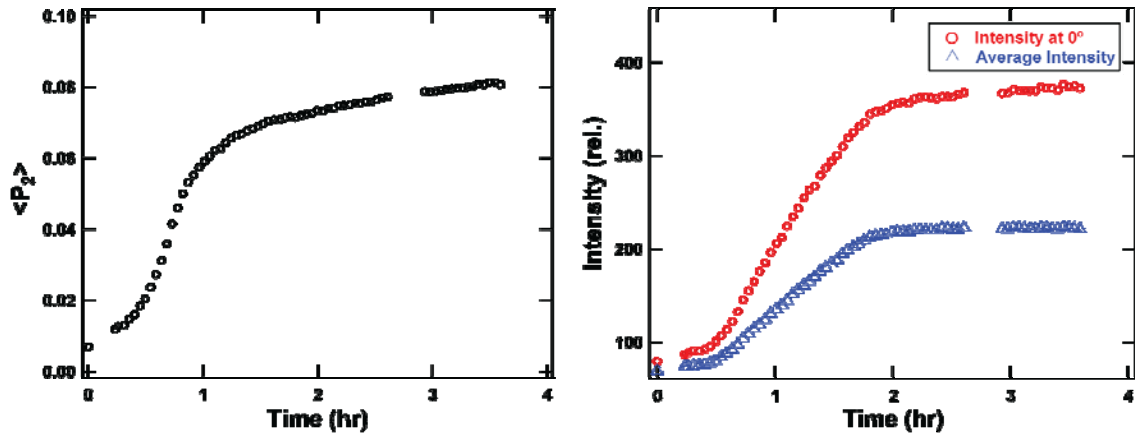


**Figure 5.5. Dynamics at low field strength**

The order parameter (left) is plotted as a function of time for a disordered sample which was quickly cooled in the presence of a 0.39T magnetic field to 100°C. The average scattering intensity and the intensity parallel to the magnetic field of the  $q^*$  peak have also been plotted as a function of time (right). Alignment in this sample occurs most quickly within 1 hour and then gradually increases at longer times.

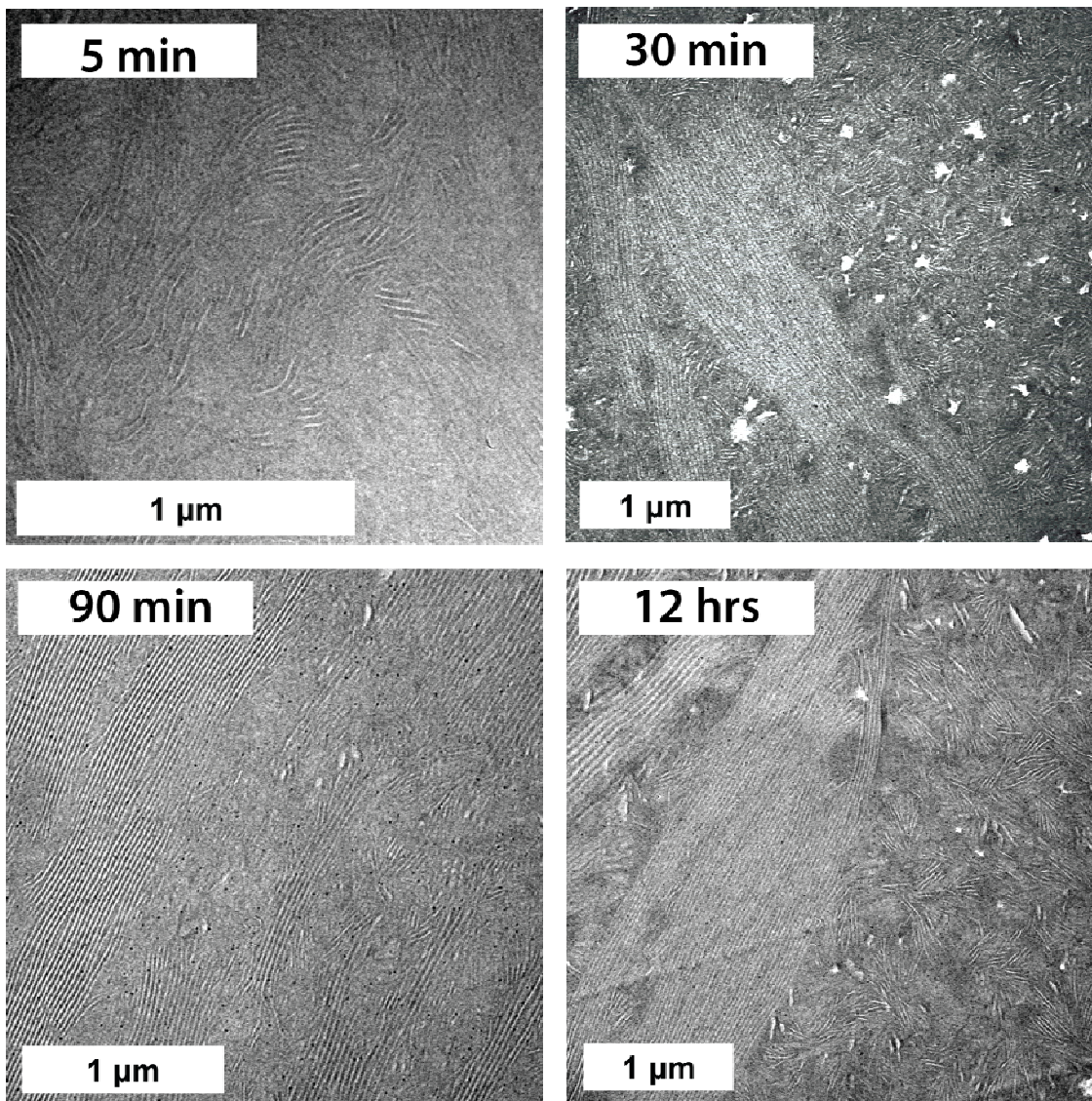


**Figure 5.6. PPV-PI morphology during alignment at low field strength**

TEM micrographs from PPV-PI samples quenched as a function of time after cooling from the disordered state (150°C) to the ordered state (100°C) in a 0.39T magnetic field. These samples are stained with OsO<sub>4</sub> making the polyisoprene domains appear dark.

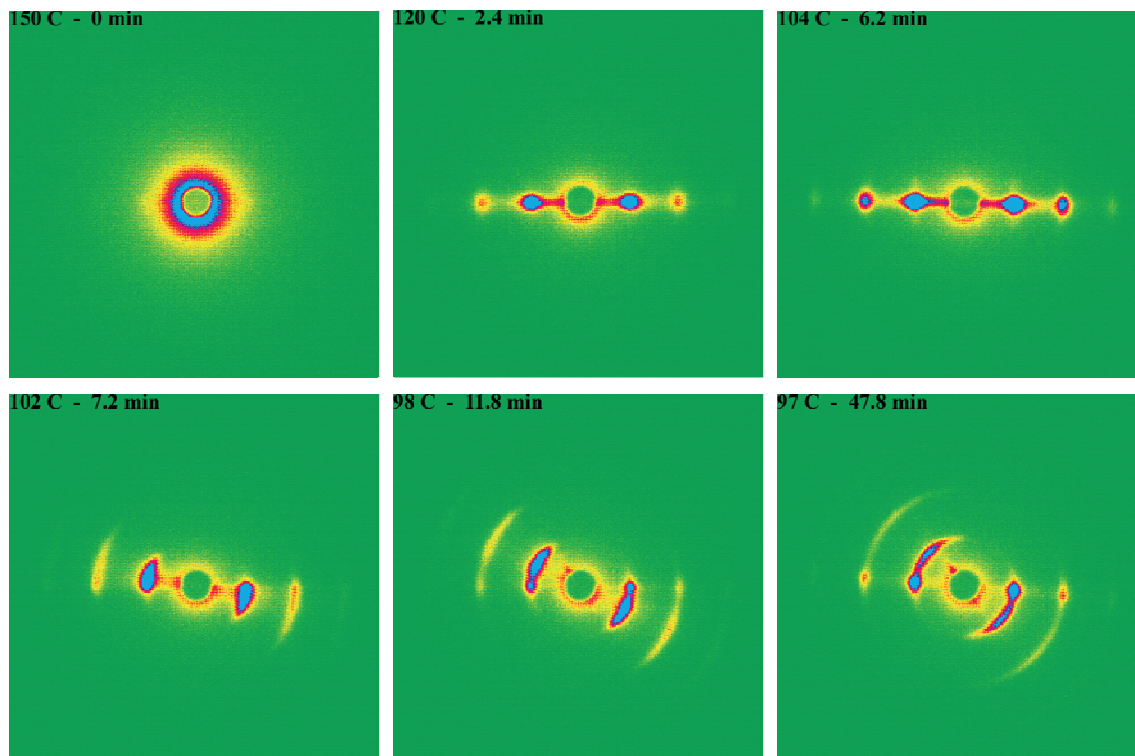


**Figure 5.7. Scattering during alignment at high field strengths upon cooling**  
2D SAXS patterns from a sample quickly cooled from the disordered state (150°C) to the ordered state (100°C) while in a 7T magnetic field.

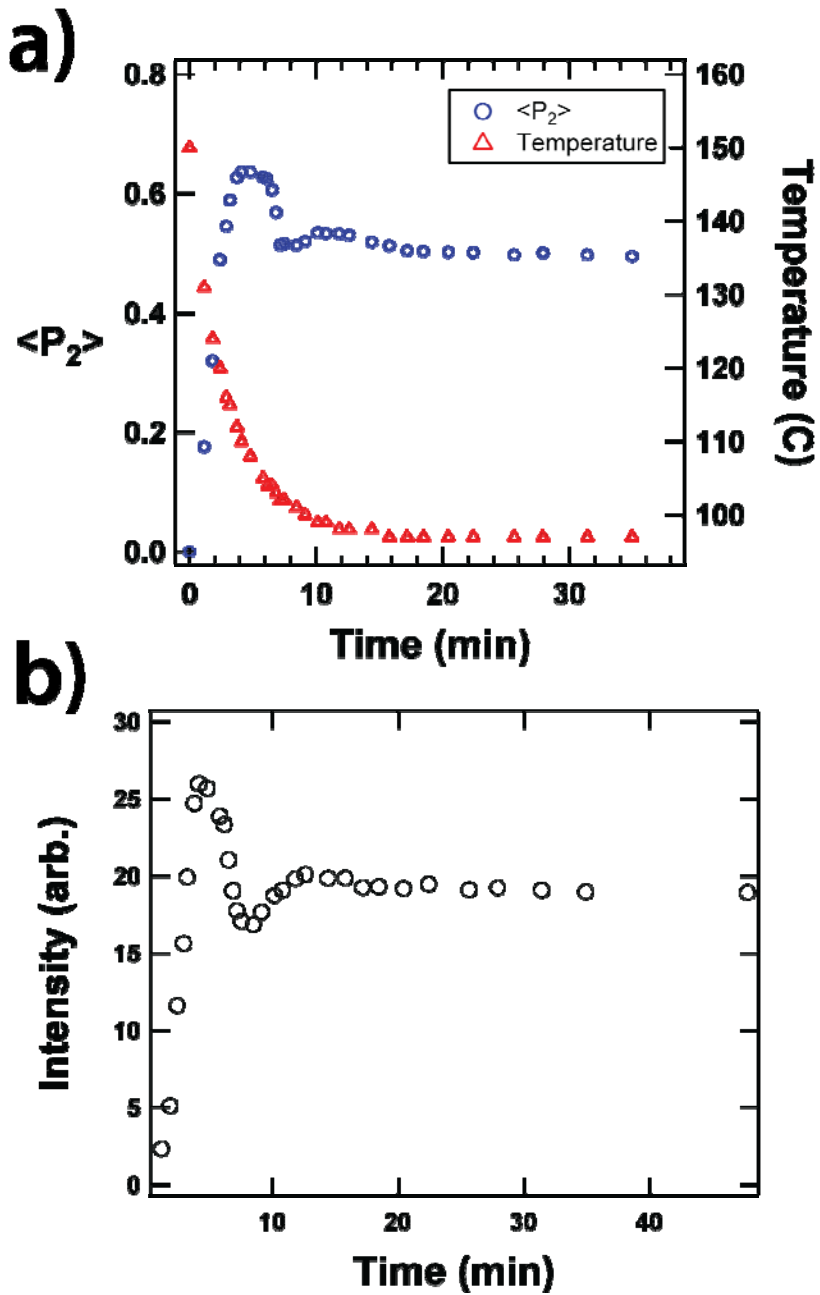


**Figure 5.8. Alignment as a function of time at high fields upon cooling**

The order parameter (a) is plotted as a function of time for a disordered sample which was quickly cooled in the presence of a 7T magnetic field to 100°C. The average scattering intensity has also been plotted as a function of time (b).



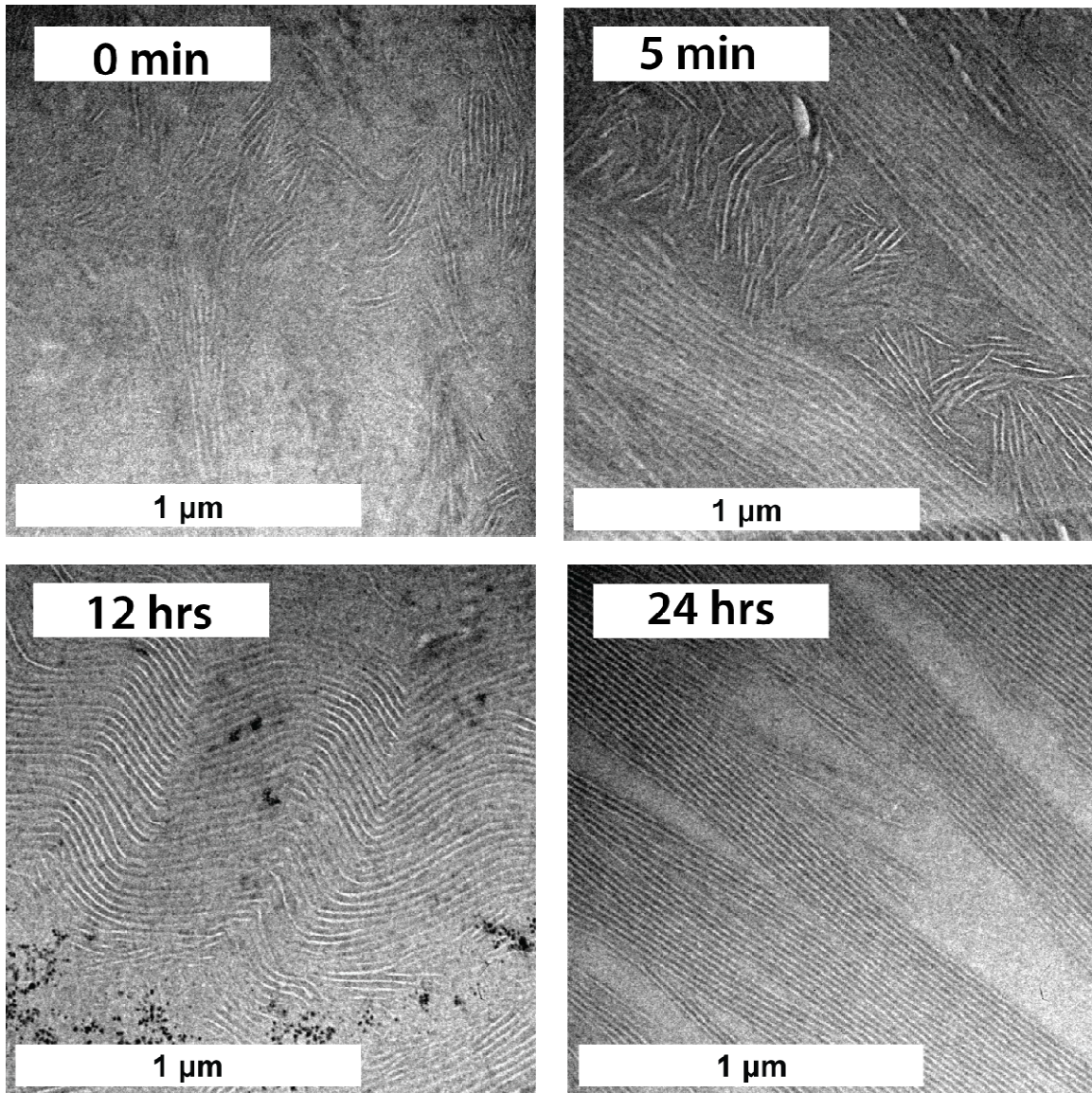


**Figure 5.9. PPV-PI morphology during alignment at high field strength**

TEM micrographs from PPV-PI samples quenched as a function of time after cooling from the disordered state (150°C) to the ordered state (100°C) in a 6T magnetic field. Representative TEM micrographs showing the defect structures associated with this block copolymer system.

to indicate that there are correlations throughout the entire sample volume being probed by the x-ray beam which could be caused by a very large block copolymer grain size.

As shown in Figure 5.7, the order parameter and average scattering intensity reach a maximum after only a few minutes. As off-axis peaks appear the order parameter and scattering intensity decrease. Over a period of hours, the order parameter would recover and increase as the off-axis peak intensity disappears. At short times, selective ordering leads to nucleation of aligned block copolymer grains producing a very high degree of alignment. Selective ordering occurs because at 147°C only perfectly aligned block copolymer grains are thermodynamically stable and between 147°C ( $T_{ODT}$  at 7T) and 115°C ( $T_{ODT}$  at zero field) only partially aligned grains should exist following the equation:  $T_{ODT}^{B=7T}(\phi) = (T_{ODT}^{B=7T} - T_{ODT}^{B=0T})\cos\phi + T_{ODT}^{B=0T}$  where the  $T_{ODT}$  of a block copolymer grain varies as a function of  $\cos\phi$  where  $\phi$  is the angle between the alignment direction of the block copolymer grain and the magnetic field. This leads to a mechanism for the nucleation of aligned block copolymer grains not present at lower fields. Similar to at low field strengths, preferential growth of aligned block copolymer grains also may occur. These two mechanisms, along with faster nucleation and growth kinetics caused by a higher degree of undercooling, lead to a dramatically faster rate of alignment at high field strengths. TEM micrographs shown in Figure 5.8 indicate that this system does in fact begin in a disordered and isotropic state and after only 5 minutes there exist aligned large anisotropic block copolymer grains coexisting with regions of poor order. At this point it is still unclear what the exact cause is of the off-axis peaks however they may be caused by a defect structure referred to as kink bands. This defect structure likely results from grain rotation and has been observed in block copolymer systems aligned using shear<sup>38, 39</sup> or electric fields.<sup>28</sup> It is possible that these defect structures could also arise from smectic liquid crystal screw defects or more complex phenomena related to a momentary disordering which is necessary to enable further alignment.

Isotropically oriented ordered block copolymer sample can also be aligned. This reduces the role of nucleation and growth on alignment and instead relies more heavily on defect annihilation and grain rotation. No appreciable alignment is observed at low field strengths in the ordered phase without first passing through the ODT because of slow defect annihilation and grain rotation observed at low field strengths. At high field strengths, alignment does occur if the temperature is increased above the melting point of PPV. To study this, an isotropically oriented block copolymer sample was heated to 120°C in a 7T magnetic field. As seen in Figure 5.10, the isotropic rings quickly transition to spots after the temperature reaches around 120°C. Interestingly, the scattering intensity and alignment decreases momentarily, the scattering pattern rotates clockwise slightly and then the scattering intensity returns and alignment continues to increase.

Examining the order parameter and scattering intensity more closely in Figure 5.11, it is apparent that little alignment occurs until the temperature reaches around 120°C after 10 minutes. There is a substantial decrease in scattering intensity during this period because as the temperature increases, thermal fluctuations and decreased grain size lead to a decrease in the intensity of the primary block copolymer peak. Between 10 and

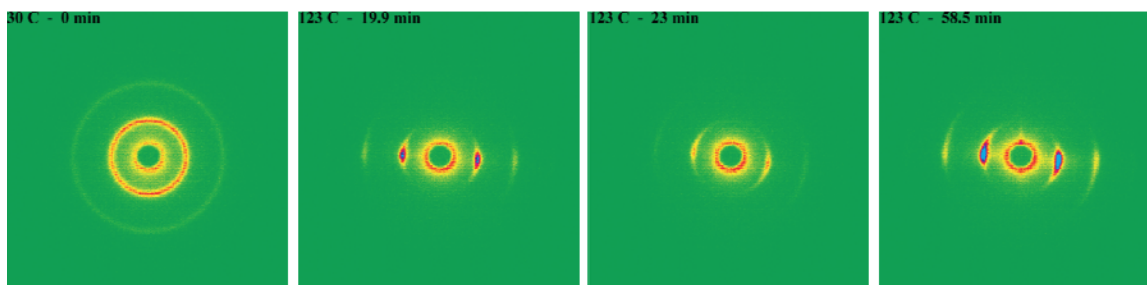


**Figure 5.10. Scattering during alignment at high field strengths upon heating**  
2D SAXS patterns from a sample which was initially isotropically oriented and then quickly heated 120°C while in a 7T magnetic field.

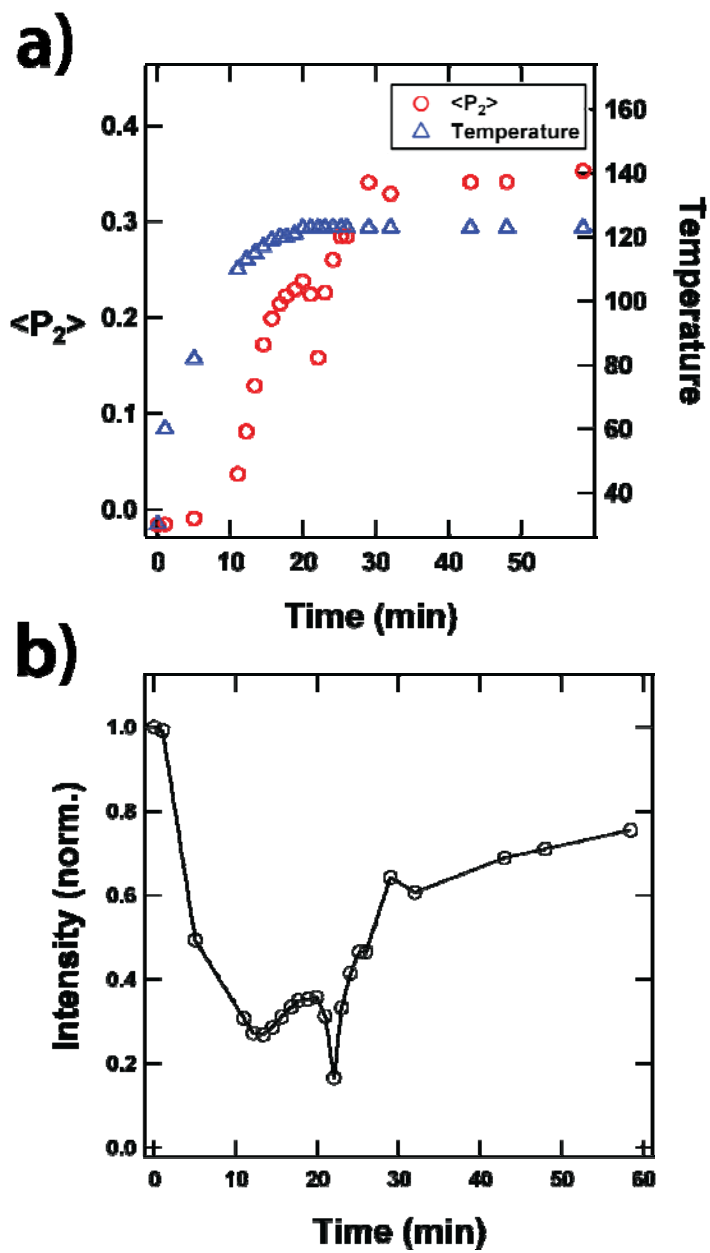


**Figure 5.11. Alignment as a function of time at high fields upon heating**

The order parameter (a) is plotted as a function of time for an isotropically oriented sample which was quickly heated in the presence of a 7T magnetic field to 120°C. The average scattering intensity has also been plotted as a function of time (b).



20 minutes there is a dramatic rise in the order parameter as the system aligns with the field. As the system aligns, the scattering intensity increases slightly as more block copolymer grains are rotated into a scattering condition with the x-ray beam. Surprisingly, at around 20 minutes there is a dramatic decrease in the order parameter and the overall scattering intensity. While it is unclear what the exact origin of this disordering process is, most likely, fluctuations in the block copolymer are locally disordering the block copolymer structure, allowing new block copolymers to nucleate and grow. This is consistent with what is observed near the  $T_{ODT}$  when electric fields are used.<sup>28, 29</sup> It may be related to grain rotation which may temporarily rotate a block copolymer grain out of Bragg condition with the x-ray beam or defect annihilation processes which may temporarily disrupt the block copolymer ordering. After 20 minutes the order parameter and scattering intensity recover to their previous values and continue to increase as a function of time. Finally, the order parameter plateaus indicating that there are kinetically trapped defects which are difficult to remove.

Temperature and field strength directly control the driving forces for alignment and affect the kinetics associated with the process. Samples have been aligned using a range of temperatures and field strengths using in situ x-ray scattering and plotted the obtained order parameter after being cooled and held at a fixed temperature in Figure 5.12. This contains information about kinetic processes as well as thermodynamic parameters and are not easily deconvoluted however some general trends become apparent. Alignment increases with increasing field strength. There is a maximum in alignment observed as a function of temperature for all field strengths occurring around 100°C. Alignment at higher temperatures is limited by smaller block copolymer grains which would couple less strongly to the magnetic field. Interestingly, for the lowest field strength (0.2T) there is a small region below the  $T_{ODT}$  where the block copolymer is ordered but does not align. This indicates that at 0.2T, alignment is insufficient to overcome the thermal energy available to the system. For all field strengths below 100°C, alignment is limited by kinetic effects such as increased melt viscosity and eventually by crystallinity of the PPV block. At lower temperatures, growth of block copolymer grains may also be more isotropic as the driving force for growing aligned block copolymer grains becomes smaller compared to the driving force for demixing.

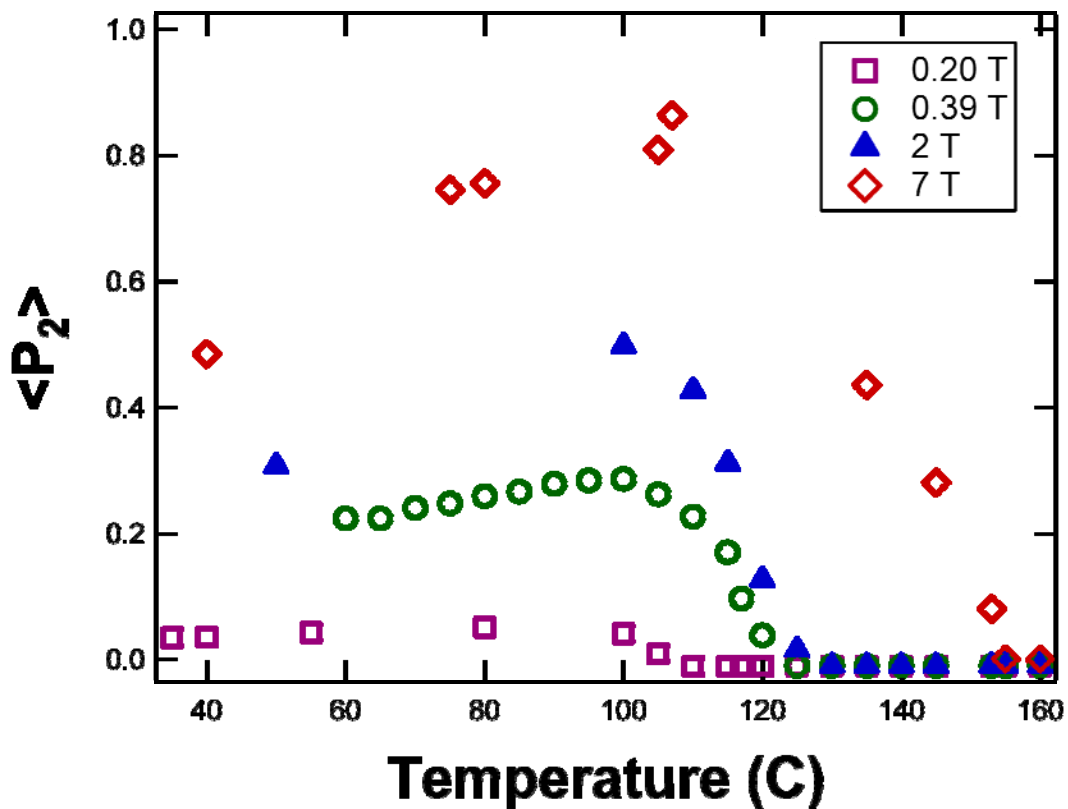


**Figure 5.12. Alignment as a function of temperature and field strength**

The order parameter is plotted as a function of alignment temperature for a range of field strengths. The order parameter was extracted from samples which were cooled from above the order-disorder transition temperature and held at the alignment temperature for over an hour. The order parameter increases as a function of field strength and has a maximum value at around 100° C.

## 5.4. Conclusions

The pathways associated with magnetic alignment in rod-coil block copolymers have been examined using a combination of time resolved in situ small angle x-ray scattering and TEM. This work has shown that at low fields isotropic nucleation and preferential growth of aligned block copolymer grains occurs and at longer times slow defect annihilation increases alignment. At higher fields, significantly higher degrees of alignment are obtained due to the increased driving force for alignment. Selective ordering may lead to nucleation of aligned block copolymer grains dramatically increasing the rate of alignment. Possibly due to the higher rate of alignment when using high fields, interesting phenomena related to defect formation and removal occurs where the overall alignment may not increase continuously as a function of time however at long times a highly aligned sample is recovered. An optimal temperature is observed as a function of magnetic field strength indicating that an efficient alignment procedure must balance the thermodynamic driving force for alignment and kinetic factors which slow block copolymer grain growth, grain rotation and defect annihilation.

## 5.5. Appendix

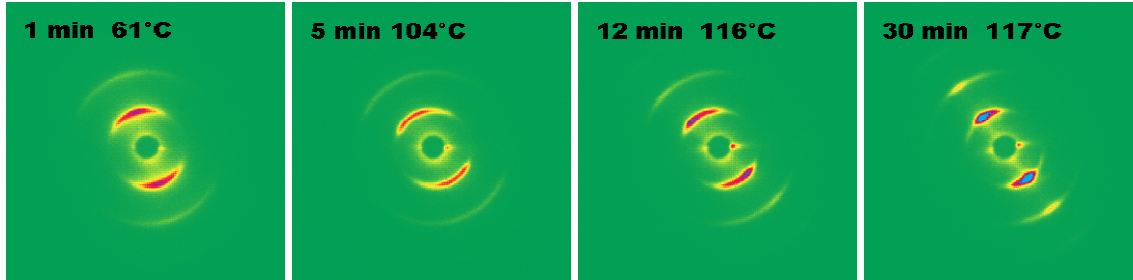


**Figure 5.13. Alignment after rotation at high fields**

2D SAXS patterns from a pre-aligned sample, rotated  $\sim 80^\circ$  and then heated to  $120^\circ\text{C}$  while in a 7T magnetic field.

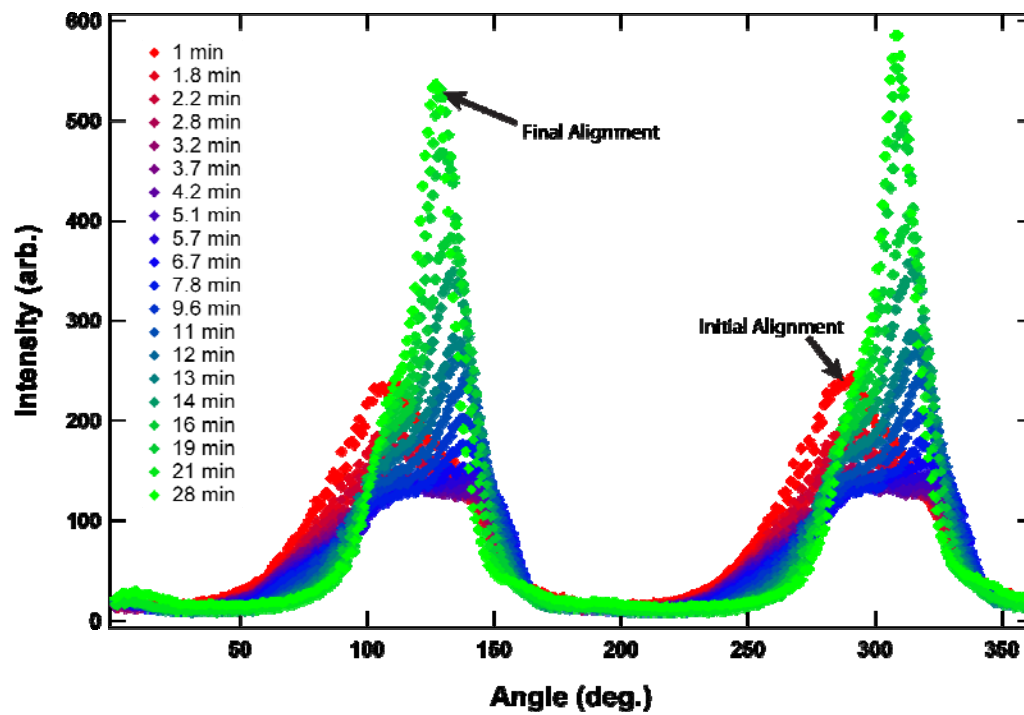


**Figure 5.14. Angular intensity of alignment after rotation**  
 Angular intensity of the primary peak ( $q^*$ ) plotted as a function of time from a pre-aligned sample, rotated  $\sim 80^\circ$  and then heated to  $120^\circ\text{C}$  while in a 7T magnetic field.

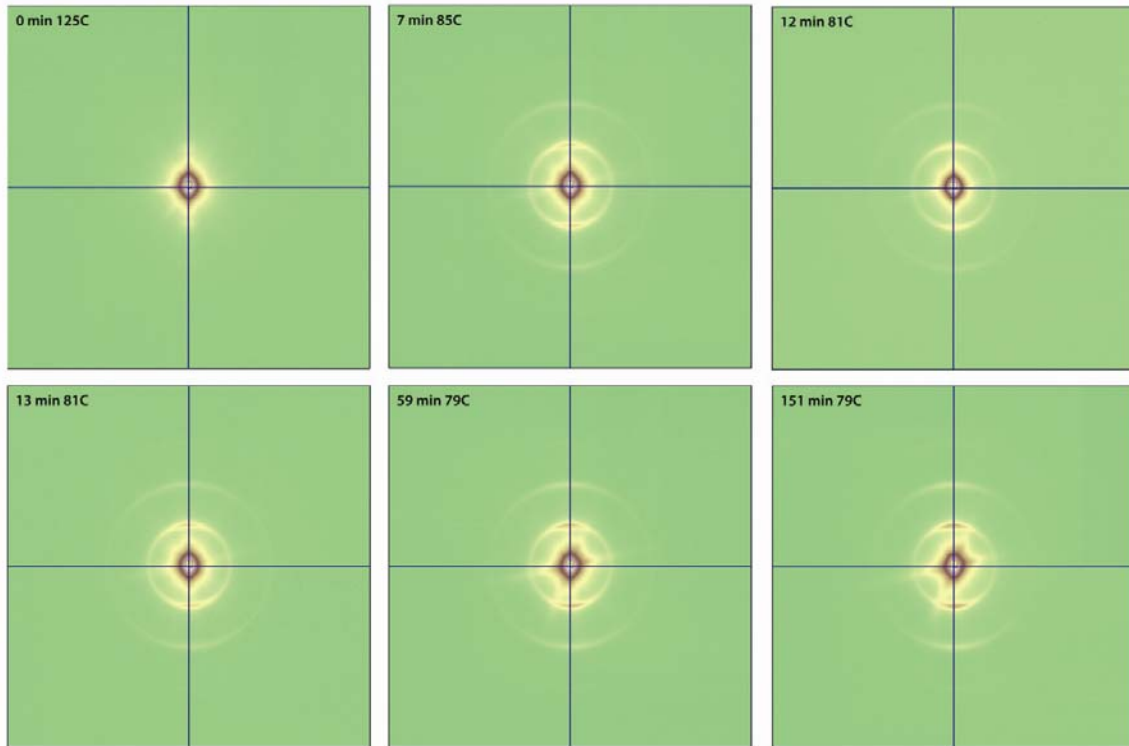


**Figure 5.15. Scattering upon cooling at 2T**  
2D SAXS patterns from a sample quickly cooled from the disordered state (150°C) to the ordered state (100°C) while in a 2T magnetic field.

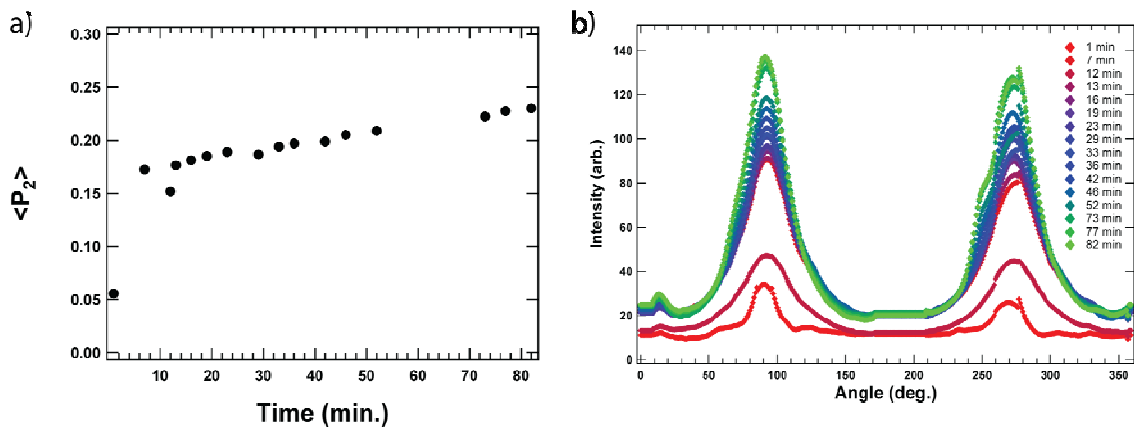


**Figure 5.16. Alignment upon cooling at 2T**

a) The order parameter and b) angular intensity of the primary peak (q\*) are plotted as a function of time for a disordered sample which was quickly cooled in the presence of a 2T magnetic field to 100°C.

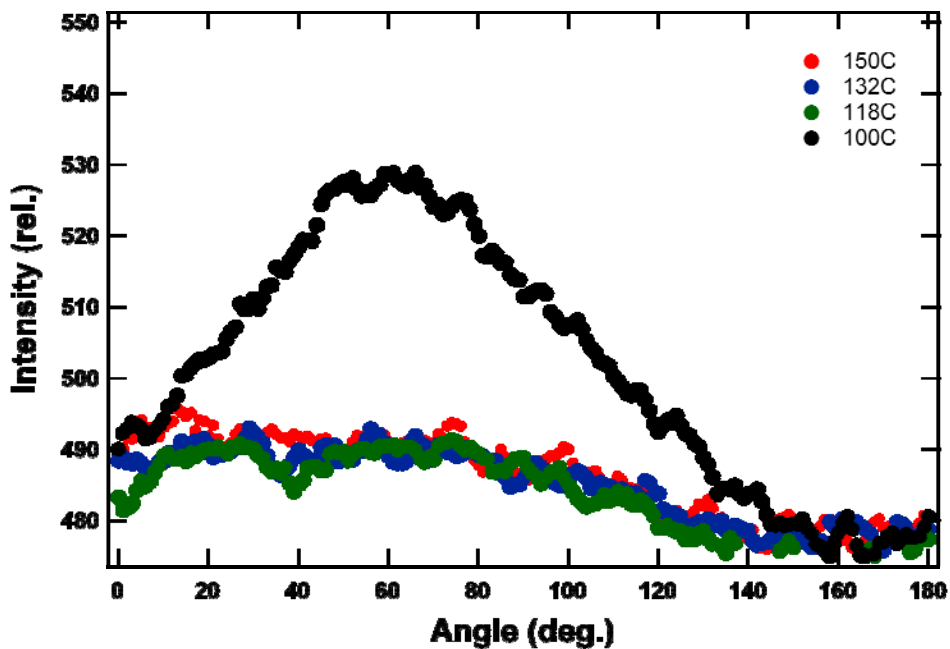


**Figure 5.17. Alignment of PPV at low field strengths**

Angular intensity of the (100) peak from PPV in the disordered state (150°C), nematic phase (132°C), and ordered smectic phase (100°C) while in a 0.39T magnetic field. Alignment of the PPV backbone only occurs in the ordered phase at 0.39T.



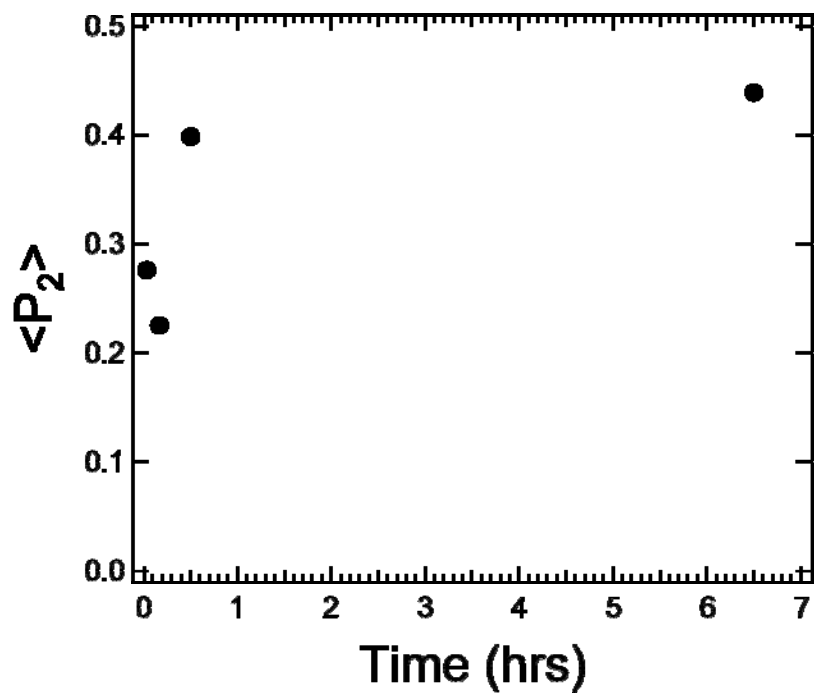


**Figure 5.18. Alignment of ex situ quenched samples at 6T**

The order parameter of samples aligned in a 6T magnetic field and quenched in liquid nitrogen. At early times a dip in the order parameter and off axis peaks are observed similar to experiments using in situ SAXS at 7T.

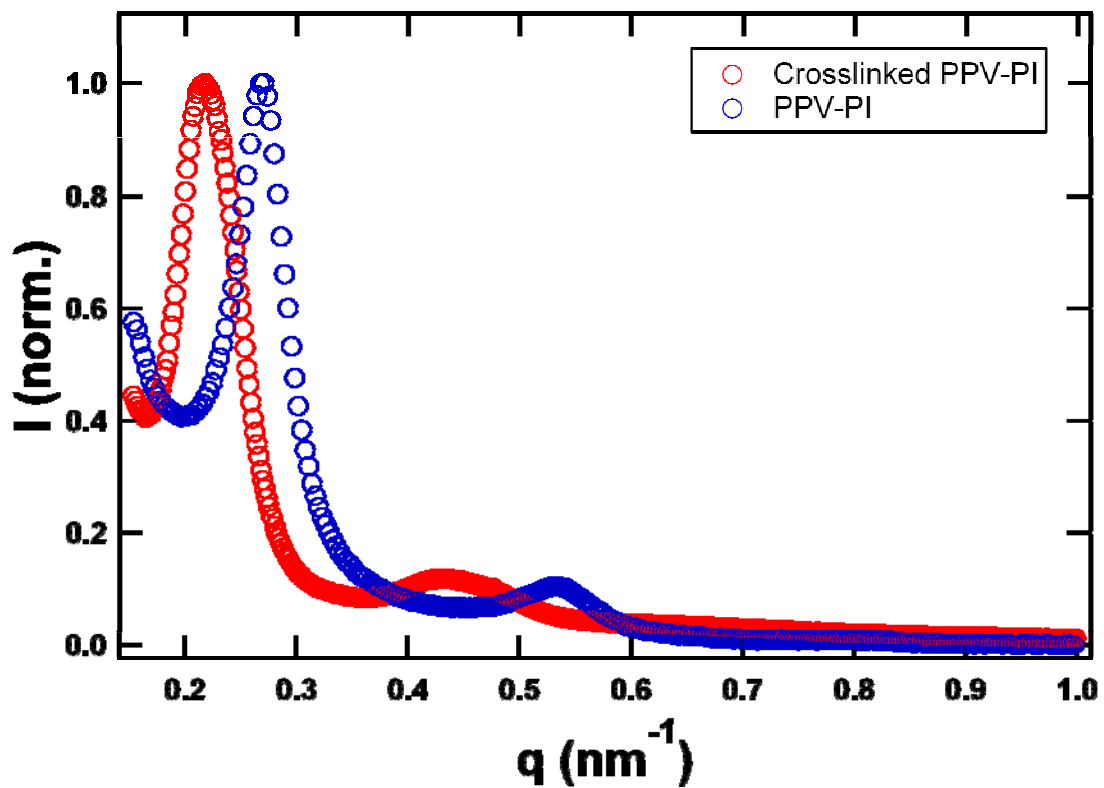


Figure 5.19. Effect of crosslinking on block copolymer morphology  
Azimuthally integrated intensity of PPV-PI before and after crosslinking with sulfur monochloride. Long range order is preserved however the domain size swells around 20%.

## 5.6. Acknowledgments

Research was supported through the Thermoelectrics Program by the U.S. Department of Energy, Office of Basic Energy Sciences, Division of Materials Sciences and Engineering under Contract No. DE-AC02-05CH11231. BM gratefully acknowledges partial support via the Dow Advanced Materials Fellowship. The Advanced Light Source is supported by the Director, Office of Science, Office of Basic Energy Sciences, of the U.S. Department of Energy under Contract No. DE-AC02-05CH11231. In-situ small angle X-ray scattering was performed at the European Synchrotron Radiation Facility on beamline BM26B DUBBLE and the Netherlands Organization for Scientific Research (NWO) is thanked for making the beam time available. Portions of this research were carried out at the Stanford Synchrotron Radiation Lightsource, a Directorate of SLAC National Accelerator Laboratory and an Office of Science User Facility operated for the U.S. Department of Energy Office of Science by Stanford University. We also thank Pawel Majewski, Dr. Chinedum Osuji, Dr. Brad Olson and Dr. Young Rae Hong for helpful discussions.

## 5.7. References

1. Segalman, R. A., Patterning with block copolymer thin films. *Materials Science & Engineering R-Reports* **2005**, 48, (6), 191-226.
2. Hamley, I. W., The effect of shear on ordered block copolymer solutions. *Current Opinion in Colloid & Interface Science* **2000**, 5, (5-6), 342-350.
3. Frederickson, G. H., Steady Shear Alignment of Block-Copolymers near the Isotropic Lamellar Transition. *Journal of Rheology* **1994**, 38, (4), 1045-1067.
4. Schoberth, H. G.; Olszowka, V.; Schmidt, K.; Boker, A., Effects of Electric Fields on Block Copolymer Nanostructures. *Complex Macromolecular Systems I* **2010**, 227, 1-31.
5. Liedel, C.; Pester, C. W.; Ruppel, M.; Urban, V. S.; Boker, A., Beyond Orientation: The Impact of Electric Fields on Block Copolymers. *Macromolecular Chemistry and Physics* **2012**, 213, (3), 259-269.
6. Suh, H. S.; Kang, H. M.; Liu, C. C.; Nealey, P. F.; Char, K., Orientation of Block Copolymer Resists on Interlayer Dielectrics with Tunable Surface Energy. *Macromolecules* **2010**, 43, (1), 461-466.
7. Galatsis, K.; Wang, K. L.; Ozkan, M.; Ozkan, C. S.; Huang, Y.; Chang, J. P.; Monbouquette, H. G.; Chen, Y.; Nealey, P.; Botros, Y., Patterning and Templating for Nanoelectronics. *Advanced Materials* **2010**, 22, (6), 769-778.
8. Grigorova, T.; Pispas, S.; Hadjichristidis, N.; Thurn-Albrecht, T., Magnetic field induced orientation in diblock copolymers with one crystallizable block. *Macromolecules* **2005**, 38, (17), 7430-7433.

9. Adachi, M. A.; Takazawa, F.; Tomikawa, N.; Tokita, M.; Watanabe, J., Magnetic orientation of microcylinders in liquid crystalline diblock copolymer and clarification of its orientation mechanism. *Polymer Journal* **2007**, 39, (2), 155-162.
10. Majewski, P. W.; Gopinadhan, M.; Jang, W. S.; Lutkenhaus, J. L.; Osuji, C. O., Anisotropic Ionic Conductivity in Block Copolymer Membranes by Magnetic Field Alignment. *Journal of the American Chemical Society* **2010**, 132, (49), 17516-17522.
11. Tao, Y. F.; Zohar, H.; Olsen, B. D.; Segalman, R. A., Hierarchical nanostructure control in rod-coil block copolymers with magnetic fields. *Nano Letters* **2007**, 7, (9), 2742-2746.
12. Osuji, C.; Ferreira, P. J.; Mao, G. P.; Ober, C. K.; Vander Sande, J. B.; Thomas, E. L., Alignment of self-assembled hierarchical microstructure in liquid crystalline diblock copolymers using high magnetic fields. *Macromolecules* **2004**, 37, (26), 9903-9908.
13. Hamley, I. W.; Castelletto, V.; Lu, Z. B.; Imrie, C. T.; Itoh, T.; Al-Hussein, M., Interplay between smectic ordering and microphase separation in a series of side-group liquid-crystal block copolymers. *Macromolecules* **2004**, 37, (13), 4798-4807.
14. Gennes, P.-G. d., *The physics of liquid crystals*. Clarendon Press: Oxford [Eng.], 1974; p xi, 333 p.
15. Majewski, P. W.; Osuji, C. O., Controlled Alignment of Lamellar Lyotropic Mesophases by Rotation in a Magnetic Field. *Langmuir* **2010**, 26, (11), 8737-8742.
16. Gopinadhan, M.; Majewski, P. W.; Osuji, C. O., Facile Alignment of Amorphous Poly(ethylene oxide) Microdomains in a Liquid Crystalline Block Copolymer Using Magnetic Fields: Toward Ordered Electrolyte Membranes. *Macromolecules* **2010**, 43, (7), 3286-3293.
17. Gopinadhan, M.; Beach, E. S.; Anastas, P. T.; Osuji, C. O., Smectic Demixing in the Phase Behavior and Self-Assembly of a Hydrogen-Bonded Polymer with Mesogenic Side Chains. *Macromolecules* **2010**, 43, (16), 6646-6654.
18. Majewski, P. W.; Osuji, C. O., Non-degenerate magnetic alignment of self-assembled mesophases. *Soft Matter* **2009**, 5, (18), 3417-3421.
19. Olsen, B. D.; Segalman, R. A., Structure and thermodynamics of weakly segregated rod-coil block copolymers. *Macromolecules* **2005**, 38, (24), 10127-10137.
20. Hartmann, L.; Tremel, K.; Uttiya, S.; Crossland, E.; Ludwigs, S.; Kayunkid, N.; Vergnat, C.; Brinkmann, M., 2D Versus 3D Crystalline Order in Thin Films of Regioregular Poly(3-hexylthiophene) Oriented by Mechanical Rubbing and Epitaxy. *Advanced Functional Materials* **2011**, 21, (21), 4047-4057.
21. Segalman, R. A.; McCulloch, B.; Kirmayer, S.; Urban, J. J., Block Copolymers for Organic Optoelectronics. *Macromolecules* **2009**, 42, (23), 9205-9216.

22. Zhu, R.; Kumar, A.; Yang, Y., Polarizing Organic Photovoltaics. *Advanced Materials* **2011**, 23, (36), 4193-+.
23. Gupta, V. K.; Krishnamoorti, R.; Kornfield, J. A.; Smith, S. D., Evolution of Microstructure during Shear Alignment in a Polystyrene-Polyisoprene Lamellar Diblock Copolymer. *Macromolecules* **1995**, 28, (13), 4464-4474.
24. Winey, K. I.; Patel, S. S.; Larson, R. G.; Watanabe, H., Interdependence of Shear Deformations and Block Copolymer Morphology. *Macromolecules* **1993**, 26, (10), 2542-2549.
25. Gopinadhan, M.; Majewski, P. W.; Osuji, C. O., Order-disorder transition and alignment dynamics of a block copolymer under high magnetic fields by in situ x-ray scattering. *arXiv:1207.1626 [cond-mat.soft]* **2012**.
26. Amundson, K.; Helfand, E.; Quan, X.; Smith, S. D., Alignment of Lamellar Block-Copolymer Microstructure in an Electric-Field .1. Alignment Kinetics. *Macromolecules* **1993**, 26, (11), 2698-2703.
27. Amundson, K.; Helfand, E.; Quan, X. N.; Hudson, S. D.; Smith, S. D., Alignment of Lamellar Block-Copolymer Microstructure in an Electric-Field .2. Mechanisms of Alignment. *Macromolecules* **1994**, 27, (22), 6559-6570.
28. Boker, A.; Elbs, H.; Hansel, H.; Knoll, A.; Ludwigs, S.; Zettl, H.; Urban, V.; Abetz, V.; Muller, A. H. E.; Krausch, G., Microscopic mechanisms of electric-field-induced alignment of block copolymer microdomains. *Physical Review Letters* **2002**, 89, (13).
29. Boker, A.; Elbs, H.; Hansel, H.; Knoll, A.; Ludwigs, S.; Zettl, H.; Zvelindovsky, A. V.; Sevink, G. J. A.; Urban, V.; Abetz, V.; Muller, A. H. E.; Krausch, G., Electric field induced alignment of concentrated block copolymer solutions. *Macromolecules* **2003**, 36, (21), 8078-8087.
30. Schoberth, H. G.; Schmidt, K.; Schindler, K. A.; Boker, A., Shifting the Order-Disorder Transition Temperature of Block Copolymer Systems with Electric Fields. *Macromolecules* **2009**, 42, (10), 3433-3436.
31. Sevink, G. J. A.; Pinna, M.; Langner, K. M.; Zvelindovsky, A. V., Selective disordering of lamella-forming diblock copolymers under an electric field. *Soft Matter* **2011**, 7, (11), 5161-5170.
32. Stepanow, S.; Gunkel, I.; Thurn-Albrecht, T.; Trimper, S., Fluctuation effects in the theory of microphase separation of diblock copolymers in the presence of an electric field. *Macromolecules* **2007**, 40, (6), 2186-2191.
33. McCulloch, B.; Portale, G.; Bras, W.; Segalman, R. A., Increased Order-Disorder Transition Temperature for a Rod-Coil Block Copolymer in the Presence of a Magnetic Field. *Macromolecules* **2011**, 44, (19), 7503-7507.

34. Olsen, B. D.; Shah, M.; Ganesan, V.; Segalman, R. A., Universalization of the phase diagram for a model rod-coil diblock copolymer. *Macromolecules* **2008**, 41, (18), 6809-6817.
35. Bras, W.; Dolbnya, I. P.; Detollenaere, D.; van Tol, R.; Malfois, M.; Greaves, G. N.; Ryan, A. J.; Heeley, E., Recent experiments on a combined small-angle/wide-angle X-ray scattering beam line at the ESRF. *Journal of Applied Crystallography* **2003**, 36, 791-794.
36. Bras, W.; Emsley, J. W.; Levine, Y. K.; Luckhurst, G. R.; Seddon, J. M.; Timimi, B. A., Field-induced alignment of a smectic-A phase: A time-resolved x-ray diffraction investigation. *Journal of Chemical Physics* **2004**, 121, (9), 4397-4413.
37. Hexemer, A.; Bras, W.; Glossinger, J.; Schaible, E.; Gann, E.; Kirian, R.; MacDowell, A.; Church, M.; Rude, B.; Padmore, H., A SAXS/WAXS/GISAXS Beamline with Multilayer Monochromator. *Journal of Physics: Conference Series* **2010**, 247, (1).
38. Polis, D. L.; Winey, K. I., Kink bands in a lamellar diblock copolymer induced by large amplitude oscillatory shear. *Macromolecules* **1996**, 29, (25), 8180-8187.
39. Polis, D. L.; Winey, K. I., Controlling kink band morphology in block copolymers: Threshold criteria and stability. *Macromolecules* **1998**, 31, (11), 3617-3625.

## Chapter 6. Conclusions and Future Outlook

The self assembly of conjugated polymers using block copolymers to control morphology has been shown to be a promising method of improving the performance of these materials. Working with these materials presents several challenges due to their relatively stiff backbone, strong intermolecular interactions and large driving force for crystallinity. By understanding how these specific challenges affect the self assembly process and how they can be tuned through synthetic and processing techniques it is possible to achieve the desired morphologies. Additionally, work done on alignment using magnetic fields presents a simple and powerful technique to improve the charge transport and introduce additional functionality by aligning both the conjugated polymer chains and the block copolymer nanostructure. This work gives a road map for tuning the self assembly of block copolymers by controlling the complex behavior and interactions inherent to conjugated polymers.

Further work is needed, taking advantage of advances in the self assembly of polythiophene block copolymers to produce optoelectronic devices where the morphology can be easily tuned. Systematic studies would help to elucidate the importance in domain size in organic photovoltaics because it is still unproven what the optimum morphology may be. Increasingly, it is even unclear if phase separation is necessary or what degree of mixing is optimal for efficient charge transfer and charge transport. Within a block copolymer system all of these variables could be easily tuned through annealing procedures and would have a large impact on the field as a whole, not only just the block copolymer community. Unfortunately, many of the conjugated polymer chemistries which may be easy to use in block copolymers do not provide cutting edge performance.

Recently a large amount of work has gone into making low bandgap polymers with very complex chemical structures. It is still unclear why some of these polymers perform well with good efficiencies and high charge mobility while others offer no improvements over existing technology. The community must be able to adapt techniques from model conjugated polymers and apply them to self assemble of block copolymer morphologies using low bandgap polymers which are able of producing record breaking efficiencies. First, the chain shape of these polymers is relatively unknown and the increasingly complex polymer backbones makes prediction of the polymer chain shape very difficult. It is hypothesized that rigid polymer chains encourage liquid crystallinity and crystallinity which can improve charge transport however the link between chain shape and these properties is still an unknown question. It is also unclear what chemical functionalities have the greatest impact the chain shape of these polymers, making it difficult to tune the degree of intermolecular interactions and molecular packing in these polymers. It is also unclear what the optimum morphology of these polymers is. It is very difficult to characterize the bulk heterojunction morphology used in devices and therefore a self assembled block copolymer system offers a simple way to systematically vary and study the effect of morphology on the performance of these materials.

Magnetic field alignment of conjugated polymers is also a very interesting topic because of its relative ease and potential to achieve very high alignment. Theoretically, magnetic field alignment should be possible on a wide variety of liquid crystalline conjugated polymers, whether they be simply homopolymers or incorporated into block copolymers. The major challenge in aligning conjugated polymers with magnetic fields is that these materials must have high enough anisotropy in their magnetic susceptibility and sufficiently ordered liquid crystalline phases while not being limited by kinetic factors such as the melt viscosity. It is also helpful to be able to access a completely isotropic liquid crystalline phase to remove any kinetically trapped structures. This requires simultaneously tuning the backbone chemistry and liquid crystalline interactions to optimize these parameters. The potential of magnetic field alignment is very substantial and should be applicable to a wide range of conjugated polymers. A simple technique for alignment of these materials also offers the possibility of creating very novel devices such as polarized OLEDs which would be extremely useful for a wide variety of applications.

In general, whenever working with block copolymers containing conjugated polymers it is crucial to constantly consider the strong intermolecular interactions and impacts of chain shape on these materials. Often achieving the desired morphology is much more challenging due to both kinetic and thermodynamic factors than in traditional block copolymers. It is necessary to make a strong link between synthetic design and morphology characterization to achieve success since it is still difficult to predict or model the behavior of these materials. With continued work in this field it should be possible to create additional design rules to improve the self assembly of these materials. In order to do this it is important to continue to investigate the intermolecular interactions and chain shape of conjugated polymers. Once the detailed chain shape and specific intermolecular interactions of conjugated polymers are more thoroughly understood, the block copolymer phase diagram must be adjusted to account for these factors. For example, block copolymer phase diagrams have been constructed for both coil-coil block copolymers and rod-coil block copolymers but it is unclear what the phase diagram may look like for a block copolymer containing a semi-flexible polymer. The intermolecular interactions in these conjugated polymers are also very complex because the aromatic backbones make the interactions very anisotropic unlike the typical isotropic interactions assumed to occur in most traditional block copolymer systems. While this is common in the liquid crystalline community, the implications of these long range interactions have never been addressed in detail when examining the self assembly of block copolymers. Lessons learned from work with conjugated polymers are very valuable and should also be applicable for a wide variety of polymers with rigid backbones or strong intermolecular interactions. By successfully using conjugated polymers in block copolymer self assembly we are beginning to develop the systems, techniques and theoretical understanding to work with very complex and functional block copolymer systems.